# PRECISION SPECTROSCOPY OF X AND GAMMA RADIATION USING THE FOCUSING CRYSTAL PRINCIPLE. A DETERMINATION OF THE LUMINOSITY IN THE WAVE-LENGTH RANGE 10 TO 500 X. U. AND A PRELIMINARY MEASUREMENT OF GAMMA RADIATION FROM GOLD $Au^{198}$.

Thesis by

David Arthur Lind

In Partial Fulfillment of the Requirements

For the Degree of

Doctor of Philosophy

California Institute of Technology

Pasadena, California

1948

## ACKNOWLEDGEMENTS

The construction and assembly of the spectrometer were carried out by Dr. J. W. M. DuMond with the assistance of Dr. W. H. K. Panofsky, Mr. R. Yost and Mr. B. E. Merkel, instrument maker, before 1942. Dr. B. B. Watson gave able assistance on a large portion of the final assembly and experimental work. Dr. J. W. M. DuMond proposed this work, and his encouragement, friendly interest and many helpful suggestions are gratefully acknowledged.

The work was financially supported by the Office of Naval Research under Navy Contract N6onr-244, Task Order IV. Many of the figures in the text are taken from reports submitted under this contract.

## Abstract

The principles of the curved crystal transmission type spectrometer are discussed with an analysis of the constructional tolerances which are necessary for spectroscopy of x-rays and gamma radiation to 1.7 Mev. energy. A description of the spectrometer which was completed and put into operation is given. The spectrometer has a two-meter focal distance with a dispersion of one mm. per X. U. at the sine screw and has a constant resolution equal to 0.1 X. U. The (310) planes of a quartz plate one mm. thick are used in the transmission arrangement. The wave-length range is from 7 X. U. to 500 X. U. with a precision of 0.01 X. U. The theoretical results of the diffraction theory in ideal and real crystals are summarized. Using these results the absolute intensity in the diffracted beam (luminosity function) is calculated as a function of wave-length under certain simplifying assumptions. An experimental determination of the luminosity function between 500 X. U. and 11 X. U. was made; the integrated reflection coefficient was found to be a function of $\lambda^2$ between these limits. These data indicate that a quartz crystal under an inhomogeneous stress behaves as would a mosaic crystal. A comparison of the reflection coefficients with theoretical values shows good agreement. At 0.4 Mev. only 0.3% of the incident quanta are diffracted by the crystal. Sources of 50 mc. or greater are needed since at present only one quantum in $10^8$ will register in a spectral line. A precision determination of one gamma-ray line in the radio-gold $Au^{198}$ spectrum was made with the result

$$E = 0.4112 \pm 0.0002 \text{ Mev.}$$

This represents the first precision determination of any gamma radiation energy. Finally, design requirements and limitations of the focusing crystal method are discussed to indicate the range of usefulness and the results which may be obtained with such an instrument.

Table of Contents

Part I

# Theory and Design of a Curved Crystal Focusing Spectrometer for X or Gamma Radiation

## Introduction

The wide range of application of the crystal diffraction technique in x-rays led many to consider this method for the study of more energetic x-rays or gamma radiation. Several attempts[1,2,3] over a period of years were made to study the radiation from the natural radioactive elements by the crystal method. The results were not remarkable, and the maximum energies studied were about 0.7 Mev. These early attempts except for Rutherford and Andrade were all made by rocking a flat crystal in a very narrow beam of incident radiation and recording the diffracted radiation by a photographic plate. The sources generally used were 100 to 200 mc. of radium. Because of the very low intensity further investigation was never attempted, in spite of the need for a method for accurately determining the energy of nuclear gamma radiations. The same problem of intensity had arisen in the use of the crystal method in x-rays, and several people had given the geometric conditions necessary for obtaining increased intensity through the focusing action of curved crystalline plates.* The first one to set down the conditions for true focusing by a curved crystal was J. W. M. DuMond[5] in 1930. However, it remained for Cauchois[6,7,8] and Johann[9] to carry out DuMond's ideas with a curved crystal. In another paper published by J. W. M. DuMond[10] is to be found a more complete history of the

*The first suggestion of this type was made by Gouy in 1916.[4] Following this many others suggested possible methods, but it should be noted that the important difference between these and the present one is that they require slits to determine the resolving power while the present method has a pair of conjugate foci.

development of the ideas as well as a preliminary description of the instrument which is the subject of this thesis.

The extreme precision of x-ray wave-length measurements suggests that the method might give comparable results for gamma-ray wave-lengths and hence tie the whole field of nuclear energy measurements to an accurate standard. It must be remembered that with the ordinary x-ray diffraction techniques the x-ray intensities available are equivalent in numbers of photons to an activity of the order of $10^4$ curies* expressed in terms of radioactive disintegrations. The artificial radioactive sources which one ordinarily has have an activity of the order of millicuries or possibly curies. Furthermore the photographic plate, ion chamber and Geiger counter can be made much more sensitive to low energy x-radiation than to high energy gamma radiation. Finally, the problem of dispersion and resolving power becomes more acute as the energy range of study increases. Hence there are essentially three problems in the design of this instrument:

1. High luminosity
2. High sensitivity gamma radiation detector
3. High dispersion and resolving power.

Luminosity and resolving power are interrelated and will be considered again in Part III.

Geometric Optics of the Curved Crystal Focusing Spectrometer

Let us assume that one wishes to make use of a widely divergent or convergent beam in a crystal diffraction spectrometer. This can be done by the use of a curved crystalline plate as was suggested by

*1 curie represents $3.7 \times 10^{10}$ disintegrations per second.

DuMond.[5] If one is to focus x-radiation from a line source by reflection from the atomic planes of a crystal, two conditions must be satisfied: (a) The angle of deviation for all rays in a bundle must be constant and fixed by the Bragg relation

$$\phi = 2 \sin^{-1}\left(\frac{n\lambda}{2d}\right) \qquad (1.1)$$

(b) The angles of incidence and reflection referred to the atomic planes must be equal. Reference to Fig. 1 will show that these two conditions are satisfied, in Case R when source and image are both real and in Case V when either source or image is real while the conjugate focus is virtual. Condition (a) determines the location of the reflecting planes, and condition (b) their direction. One can see that if the source, image and crystal planes all lie on a circle with center at O, the arc $(S_1I_1)$ or $(S_2I_2)$ measures twice the angle of deviation for all parts of the crystal. Furthermore, if the crystal has as its center of curvature the point $C_2$, i. e. in Case R the center of curvature of all the crystal planes used for Bragg reflection is at $C_2$, and if arcs $(S_1C_2)$ and $(I_1C_2)$ are equal, then condition (b) will be satisfied for all parts of the crystal simultaneously. In Case V the crystal planes may be imagined to pass through the center $C_1$; if S is the virtual source, I will be the real image. I may be the source in which case S will be a virtual image point. In this case it is evident that again conditions (a) and (b) will be satisfied. It is apparent that the Case V or transmission type will be better suited for use in the short wave-length region of small Bragg angles $\theta_B$.

Cauchois[6] made the first careful analysis of the focusing conditions and showed that the crystal need not be ground out to contact

the focal circle but could be a section of a right cylinder which was tangent to the focal circle at $C_2$. She analyzed the construction tolerances and focal caustic due to failure of condition (a). For this work only part of her analysis will be needed. Referring to Fig. 2 and assuming that the reflection by the crystal planes occurs only on the neutral axis $P'C_2P$, the dispersion on the focal circle will be given by the following calculation:

$$n\lambda = 2d \sin \theta_B$$

$$n \Delta\lambda = 2d \cos \theta_B \Delta \theta_B$$

$$\frac{\Delta\lambda}{\lambda} = \cot \theta_B \Delta \theta_B$$

To calculate the dispersion on the focal circle let $\ell$ be the distance measured along its circumference. Then

$$\Delta\ell = R \Delta\theta_B$$

$$\frac{\Delta\lambda}{\Delta\ell} = \frac{\lambda \cot \theta_B}{R}$$

For $\theta_B \ll 1$

$$\frac{\Delta\lambda}{\Delta\ell} = \frac{2d \cos \theta_B}{Rn} \cong \frac{2d}{Rn} \qquad (1.2)$$

The other quantity of interest is the resolution $\frac{\Delta\lambda}{\lambda}$

$$\frac{\Delta\lambda}{\lambda} \cong \frac{2d}{Rn} \frac{\Delta\ell}{\lambda} \qquad (1.3)$$

In any instrument $\Delta\ell$ is determined by construction tolerances and perfection of crystal lattice structure as well as source size, but it must be noted that the geometric perfection of focus must increase with increasing energy of radiation if uniform precision is to be maintained.

In the transmission type of spectrometer in which the planes are

approximately normal to the plate surface there is no correction for the index of refraction of the crystal.* (See Fig. 3.) This is not true for the reflection type. The change in wave-length at the surface just compensates for the change in angle, so the Bragg equation still holds when referred to the external angles and wave-lengths as long as the external angles of incidence and reflection are equal.

In Fig. 2 is shown the approximate transmission spectrograph geometry. Since it is necessary to use a crystal of some thickness and since the crystal deviates from the focal circle, the image of the source S will have an aberration width $\Delta\lambda_1$ on the wave-length scale corresponding to the width $\Delta l_1$ on the focal circle. Assume the neutral axis of the crystal ($P'C_2P$) lies tangent to the focal circle at $C_2$. By a simple geometric analysis

$$\frac{\Delta\lambda_1}{\lambda} = \frac{\cos\theta_B(1 - \cos\alpha)}{\cos(\alpha + \theta_B)} \qquad (1.4)$$

$\theta_B$ is the Bragg angle, and $\alpha$ is the half-angle of the aperture. For $\theta_B << 1$ and $\alpha << 1$ one obtains for the relative broadening

$$\frac{\Delta\lambda_1}{\lambda} \simeq \frac{\alpha^2}{2} \qquad (1.5)$$

If one assumes the crystal is perfect throughout its depth and if the crystal lattice is distorted elastically, the increased lattice

*The dynamical theory of x-ray scattering in crystals predicts this result. However, a correct expression for the correction can be obtained by applying Snell's law for refraction at the surface and Bragg's law in the interior of the crystal. A simple derivation of Snell's law leads to the relation

$$\frac{\sin\theta_1}{\sin\theta_2} = \frac{\lambda_1}{\lambda_2}$$

which shows that Bragg's law is correct when applied to $\lambda_1$ and $\theta_1$.

constant on the convex side will compensate so that all rays through the depth of the crystal will focus at I. The rays diffracted from the outside edge will suffer a smaller deviation than those from the inside edge on account of the larger lattice spacing. This effect is exactly sufficient to cause all rays to pass through the image point I. If instead the lattice spacing is constant throughout the depth and if t is the crystal thickness, there will be an additional broadening

$$\frac{\Delta\lambda_2}{\lambda} = \frac{t}{2R}\left(1 + \frac{\cos\theta_B}{\cos(\theta_B + \alpha)}\right) \qquad (1.6)$$

which for the conditions $\theta_B << 1$ and $\alpha << 1$ reduces to

$$\frac{\Delta\lambda_2}{\lambda} \simeq \frac{t}{R} \qquad (1.7)$$

Expression (7) will suffice for an analysis of the effect of errors of placement of the crystal relative to the focal circle provided $C_1$, the center of curvature, lies on the focal circle.

The crystal will be assumed curved to a perfect cylinder of radius R. First, the crystal must lie tangent to the focal circle at $C_2$. (See Fig. 2.) If the crystal is centered on $C_2$ but is rotated by an angle $\phi$ about $C_2$, the relative widening will be of the order $\phi\alpha$. $\phi$ can easily be made less than $5 \times 10^{-4}$, so this term is much smaller than the inherent widening due to the approximate geometry. Second, if the crystal is displaced by an amount t along $C_1C_2$, there will be a defocusing of $\frac{t}{R}$, but again $\frac{t}{R}$ may be easily held to $2 \times 10^{-4}$. Finally, the focal circle diameter must be set equal to R, the radius of curvature of the crystal. Suppose $D_f = R \pm \varepsilon$, then the relative widening will again be

$$\frac{\Delta\lambda_3}{\lambda} = 2\,\frac{\varepsilon}{R}\,\frac{\alpha}{\theta_B} \qquad (1.8)$$

In fact the procedure for assembling and adjusting an instrument requires that one first set the center of the crystal over the point $C_2$. After determining the focal distance R, the center O is set to bisect the radius $C_1C_2$, and finally I is set on the focal circle with center at O. These various adjustments can be made to 1 part in 1000 if not better. However, even if these conditions are not met, the aberration will be given approximately by (8) where $\varepsilon$ is the distance out of focus in the zero position; this can be checked as will be described later.

A discussion of the other adjustments and tolerances will be deferred until the instrument is described. However, the bending of the crystal turns out to be the crucial factor for the success of the method. The analysis to this point has assumed that the crystal is bent to a perfect cylinder with no aberration. This will never be the case. For a transmission spectrograph the crystal planes which are to be used must lie very nearly normal to the crystal plate. Small deviations from this condition can be compensated for by setting the zero of the wave-length scale at the point on the focal circle which is the intersection of the crystal planes. This point is designated the $\beta$ point. The planes must, however, be uniformly oriented with respect to the external geometry of the plate, and in the bent position the generators of the cylinder must be accurately parallel. The crystal planes need be only approximately parallel to the axis of the cylinder since a slight tilt will only raise or lower the image normal to the focal circle by a small amount. It is the accuracy with which the

crystal planes intersect at one point, i. e. $C_1$ (Fig. 2), which will determine the resolving power as well as the luminosity of the instrument. This aberration is in part a result of non-uniform curvature, but also in part due to irregularities in the crystal structure, i. e. mosaic structure. These aberrations must be such that $\frac{\Delta}{R}$, where $\Delta$ is the aberration width at the center of curvature, be less than $5 \times 10^{-5}$ if the instrument is to have a resolution of 0.1% around 1 Mev. quantum energy.

The transmission type spectrograph may be used with either a real source or a virtual source (Fig. 4). If a virtual source is used, the true source is placed at A. Those rays from A which would pass through V will be diffracted to R as a real image, because they all make the same angle with the crystal planes. A photographic plate may be placed along the focal circle, or a counter and slit may be used to explore the spectrum. Of course it is necessary to prevent direct radiation from A reaching R. If the point R is used as a real source, then there exists its virtual image at V from which all diffracted rays appear to diverge. In this case a counter or ion chamber must be used as the detector and must be shielded from the direct beam. There will be a considerable increase in luminosity of the instrument for this case as indicated in the analysis given in Part III. When the Bragg angle is small as in the case of gamma rays, both arrangements require a collimator to prevent the direct beam from reaching the detector. It is the collimator which geometrically limits the minimum wave-lengths which may be studied.

Description of the Instrument

The mechanical design of this instrument was done by Dr. J. W. M.

DuMond in 1938. The instrument was complete except for detector and crystal in 1945. It was decided that a real source and virtual image would be used, because of the increased intensity afforded by this arrangement.

Lead Collimator

The collimator was designed to have a window, i. e. to transmit radiation, of half-width of approximately $0.4^{\circ}$ and to cut off all scattered radiation outside this angle. The angle $0.4^{\circ}$ represents the minimum Bragg angle which can be used and corresponds to 1.75 Mev. energy (7 X. U.). Since there may be a very high radiation density passing directly through the crystal (Fig. 5), it is desirable to avoid secondary scattering from the side walls of the collimator. The collimator is shown in Fig. 5 (not to scale) and by E of Fig. 8. The length is 31.4 inches, and the faces of the slots taper to intersect at a distance of 75.5 inches. There are 7 slots, 2 inches in height, spaced 0.25 inches center to center at the small end and 0.35 inches at the large end; slots and partitions are of equal width. The partitions and spacers are die-cast of 96% lead and 3% antimony and are assembled with one inch slabs of lead on each side by clamping between steel plates. The total weight is 500 pounds. A carriage supports this collimator, and leveling screws as well as transverse adjustment screws are provided.

Fig. 6 shows an experimental window curve of the collimator taken with a source placed at R. This shows that the source is very close to the true focal distance. The radiation outside the geometric window is very small and diminishes rapidly as the angle increases. This radia-

tion is due in part to transmission in the lead and in part to scattering. Note that in Fig. 6 the ordinate scale is changed by the factor $10^3$ between -10 and + 10. The irreducible background as indicated is due to the local radiation level.*

Kinematic Design

In practice the collimator is fixed in orientation. This fixes the line CV (Fig. 7). Hence the motion of the system must be such that the angles R'CB and BCV' are equal at all settings and the point R remains on the focal circle. Also it is necessary to allow R to pass through V to permit study of reflections from both sides of the crystal planes, so that the determination of the diffraction angle $\theta$ does not depend on an exact knowledge of the location of the $\beta$ point.** This is extremely important when working at very small diffraction angles, for the measurements of the diffracted line on both sides of the crystal planes give the wave-length as well as the location of the $\beta$ point. Since the line CV is fixed, the focal circle which is fixed with respect to the crystal must swing through an angle $\theta$ (relative to the frame of the instrument) while the source swings through the equal angle $\theta$ with respect to the focal circle and at the same time is constrained to lie on it by the radius bar OR.

The instrument consists of the triangular base frame of eight-inch channels, the corners of which have leveling screws and adjustable

*It is most convenient to plot the collimator transmission curve as a function of the wave-length screw. Actually the width is twice the apparent width given by Fig. 6, because only the distance R (Fig. 5) is represented by the screw reading.

**Only if the crystal planes were truly normal to the crystalline plate would the line CO intersect the $\beta$ point as indicated in Fig. 7.

pads. (See Fig. 8.) The pad A carries the main pivot system which determines the axis of the crystal and supports the focal circle beam F and source beam S. The axes of rotation of these beams are accurately determined by adjustable cone type bearings while their weight is supported by ball thrust bearings. The two pads B and C support the ends of the track T which is pivoted about the point V. The screw carriage Q rides in the track T and is so constructed that the focal circle beam always passes through its center and always remains normal to it. Since T is pivoted at V' (Fig. 7), the beam F must be permitted to slide normally to Q. With the exception of this motion Q and F may be considered a rigid system pivoted about C to which the focal circle and hence the crystal are attached. The table L rides on the screw carriage Q and supports the opposite end of the source beam S to which it is fixed so that distances R'C and V'C (Fig. 7) are constrained to be equal. The source carriage N rides on the source beam and is constrained to move only along R'C. The point O, the center of the focal circle, is connected to the carriage N by a radius bar as shown in Fig. 8. The displacements of the carriages Q and L are controlled by two screws of equal pitch driven in opposite directions of rotation inside the carriage Q. The lower screw runs through a nut fixed at V' and drives the carriage Q while the upper drives the carriage L through a nut at R'. These screws have backlash takeups and in addition are spring loaded to take up any residual backlash. All the bearings are of the antifriction type except the main pivotal location bearings at the spindle M (Fig. 8).

The screw carriage Q always runs normally to the axis COB (Fig. 7).

Since the two screws have accurately equal pitches and are driven at equal rates, the distances R'B and V'B are equal. In addition the distances R'C and V'C being equal insures that R'V and V'B shall measure the sines of the equal angles $\theta$. This means that the screw may be calibrated directly in wave-length units. The distances CR' and CV' are such that with the quartz (310) planes the 26 threads per inch pitch of the screw yields a calibration of almost exactly one X. U. per revolution. The screw is provided with a revolution indicator Z and a vernier W,Y (Fig. 8) to read to 0.001 revolution or 0.001 X. U. The two screws are precision screws lapped with great care. As a check they were calibrated by means of a microscope and a standard decimeter scale. The errors seemed to be periodic with a period of one revolution. Their maximum value was about 0.005 X. U. which is small enough to be neglected until experimental results demand otherwise.

The crystal holder is supported on the table P which is rigidly mounted on the main spindle M. This spindle is free to rotate with respect to F and S except that F is provided with an arm J which may be clamped to the crystal spindle and which allows one to make small angular adjustments of the crystal table with respect to the beam F. This permits one to set the crystal tangent to the focal circle determined by O and then rotate the crystal and circle to set $\beta$ accurately on the line BC. Then the $\beta$ point will be set at the zero of the wave-length scale. The crystal holder table is provided with screws for sliding the holder so that the center of the crystal may be set on the axis of rotation. At the same time the crystal can rotate about a horizontal axis to set the axis of curvature parallel to the axis of

the spindle M.

The center O may be moved along the arm J so that OC = R/2 is the correct focal circle radius (Fig. 7). Then the carriage N is rolled along the beam S until RO = OC = R/2 and clamped to the radius bar.

The principles of "kinematic design" were used except in a few instances. The high precision requires that the geometry be precise. Subsequent experience has shown that what troubles did occur in the instrument arose at those points where the principles were violated.

The instrument was checked throughout after assembly to insure that no interference would cause mechanical loading and deformation from the assumed geometry. The base triangle, i. e. the plane defined by the surfaces of the three corner pads, was carefully leveled to 0.01 inches. The main pivot axis at C (Fig. 7) had to be accurately normal to the base plane defined by the three pads because, owing to the fact that the beams F and S pivot at different heights, their centers of rotation would not otherwise coincide. If the actual geometry lay in a plane, this problem of alignment would not occur. The only thing that can be done is to take extreme care in design and construction.

Crystal Clamping Blocks and Crystal

The crystal chosen for this work was quartz because of its mechanical properties and perfect crystal structure. Also crystals of hexagonal symmetry have smaller grating spacings than those of any other class. The planes chosen were the (310) planes because they had been reported to have a high luminosity. The slabs were cut 3/16 of an inch thick from a large natural crystal so that the (310) planes lay within $1^{\circ}$ of the normal to the slab and parallel to one set of edges.

The slabs were then polished optically flat on one face, turned over, milled to a thickness of 1 mm. and polished to an optical flat again. Thus, with some precautions to relieve strains set up in working, the plates were made optically flat, uniformly thick slabs with known orientation of the crystal planes.

The crystal holder is shown in Fig. 9. Only the convex block determines the curvature of the quartz plate clamped against it. The concave block is ground to approximately the same curvature. A thin rubber diaphragm between it and the plate is sufficient to make the plate contact the convex block. The assembly is held together with four screws and compression springs to equalize the pressure. The central web of the aperture was considered desirable to prevent bowing of the plate from "anticlastic curvature".

The clamping blocks were completely machined before any heat treatment or grinding was done. The material was a special stainless steel,* suggested for its stability by C. G. Peters of the National Bureau of Standards. Fortunately the heat-treated pieces aged for four years before the final grinding and polishing operation. Since the radius of curvature chosen for the instrument was two meters, it was a problem to devise a means to grind a perfect cylinder, the generators of which were parallel to the side faces of the blocks. This last condition was necessary in order to orient the focal axis. The procedure for this figuring has been adequately described elsewhere.(11) The aperture in the blocks for the radiation to pass through consists of two

*Composition as follows: Cr 13.5%, C 0.35%, Mn 0.40%, Si 0.50%. It can be obtained from either Firth Sterling or Allegheny Ludlum Steel Companies.

slots 14 mm. high by 44 mm. wide presenting a total area of $1.23 \times 10^3$ sq. mm. This is the limiting aperture of the system.

The quartz crystal and blocks had to be very carefully cleaned before clamping, because small particles would prevent an optical contact between crystal and convex block. The check of uniformity of curvature was made by watching the fringes between the plate and the ribs. After the plate was set up and tested for focus, the plate was rotated until the planes lay parallel to the generators. The vertical displacement of a short segment of the line image of a spectral line on opposite sides of the $\beta$ point was measured. From the vertical separation between images it was possible to calculate the rotation necessary. The focal properties of the crystal remained remarkably constant for a period of over a year, and it was quite easy to reproduce the focal length when crystals were exchanged.

Experimental Test of Focus

The check of the crystal focus and incidentally the crystal perfection was made by a photographic method first. The photographic film was set up at R (Fig. 7) since a real image was desired. A tungsten target x-ray tube excited at 70 kv. and 10 ma. was used as a source. Since the focal spot is small, the tube was moved so that successive exposures could be made with the zones of the crystal as shown in Fig. 10 by the tungsten $K\alpha$ radiation. All exposures were taken on the same film by successively covering with lead shields all but a narrow horizontal band of film. The position of the line from successive zones was measured on a comparator and with the corresponding ray direction was plotted as in Fig. 10. In the figure the scale parallel to the

focal plane is 100 times full scale while normal to the focal plane, it is full size. Once a focal picture is plotted, the exact position for best focus is known as well as the width of the focus.

A second method for checking the focus consists of setting up a very narrow slit (0.025 mm.) at R with the tube behind it and plotting the diffracted intensity as a function of the angle $\theta$ for various zones of the crystal (defined by appropriate stops). The centers of these curves determine the $\mathcal{S}$ points for the various zones and when plotted as described above form a focal picture similar to Fig. 10. This method is preferable once the instrument is set up for real sources. A tolerance value for the width of focal aberration was set at 0.1 mm. for a two-meter radius of curvature. This is chiefly determined by the focal volume necessary for radioactive material. Since the positions of lines can be located to about 1/10 of their width, this permits measurements to 0.01 mm. or 0.01 X. U. Actually the focal width could be made about 0.05 mm.

Since the curvature aberration gives rise to a constant width of line, the resolving power must diminish for shorter wave-lengths. It will be instructive to compare aberrations due to other causes to show the precision necessary in alignment.

(a) Aberration due to finite aperture

$$\frac{\Delta\lambda}{\lambda} \simeq \frac{\alpha^2}{2}$$

Aperture half-width = 22 mm.

Focal distance = 2000 mm.

$$\frac{\Delta\lambda}{\lambda} = 6 \times 10^{-5}$$

(b) Aberration due to crystal thickness assuming constant lattice spacing through the crystal

$$t = 1 \text{ mm.}$$

$$\frac{\Delta\lambda}{\lambda} \cong \frac{t}{R}$$

$$\frac{\Delta\lambda}{\lambda} \cong 5 \times 10^{-4}$$

(c) Failure of crystal to lie tangent to the focal circle

$$\frac{\Delta\lambda}{\lambda} \cong \alpha\phi$$

$\phi$ is the angle of rotation of the crystal relative to the focal circle and can be made less than $5 \times 10^{-4}$.

$$\frac{\Delta\lambda}{\lambda} \cong 5 \times 10^{-6}$$

(d) Failure to set at true focal point

This leads to a constant aberration for small angles.

$$\Delta\lambda \cong 2\alpha\varepsilon$$ where if $\varepsilon$ is in mm., $\Delta\lambda$ will be in X. U.

$$\varepsilon \cong 3 \text{ mm.}$$

$$\text{So } \Delta\lambda \cong 6 \times 10^{-2} \text{ X. U.}$$

From these figures it is evident that a simple focus test will give the position of best image over all angles as long as the angle is small, and the aberration due to non-uniform curvature is predominant.

Detection System

The detection of the diffracted radiation is a major problem since high resolution implies low intensity and thus, means that one must have high detection efficiency. The possible detectors of radiation for this purpose are photographic plate, ion chamber, Geiger counters,

scintillation counters, or crystal counters. Only the last three are feasible, and of these only the Geiger counters have been developed to the stage where they could be made to work with certainty although now the scintillation counter offers considerable promise.

The sensitivity of Geiger counters to gamma radiation has been discussed by several authors.[12,13] In principle only those quanta which produce secondary electrons which may reach the active volume (assumed to be the whole volume of the ordinary cylindrical counter) can be counted. Assume for the moment that the counter wall is a flat sheet of material. The three modes of production of secondary electrons are (1) photo-effect, (2) Compton effect and (3) pair-production. The range of photo electrons is

$$R_\tau = R(h\nu - E_K) \tag{1.9}$$

where one takes the range for electrons of energy $h\nu - E_K$ in the material. For Compton electrons one may take as the average range

$$\overline{R_\sigma} = 0.6\, R_{max} = 0.6\, R\left( \frac{2\frac{h\nu}{mc^2}}{1 + 2\frac{h\nu}{mc^2}}\, h\nu \right) \tag{1.10}$$

and for pair electrons

$$\overline{R_\chi} = R\left(\frac{h\nu - 2mc^2}{2}\right) \tag{1.11}$$

Taking as $\tau$, $\sigma$, and $\chi$ the linear absorption coefficients for photo, Compton, and pair effects respectively the intrinsic sensitivity* of a counter is

$$\varepsilon = 2C\,(\tau R_\tau + \sigma \overline{R_\sigma} + 2\chi \overline{R_\chi}) \tag{1.12}$$

One may calculate by means of curves such as Bleuler and Zunti[14]

*By intrinsic sensitivity is meant the fraction of all photons passing through the counter which register counts.

have published for the penetration of electrons through matter the value of the constant C with given geometry. However, equation (1.12) gives the energy and material dependence of $\varepsilon$, and once the curve of $\varepsilon$ vs. E and Z is normalized, counters may be designed with known sensitivity. Fig. 11 is one such curve.[13] It should be noted that all sensitivities given are for cylindrical counters of optimum wall thickness, i. e. the thickness just equal to the range of the most energetic secondary electrons.* Fig. 12 is a range energy curve for electrons in aluminum. With these curves it is possible to estimate counter efficiencies and to design a counter of optimum efficiency for each energy.

For the energy range of interest, i. e. 25 Kev. to 1.7 Mev., only the photo and Compton processes are of importance. Since $\tau$ varies as $Z^5$, it is advantageous to use plates of high Z. However, at very low quantum energies, i. e. near the K edge of the absorbing material, the photo electrons will have little energy so the efficiency falls off rapidly with decreasing energy. In this case a Xenon filled counter with a thin window may be used.

Description of the Counter

Two counters were built for this instrument, the one to operate in the x-ray range and up to about 0.5 Mev. and the other to operate from 0.5 Mev. to 1.7 Mev. The wall materials were chosen as a compromise between high Z and ease of construction.

---

*The electrons liberated inside the body of the wall have preferred directions depending on the process, but they suffer so many collisions before losing much energy that one may assume they have spherical distribution and diffuse as would a gas out of the wall. This is true only for low energies (less than 2 Mev.).

The x-ray counter G is shown in Fig. 8 in a cut-away view and in Fig. 13. Since the beam emerging from the collimator is approximately two inches square in cross section, the counter was designed with a three-inch diameter sensitive section. To gain sensitivity several identical sections were stacked along the axis so that the beam passed through all sections. The problem became one of obtaining a wide plateau and uniformity of threshold for each section so the over-all counter would exhibit a flat plateau. The case is made entirely of steel, copper plated and silver soldered together in a hydrogen furnace. The inside diameter is $3\frac{1}{4}$ inches; the length, 8 inches. The one end carries a Stupakoff glass insulator bushing for the central wire and a pumping lead. The opposite end carries a grill which is cut out to match the slots of the collimator to support the thin foil window. A soft aluminum gasket in a vee groove serves as the vacuum seal. The clamping ring is a grill identical to the inside one so that the unit could be pressure tested. This case could be opened and resealed in a very short time which enabled one to change the number of units or plate materials.

The counter sections themselves consist of circular disks or screens three inches in diameter spaced 5/8 inches apart by rings which just slip in the cylindrical case. For the x-ray counter 100 mesh 0.005 inch monel wire screens plated with silver to a depth equal to the range of 70 Kev. electrons (about 0.001 inch) were used. These screens were punched with a 5/8 inch hole at the center. The wire consisted of four radial 0.010 inch tungsten wires silver soldered to a monel tube 0.050 inch outside diameter so as to form a four pronged spider. The

end of each wire was beaded with glass to protect the end from point discharge. Each spider was etched by A. C. electrolysis in NaOH solution to clean the wires of all scale and sharp points. A 0.040 inch drill rod was soldered in the Stupakoff bushing and extended down the axis of the counter. As each disk was set in the counter, a spider was slid on the central mounting wire and centered between each pair of disks. In this manner a maximum of four complete sections was built up. The free end of the central rod was supported in a glass bushing to keep the spiders centered in their cells.

The second counter for gamma rays was somewhat different in construction, but the internal geometry differed only in that the disks were a 50% Bi, 40% Pb, and 10% Sn alloy for high atomic number and were 0.015 inches thick, this being the range of 1 Mev. electrons in the material. These plates were given a light silver plating to cut out alpha contamination from the lead. No other special cleaning or washing was done except that the parts were freshly plated and never touched during assembly.

A mixture of 3% petroleum ether and argon gave the best results as a filling gas. The total pressure was about 20 cm. of Hg which gave a threshold at 1000 V. The counting range for any one section was of the order of 300 volts wide, but the counters of 4 sections showed flat plateaus of from 100 to 200 volts. The counter was set up at about one meter from a radium needle with adequate shielding on all sides except for the window. With a beam of radiation of cross section 1 $cm.^2$ passing through the counter, the counting rate over the face of the counter remained constant to the geometric edge except

for the region in the vicinity of the central wire. The relative counting rate through each slot of the grill was determined by placing the radium needle in successive slots of the collimator; the data are shown in Fig. 14. No source of monoenergetic gamma radiation was available for the range of energies for which the counters were designed. However, an efficiency calculated from an extrapolated absorption curve for a radium source yielded an efficiency of 8% for 1 Mev. radiation. These counters were sufficiently stable and reliable that no trouble was experienced once the counter was sealed off. If very high efficiencies are desired, it appears that a scintillation counter possessing a higher intrinsic efficiency per unit volume of counter would be better than a Geiger counter of many sections because of the impossibility of completely shielding the counter.

Because of low counting rates every precaution to reduce the counter background was used. The main detection counter was fitted into the lead shielding H (Fig. 8) so that the grill in the window end of the counter matched the slots of the collimator. The lead shielding was cut away around the top of the main counter to make space for six conventional anticoincidence counters D. Hence the detector was shielded by three inches of lead on the top semicylinder and by four inches on the lower as well as on the back end. The lead reduced the local background while the anticoincidence counters served to subtract almost all cosmic ray counts. With this arrangement the background counting rate was reduced to 33 counts per minute. Without the anticoincidence counters the rate was 62 counts per minute and without shielding about 150 counts per minute.

the counting rates are rather slow, no attempt is made to make fast counting circuits. The value of $R_{18}$ sets the dead time at about 500 $\mu$s. The output is fed directly to a scale of 16 scaler and register. This circuit insures that all true coincidences will be canceled out. This is necessary whenever very weak sources are to be used.

Source Holder

The instrument is used for the most part with real sources. On the source carriage N is mounted a turntable on which the actual source holder can be set. The turntable permits centering the source so that its axis is vertical and hence parallel to the crystal focal axis. The table axis coincides with the point R (Fig. 7). Hence the radius arm connecting R and O insures that the source remains on the focal circle. The table may be clamped so that it does not rotate with respect to the source beam S, or else it may be clamped so that it rotates about O with the radius arm. The latter arrangement is used only when the photographic cassette U is mounted on the table. A lead bomb sits on the table. Within it the source holder K is placed with an adjustment for proper alignment with respect to the crystal. The lead shield and cap complete the source bomb so that except in the direction of the crystal there are three inches of lead on all sides of the source. The lead tunnel leading from the source to the crystal helps to keep scattered radiation out of the counters as well as out of the room. A similar tunnel is used in the case of x-ray photographic spectra with the cassette U to keep the background blackening on the film low.

## Part II

## Theoretical Results of Diffraction Theory as Applied to Crystals

### The Elementary Interaction of Radiation with an Atomic System

The treatment of the problem of scattering of radiation by an atomic system in the non-relativistic theory has been given by several authors.(16,17)* Their results indicate that the relations for the scattering of an electromagnetic wave by an atomic system are of the same form whether calculated by a rigorous quantum mechanical method or by a classical method.

The classical method for calculation of the scattering by an electron assumes that when a plane electromagnetic wave falls on an elastically bound electron, the harmonic oscillation of the electron results in an oscillating dipole moment of magnitude

$$\vec{P}_e = - \frac{e^2}{m\omega_o^2} \vec{E}_o \qquad (2.1)$$

where $\vec{E} = \vec{E}_o e^{i\omega_o t}$ is the field the electron experiences because of the incident wave. From the classical electromagnetic theory the intensity of radiation from a dipole at a large distance is given by

$$I_e = \frac{c}{8\pi} \left(\frac{\omega_o^2}{c^2 R} P_e \sin \phi\right)^2$$

$$= I_o \left(\frac{e^2 \sin \phi}{mc^2 R}\right)^2 \qquad (2.2)$$

The quantity $I_o$ is the incident intensity, and $\phi$ is the angle between the incident polarization direction and the direction of observation. Reference to Fig. 16 will show that if the polarization is in the plane

---

*In this part the treatment given by Zachariasen(18) in Theory of X-Ray Diffraction in Crystals is followed in order to have for easy reference the results of the theory.

of the propagation vectors $\sin \phi = \cos 2\theta$. If normal to the plane, then $\sin \phi = 1$. If the incident radiation is unpolarized $\overline{\sin^2 \phi} = \frac{1 + \cos^2 2\theta}{2}$, and the average scattered intensity is given by

$$I_e = I_o \left(\frac{e^2}{mc^2 R}\right)^2 \left(\frac{1 + \cos^2 2\theta}{2}\right) \tag{2.3}$$

Set $\frac{e^2}{mc^2} = r_o$

Then $$I_e = I_o \left(\frac{r_o}{R}\right)^2 \left(\frac{1 + \cos^2 2\theta}{2}\right)$$

For some purposes it will be convenient to represent the intensity scattered at the angle $\theta$ in terms of a cross section for scattering. If the incident intensity is $I_o$, the number of incident photons per second per cm.$^2$ is $\frac{I_o}{h\nu}$; likewise, $\frac{I}{h\nu_s}$ is the number scattered into an area of one cm.$^2$ at an angle $\theta$ with incident direction at a distance R from the origin. Now $\frac{IR^2}{h\nu_s}$ is the number scattered into a solid angle $d\Omega$ per second at the angle $\theta$. Then

$$\frac{d\sigma}{d\Omega} = \frac{IR^2}{I_o} \left(\frac{\nu}{\nu_s}\right) = \left(\frac{\nu}{\nu_s}\right) r_o^2 \left(\frac{1 + \cos^2 2\theta}{2}\right)$$

is the cross section per unit solid angle for scattering at the angle $\theta$. Since there is no change of frequency, $\nu = \nu_s$ so

$$\frac{d\sigma}{d\Omega} = r_o^2 \left(\frac{1 + \cos^2 2\theta}{2}\right) \tag{2.4}$$

The calculation of the scattering by an atom proceeds in the same manner except that in this case the different electrons are spread over the region of space occupied by the atom and at the same time are in motion relative to the center of mass. The scattered waves from each electron with their appropriate phase factors resulting from the different positions of the electrons in the atom must be added together

and an instantaneous intensity calculated. This intensity must then be averaged over time and expressed in terms of the spatial electron distribution functions for the various classes of electrons in the atom. Let $\sigma_i$ be the probability distribution function for the ith class of electrons such that $\sigma_i d\tau$ is the probability of finding the ith electron in the volume $d\tau$ on the average. Thus if $E_e$ is the amplitude scattered by a single electron, the mean scattered amplitude from all classes of electrons is

$$E_e \sum_i \phi_i \tag{2.5}$$

where

$$\phi_i = \int \sigma_i e^{i\vec{s}\cdot\vec{r}} d\tau$$

The exponential factor is a phase term in which $\vec{s}$ is the phase vector (Fig. 16). Let $\vec{k_o}$ and $\vec{k}$ be incident and scattered wave vectors*; then the vector equation holds

$$\vec{s} = \vec{k} - \vec{k_o}$$

$\vec{r}$ is the position of the volume element $d\tau$. The total scattering will be

$$I_{tot} = I_e \iint \sum_j \sum_k \sigma_j \sigma_k e^{i\vec{s}\cdot(\vec{r_j}-\vec{r_k})} d\tau_j d\tau_k$$

$$I_{tot} = I_e (Z + \sum_{j \neq k} \phi_j \phi_k^*) \tag{2.6}$$

Notice that both terms $I_e$ and the bracket are functions of the angle of scattering. The coherent scattering will be given by

$$I_c = I_e \left| \sum_i \phi_i \right|^2 \tag{2.7}$$

The meaning of the term coherent needs a word of explanation. From the form of the expression for $I_c$ it is evident that it is the square of the mean amplitude and would be calculated on the assumption

---

*The vector $k_o$ has the direction of the incident wave and a magnitude $|k_o| = \frac{1}{\lambda}$ $\lambda = \frac{\lambda}{2\pi}$

that all electrons would scatter without change of frequency so there is a definite phase relation between the scattered amplitudes. Only then could the amplitudes be additive. Since the charge distribution for atoms is known at least approximately, one can calculate $\sum_i \phi_i$ by the relation

$$f = \sum \phi_i = \int \rho \, e^{i\vec{s}\cdot\vec{r}} d\tau \qquad (2.8)$$

$\rho$ is the electron density distribution function, and for cases of spherical symmetry f becomes

$$f = \int_0^\infty \rho(r) \frac{\sin sr}{sr} \, dr \qquad (2.9)$$

f is known as the atomic structure factor, tables of which are given as a function of $\frac{\sin \theta}{\lambda}$. It is numerically the effective number of electrons which would scatter in phase. Anomalous dispersion does not contribute to f for the energies which will be interesting and hence can be ignored entirely. It will change the scattering only in the region where the quantum energy is close to the K, L, or M ionization energies. For the usual crystals of low atomic numbers these energies are less than 10 Kev. and far below the lowest quantum energies of interest.

The expression (2.7) for $I_c$ has been checked by experiment for the x-ray region of from 1 to 5 Å and found to be correct. It is necessary, however, to investigate more carefully the results to be expected if the quantum energy is increased to a value of the order of $mc^2$. Sommerfeld[17] has reproduced Wentzel's treatment of scattering of x-rays by an atomic system using the perturbation theory of non-relativistic quantum mechanics. The problem is to calculate the radiation scattered by the electrons bound to the atomic system. Physically the

following phenomenon takes place: The photon may interact with some electron of the atomic system, but if none of the binding energies are near the quantum energy, there will be very little photo effect. Hence, either the electron recoils under the momentum of the photon and Compton scattering occurs, or else the electron is so tightly bound to the nucleus that it cannot recoil and hence the nucleus takes up the momentum while the photon is scattered with unchanged frequency. In the first case the displaced line shows the momentum distribution of the initial electron state as well as the recoil momentum imparted by the radiation. In the second the scattered radiation, having a definite phase relationship with the incident radiation and the same frequency, is coherent with it. In terms of the quantum theory all possible compound states are formed in which the photon is absorbed by the atom (assuming the atom is initially in its lowest state). Those which return the atom to its initial state with the emission of a photon represent coherent scattering because of a definite phase relationship between incident and scattered probability amplitudes. Those final states for which the atom is ionized, i. e. the electron is ejected, represent Compton scattering while those which leave the atom complete but in a different state represent "Smekal" jumps. The probabilities for the three types of scattering can be represented as cross sections in the same manner that the scattering by a single electron is given by the Thomson cross section.

Sommerfeld derives the general dispersion formula by the usual approximation of the radiation field as a perturbation on the atom. Using this formula he proceeds to calculate the dipole moment corre-

sponding to the Compton scattered radiation; the coherent or unshifted radiation is one term in the general expression. The assumptions used are as follows:

(a) The electron binding energies are much less than the photon energy, i. e. $|E_k| << h\nu$.

(b) The recoil energy is small compared with the photon energy, i. e. $|E_\ell| << h\nu$. This will certainly be the case for coherent scattering where $|E_k| = |E_\ell|$.

(c) Non-relativistic wave functions are used throughout. For atoms of low atomic number this is certainly a valid procedure.

Under these assumptions the moment becomes

$$\vec{P_k} = - \frac{e^2}{m\omega_o^2} \vec{E_o} \int \psi_k^* \psi_k e^{i\vec{s}\cdot\vec{r}} d\tau \qquad (2.10)$$

where it is assumed that the final state of the electron is identical to its initial state so that there is no change of quantum energy. Since $\sigma_k = \psi_k^* \psi_k$ is the probability distribution function for the kth electron, one may write for the integral

$$f_k = \int \psi_k^* \psi_k e^{i\vec{s}\cdot\vec{r}} d\tau$$

With these approximations, which appear valid, the result of the non-relativistic calculation for the atomic structure factor turns out to be identical with the calculation on a classical basis. Franz[19,20,21] using the relativistic equations of Dirac has calculated the coherent component of scattering with a result which is identical with that already obtained for atoms of low Z such as one has in quartz.

The scattering by an atom is given by a relation analogous to equation (2.3)

$$I = I_o \left(\frac{r_o}{R}\right)^2 \left(\frac{1 + \cos^2 2\theta}{2}\right) f^2$$

where I is the average scattered intensity, $I_o$ the incident intensity of unpolarized radiation, and f the atomic structure factor. The differential cross section for scattering is given by:

$$\frac{d\sigma_{atom}}{d\Omega} = r_o^2\left(\frac{1+\cos^2 2\theta}{2}\right)f^2 \qquad (2.11)$$

If one uses the Fermi-Thomas atom model for the distribution function, it is possible to evaluate f as a function of $\frac{\sin\theta}{\lambda}$. (22a) Because $\frac{\sin\theta}{\lambda}$ is proportional to the momentum given to the electrons, f/Z should for constant $\frac{\sin\theta}{\lambda}$ increase with Z since more electrons are bound tightly enough to transfer the photon momentum to the nucleus. The differential cross section $\frac{d\sigma_{atom}}{d\Omega}$ for coherent scattering decreases with $\lambda$ because $f(\frac{\sin\theta}{\lambda})$ diminishes rapidly with increasing argument. However, if the scattering is observed at the angle $\theta$ such that $\frac{\sin\theta}{\lambda}$ is constant as is the case for crystal diffraction from planes of fixed spacing with fixed order number, then the scattering observed at the angle $\theta$ will remain constant or increase slightly because of the $\cos^2 2\theta$ factor.

Interaction of Radiation with a Perfect Crystalline Medium

The theory of the interaction of radiation with a crystalline medium has been completely developed on the basis of the electromagnetic theory by Darwin(23), Ewald(24), Prins(25) and Kohler(26). The results presented in the remainder of this part are taken from Zachariasen.(18)

For a discussion of the results of the dynamical theory of reflection in crystals one needs the structure factor for a single cell of the crystal. Consider a single unit cell of the crystal lattice with the reference vectors $\vec{a}_i$ (i = 1,2,3) defining the cell. The positions

of the atoms in the cell are given by

$$\vec{r}_k = \sum_{i=1}^{3} x_{ki}\vec{a}_i$$
$$0 \leq x_{ki} \leq 1$$

The scattering cross section of each of the individual atoms is given by $r_o^2(\frac{1+\cos^2 2\theta}{2})f_k^2$. The cross section for scattering by the cell is computed in the same manner as for a single atom except that instead of the integration over the atom, one integrates over the cell. Hence

$$\sigma_{cell} = r_o^2(\frac{1+\cos^2 2\theta}{2})(\sum_k f_k e^{i\vec{s}\cdot\vec{r}_k})^2 \qquad (2.12)$$
$$F = \sum_k f_k e^{i\vec{s}\cdot\vec{r}_k}$$

The electron distribution in the crystal may also be considered as a triply periodic continuous function in space and hence may be expanded as a Fourier series. Let $\Omega(\vec{r})$ be the electron distribution function for the cell which may be expanded by the relations

$$\Omega(\vec{r}) = \sum_H \Omega_H e^{-i2\pi\vec{B}_H\cdot\vec{r}} \qquad (2.13)$$
$$\Omega_H = V^{-1}\int \Omega e^{i2\pi\vec{B}_H\cdot\vec{r}} d\tau$$

The expression for the structure factor in terms of $\Omega$ is given as

$$F_H = \int \Omega e^{i2\pi\vec{B}_H\cdot\vec{r}} d\tau \quad \text{or} \quad \Omega_H = \frac{F_H}{V} \qquad (2.14)$$

$\vec{B}_H$* is the lattice vector in the reciprocal lattice. H represents the triple of Miller indices for the expansion term and

$$\Omega_{ooo} = \frac{Z}{V}$$

Z is the total number of electrons in the unit cell and V the volume of the cell.

---

*$\vec{B}$ is related to the vectors $a_i$ as follows:

$$\vec{B} = H_1\vec{b}_1 + H_2\vec{b}_2 + H_3\vec{b}_3$$

where $(\vec{b}_i\cdot\vec{a}_j) = \delta_{ij}$. The volume of the reciprocal cell is just 1/V and $|B_H| = 1/d_H$. $d_H$ is the lattice spacing for the H planes.

The direction of propagation in such a medium is related to the wave-length of the radiation and the wave-length of the periodicity of structure, i. e. the place spacing, by the Bragg law

$$n\lambda = 2d \sin \theta_B \tag{2.15}$$

and by the condition that the angle of incidence with the crystal planes equals the angle of diffraction. This law may be expressed more concisely in terms of the reciprocal lattice vectors $\vec{B}$ by the vector equation

$$\vec{k_H} - \vec{k_o} = 2\pi\vec{B_H} \tag{2.16}$$

$$|B_H| = \frac{1}{d_H}$$

Fig. 17 is the representation of equation (2.16) in the reciprocal lattice. The lattice points which lie on the sphere correspond to the allowed directions of propagation in the crystal. It may be necessary to vary the length of $k_o$, i. e. change the wave-length to satisfy the vector relation, or rotate the sphere about the point 0. Changing $k_o$ corresponds to taking a Laue photograph while rotation of a fixed $k_o$ about 0 corresponds to the Bragg method. This simple law gives the allowed directions of propagation but says nothing about the intensity or how it varies when this condition is not satisfied.

The calculation of the expressions for intensity as a function of the angle of diffraction is rather involved. The Maxwell equations for the electromagnetic wave incident on the crystalline medium are set up with appropriate boundary conditions. The index of refraction of the medium is expressed in terms of the electronic density and frequency, and the Bragg law is introduced to limit the consideration to only those directions for which propagation is allowed. This set of

equations with boundary conditions, when solved, will give the intensity which will be transmitted as a function of angle and wave-length.

The results which one needs to understand are the factors influencing the width of the diffraction pattern and reflection as a function of angle both for "thin" and "thick" crystals. Whether a crystal is "thin" or "thick" will depend on the "extinction distance" due to diffraction of the energy by the successive crystal planes from the incident beam into the reflected beam. If the intensity of the incident radiation is not appreciably attenuated by such primary extinction in passing through the crystal, it will be considered "thin"; if there is complete extinction, it will be considered "thick". Many crystals have discontinuities or distortions in the lattice so that they are only locally periodic. The nature of diffraction by these crystals is not very well known partially because the nature of the lattice disturbances is not known. Some ideas about the mosaic structure may result from a study of the reflection coefficients since the energy dependence of the reflection coefficient will give an idea of the size of the domains of periodicity.

Consider a plane electromagnetic wave incident on the boundary of a crystal. Due to the small polarization, the dielectric constant $\varepsilon$ will be different from unity.

$$\varepsilon \cong 1 + 4\pi\alpha \tag{2.17}$$

where $\alpha$ is the polarizability per unit volume.

Set $$\psi = 4\pi\alpha = \sum \psi_H e^{-i2\pi \vec{B}_H \cdot \vec{r}}$$

The polarizability of a single elastically bound electron as calculated by its coherent scattering is given by

$$\alpha = -\frac{e^2\lambda^2}{4\pi^2 mc^2} = -\frac{r_o\lambda^2}{4\pi^2}$$

and for a volume distribution of electrons by

$$\alpha = -\frac{r_o\lambda^2}{4\pi^2}\Omega \tag{2.18}$$

The Fourier expansion coefficients are

$$\psi_H = -\frac{r_o}{\pi}\lambda^2\frac{1}{V}\int\Omega e^{i2\pi\vec{B}_H\cdot\vec{r}}d\tau \tag{2.19}$$

But $$F_H = \int\Omega e^{i2\pi\vec{B}_H\cdot\vec{r}}d\tau$$

so $$\psi_H = -\frac{r_o}{\pi}\left(\frac{F_H}{V}\right)\lambda^2 \tag{2.20}$$

Now the index of the medium is

$$n = 1 + \tfrac{1}{2}\psi$$

and if n is complex, there will be an attenuation or absorption due to the imaginary part of n; hence n is assumed to be complex to take care of the absorption in the crystal by photo or Compton processes.

Then $$\psi = \psi' + i\psi'' \tag{2.21}$$

The total absorption coefficient is related to $\psi''$ by the expression

$$\mu = -\frac{2\pi\psi''}{\lambda} \tag{2.22}$$

However, it is assumed for this work that the crystals have very little absorption, so $\mu \cong 0$.

The calculation of the intensity transmitted for any incident wave vector and for definite boundary conditions yields a result which depends on the function $\psi$ and the boundary conditions. Inside the crystal only in the neighborhood of those directions for which the Bragg relations hold can there exist waves which are propagated with appreciable intensity. One of these directions is the direction corresponding to the incident beam and the other, that for the diffracted beam. For

the case of Laue reflection (Fig. 18) when the reflecting planes are not parallel to the incident face, the wave field consists of the incident beam only, on the side of incidence. As the beam passes through the crystal, the Ewald theory predicts that the energy is periodically exchanged between the two allowed directions of propagation; the one beam has its maximum of intensity when the other is at its minimum. For Bragg reflection (the case in which the reflecting planes are parallel to the entry surface) the energy is shifted to the diffracted beam and then escapes before it can suffer a multiple reflection. The parameter which describes the nature of the diffraction pattern best is the extinction distance measured by the number of atomic planes traversed. It is the number of planes, which are effective for reflection, crossed before the incident wave is extinguished by the transfer of its intensity to the reflected wave and is a function only of the effective electronic density in those planes.

The analytic results of the diffraction theory are given below. Two cases are possible as shown in Fig. 18. The Laue case for zero absorption is the one of interest for transmission spectrographs. The theory as outlined leads to the following results for the Laue case.[18] For the case of plane waves the energy flux per second is $P_o$ and $P_H$ for incident and reflected beams respectively, i. e.

$$P_H = S_H I_H \qquad S_H = \text{area of diffracted beam}$$

$$P_o = S_o I_o \qquad S_o = \text{area of incident beam}$$

so

$$\frac{P_H}{P_o} = \frac{1}{|b|}\,\frac{I_H}{I_o}$$

$$\frac{P_H}{P_o} = \frac{\sin^2\left[A\sqrt{1+y^2}\right]}{1+y^2} \qquad (2.23)$$

where
$$y = \frac{\frac{1-b}{2}\psi_o + \frac{b}{2}\alpha}{|b|^{\frac{1}{2}} K |\psi_H|} \tag{2.24}$$

$$A = \frac{k_o}{2} K|\psi_H| \frac{t_o}{(\gamma_o \gamma_H)^{\frac{1}{2}}} \tag{2.25}$$

In these expressions

$$b = \frac{\gamma_o}{\gamma_H}$$

where $\gamma_o$ is the cosine of the angle of incidence and $\gamma_H$ is the cosine of the angle of diffraction for the beam reflected from the planes (H).

$$\alpha \cong 2(\theta_B - \theta) \sin 2\theta_B \tag{2.26}$$

The angle $\theta_B$ is the Bragg angle of incidence with the crystal planes. The approximations made in b and $\alpha$ are that one assumes the propagation vectors in the crystal have the same direction as those outside. $K = 1$ for the case of polarization normal to the plane of the incident and reflected wave vectors, and $K = \cos 2\theta$ for polarization in this plane. $t_o$ is the thickness of the crystal slab.

To see the physical meaning of the relations, set $b = 1$ (a good approximation for the case of crystal planes very nearly normal to the surface).

$$\gamma_o = \gamma_H = \cos \theta_B$$

Whence
$$A = \frac{k_o K|\psi_H| t_o}{2 \cos \theta_B}$$

But
$$|\psi_H| = \frac{r_o}{\pi} \left(\frac{F_H}{V}\right) \lambda^2 \tag{2.20}$$

so
$$A = r_o \lambda \left(\frac{F_H}{V}\right) \frac{K t_o}{\cos \theta_B} \tag{2.27}$$

But also by the Bragg relation $\lambda = \frac{2d_H}{n} \sin \theta_B$

$$A = 2r_o \left(\frac{F_H}{V}\right) \frac{Kd_H \tan \theta_B t_o}{n} \tag{2.28}$$

Hence the thickness of the crystal slab is given by equation (2.28) in terms of the extinction depth $t_x$

$$t_x = \frac{n}{2r_o \left(\frac{F_H}{V}\right) Kd_H \tan \theta_B} \tag{2.29}$$

Expressed in terms of the number of planes which are effective for extinction $N_H$

$$\frac{t_x \tan \theta_B}{d_H} = N_H$$

$$N_H = \frac{n}{2r_o K \left(\frac{F_H}{V}\right) d_H^2} \tag{2.30}$$

$$y = \frac{(\theta_B - \theta) \sin 2\theta_B}{|\psi_H| K} = \frac{\pi (\theta_B - \theta) \sin 2\theta_B}{r_o \lambda^2 \left(\frac{F_H}{V}\right) K}$$

Using the Bragg relation

$$y = \frac{\pi n \cos \theta_B (\theta_B - \theta)}{r_o d_H \left(\frac{F_H}{V}\right) K \lambda} \tag{2.31}$$

The deviation from the Bragg angle is measured in units of

$$w' = \frac{r_o d_H K \left(\frac{F_H}{V}\right) \lambda}{\pi n \cos \theta_B} = \frac{2r_o d_H^2 K \left(\frac{F_H}{V}\right) \tan \theta_B}{\pi n}$$

or in terms of the number of planes

$$w' = \frac{\tan \theta_B}{\pi N_H} \tag{2.32}$$

This result is more understandable if one remembers that $\frac{d\lambda}{\lambda} = \frac{d\theta}{\tan \theta_B}$ for Bragg reflection so

$$\frac{d\lambda}{\lambda} = \frac{n}{\pi N_H} \tag{2.33}$$

i. e. the resolving power is a function only of the number of planes

which are operative.

To calculate the exact diffraction pattern consider two cases:
Case A: $A >> 1$, i. e. $t >> t_x$ or the crystal is "thick". The $\sin^2\left[A\sqrt{1+y^2}\right]$ term of equation (2.23) will oscillate rapidly as a function of y. If A is large enough, the variations in thickness and finite resolution of experimental apparatus will average over this term so

$$\frac{P_H}{P_o} = \frac{1}{2(1+y^2)} \tag{2.34}$$

The half-width of the pattern will occur at $y = 1$ or

$$\theta_B - \theta = w_\theta = \frac{r_o d_H K(\frac{F_H}{V})\lambda}{\pi n \cos\theta_B} = \frac{\tan\theta_B}{\pi N_H} \tag{2.35}$$

For "thick" crystals the diffraction width is proportional to $\tan\theta_B$ or by the Bragg relation proportional to $\lambda$ for short wave-lengths. The parallel polarization component has a smaller half-width because its extinction distance is longer.

A quantity which will be needed frequently is the integrated reflection coefficient. This quantity is defined as

$$R_\theta = \int_{-\infty}^{\infty} \frac{P_H}{P_o}\, d\theta \tag{2.36}$$

$R_\theta$ represents thearea under the reflection power curve (Fig. 19). Experimentally if one allowed a beam of divergence, large compared with the width of the curve shown, to fall on a crystal, only those rays falling at angles within the curve would contribute to the transmitted energy. $R_\theta$ represents the ratio of total reflected power to incident power per unit solid angle. $R_\theta$ is therefore dimensionally an angle and represents the angle over which complete reflection may be assumed

to occur if a beam of divergence, wide compared to w, falls on the crystal.

$$R_\theta = \frac{\pi}{2} w_\theta$$

$$= \frac{\pi |\psi_H| K}{2 |b|^{1/2} \sin 2\theta_B} = \frac{r_o d_H (\frac{F_H}{V}) K \lambda}{2n \cos \theta_B} \qquad (2.37)$$

Notice that $R_\theta$ is a function of $\lambda$ to the first power only. This is due to the fact that if extinction is complete, the total energy reflected depends only on the width of the pattern.

Case B: $A \ll 1$, i. e. $t \ll t_x$ or the crystal is "thin". In this case the number of planes that are effective is given by $N_H = \frac{t_o \tan \theta_B}{d_H}$ and will decrease with $\lambda$. From equations (2.28) and (2.31)

$$Ay = \frac{\pi n t_o (\theta_B - \theta)}{d_H} \qquad (2.38)$$

From equation (2.38) it is seen that when A is small, y must become large for very small values of $\theta_B - \theta$, or $y^2 + 1 \cong y^2$ so

$$\frac{P_H}{P_o} = \frac{\sin^2 Ay}{y^2} \qquad (2.39)$$

This function may be replaced by a smoothing function with the same area and the same maximum value, because the fluctuations can never be observed.

$$\frac{P_H}{P_o} = A^2 e^{-\frac{A^2 y^2}{\pi}} \qquad (2.40)$$

The half-width is given by $\frac{(Ay)^2}{\pi} = \ln 2$ or

$$w_\theta = \sqrt{\frac{\ln 2}{\pi}} \frac{d_H}{t_o n} \qquad (2.41)$$

The angular width of the pattern will remain constant as a function of $\lambda$. Since there is little extinction, the whole depth of the crystal is uniformly irradiated. This being the case the number of planes

effective for diffraction is proportional to tan $\theta_B$ or to $\lambda$ for small angles, and hence the angular width of the pattern must remain constant.

The integrated reflecting power should decrease as $\lambda^2$ since $P_H/P_o$ is proportional to $\lambda^2$, and the width is constant.

$$R_\theta = \frac{\pi A |\psi_H| K}{|b|^{1/2} \sin 2\theta_B} \tag{2.42}$$

Since b = 1

$$R_\theta = \frac{r_o^2 (\frac{F_H}{V})^2 K^2 \lambda^2 d_H t_o}{n \cos^2 \theta_B} \tag{2.43}$$

Notice that the reflection coefficient is proportional to the thickness $t_o$ of the crystal, and the width of the pattern is inversely proportional to $t_o$. When the incident radiation is unpolarized, the value of $R_\theta$ is given by

$$R_\theta = \frac{Q t_o}{\gamma_o} \tag{2.44}$$

$$Q = r_o^2 \left(\frac{F_H}{V}\right)^2 \frac{\lambda^2 d_H (1 + \cos^2 2\theta_B)}{2n \cos \theta_B}$$

The cases intermediate between "thick" and "thin" crystals may be summarized by giving the value of R in terms of the variable y as a function of A. This curve is shown in Fig. 20. This summarizes the results of the dynamical theory for the purposes at hand. It is not necessary to consider the results for the cases when absorption is present, because of the high quantum energies which make absorption quite negligible. Only in the event that a high atomic number crystal were used would the results be changed substantially, and intuition will give qualitative ideas of the effects to be expected.

X-Ray Diffraction by Real Crystals

The exact nature of the imperfections in any real crystal is not

known. A great amount of work has been done on this topic by the analysis of the diffuse x-ray scattering. The problem at hand is to find how the value of the integrated reflection coefficient will vary with wave-length and what types of real crystals will be most suited for use in a curved crystal spectrometer.

Rather than consider the nature of mosaic structure in detail, assume that there exist limited domains of the crystal over which coherent scattering can occur, and furthermore, assume that these domains may be distributed in angular orientation. These may not necessarily have sharply defined boundaries such as the so-called "slip planes" of plastic solids. Inside these domains of coherence it is assumed that the crystal has an ideal periodic lattice. Then within these regions the results of the previous section on perfect crystals may be applied. These domains will be "thick" or "thin" as the extinction within them is complete or small. However, the domains may not be uniform in size or structure factor, so exact calculations of the reflection coefficient may not be possible. The important facts which one desires are (a) the integrated reflection coefficient as a function of $\lambda$ and total crystal plate thickness $T_o$ and (b) the diffraction pattern width or crystal resolution as a function of $\lambda$ and $T_o$.

For the purposes of analysis assume that the domains of coherence are distributed in angular orientation by a Gaussian distribution about the average orientation.

$$W(\Delta) = \frac{1}{\sqrt{2\pi}\eta} e^{-\frac{\Delta^2}{2\eta^2}} \qquad (2.45)$$

$\Delta$ is the angular deviation from the mean orientation of some set of planes (H) of interest. $W(\Delta)$ gives the probability of finding a domain

with orientation $\Delta$. Let $T_o$ be the thickness of the crystal plate, and assume that $\gamma_o = \gamma_H$. Also one must assume that the size of the domains of coherence is small enough that the distribution function above applies for a very thin slab of the crystal.* The intensity reflected by a layer dT of the crystal is $\sigma\, dT$. Let $t_o$ be the mean thickness of the domains, so there will be $\frac{dT}{t_o}$ layers of crystal blocks. The reflection coefficient of one layer will be

$$\int_{-\infty}^{\infty} W(\Delta)\, \frac{P_H}{P_o}\, (\theta - \theta_B + \Delta)\, d\Delta$$

For most cases $W(\Delta)$ is wide compared with the function $P_H/P_o$ in angular width, so

$$\int_{-\infty}^{\infty} W(\Delta)\, \frac{P_H}{P_o}\, (\theta - \theta_B + \Delta)\, d\Delta \cong W(\theta_B - \theta) R_\theta \tag{2.46}$$

The reflecting power of the layer dT is

$$\sigma\, dT = W(\theta_B - \theta)\, R_\theta\, \frac{dT}{t_o} \tag{2.47}$$

In passing through the layer there will be an attenuation of both incident and reflected beams by absorption and an exchange of energy as the result of reflection. Let $\mathcal{P}_o(T)$ and $\mathcal{P}_H(T)$ be the power in each beam. Then

$$\begin{aligned} d\mathcal{P}_o &= -\mu_o \mathcal{P}_o \frac{dT}{\gamma_o} - \sigma \mathcal{P}_o dT + \sigma \mathcal{P}_H dT \\ d\mathcal{P}_H &= -\mu_o \mathcal{P}_H \frac{dT}{|\gamma_H|} - \sigma \mathcal{P}_H dT + \sigma \mathcal{P}_o dT \end{aligned} \tag{2.48}$$

for the Laue case. If the boundary conditions are inserted for a flat slab of thickness $T_o$, the result becomes

$$\frac{\mathcal{P}_H(T_o)}{\mathcal{P}_o(0)} = \operatorname{sh} \sigma T_o\, e^{-\left(\frac{\mu_o}{\gamma_o} + \sigma\right) T_o} \tag{2.49}$$

---

*This method of calculation could not be applied if the size of the mosaic units were comparable with the plate thickness.

The explicit expression for $\sigma$ will depend on the exact nature of the mosaic structure; an approximate form is given by equation (2.47). The term $\mu_o + \gamma_o\sigma = \mu$ is known as the secondary extinction coefficient in contrast to the primary extinction which is implicitly taken into account in the function $P_H/P_o$ given by equation (2.23). If $\mu_o$, the true absorption coefficient, is small, $\gamma_o\sigma$ represents the total extinction. It may be large even though the primary extinction be small, because it depends on the size of domains and their angular orientation as well as $R_\theta$. Several different cases are possible, and it will be interesting to compare the integrated reflection coefficient

$$\mathcal{R}_\theta = \int \frac{\mathcal{P}_H(T_o)}{\mathcal{P}_o(0)}\, d\theta$$

in these cases and determine the wave-length dependence of both $\mathcal{R}_\theta$ and the crystal resolution.

Case A: Negligible Primary and Secondary Extinction

This case corresponds to coherence domains, small compared with the primary extinction distance, so that the power reflected by each domain is small and at the same time the power reflected by a layer of domains is very small. If these conditions hold,

$$\gamma_o\sigma = W(\theta_B - \theta)Q \qquad (2.50)$$

From equation (2.49)

$$\frac{\mathcal{P}_H(T_o)}{\mathcal{P}_o(0)} \quad \frac{e^{-\frac{\mu_o T_o}{\gamma_o}}}{2}\,(1 - e^{-2\sigma T_o})$$

The true absorption term will be of no interest. If $2\sigma T_o << 1$, then

$$\frac{\mathcal{P}_H(T_o)}{\mathcal{P}_o(0)} = \sigma T_o = \frac{W(\theta_B - \theta)QT_o}{\gamma_o} \qquad (2.51)$$

The width of the pattern is the width of W and hence independent of

wave-length. Performing the integration on equation (2.51), one obtains

$$\mathcal{R}_\theta = \frac{QT_o}{\gamma_o} \tag{2.52}$$

$\mathcal{R}_\theta$ is independent of the domain size but depends on $\lambda^2$ and in general will be much larger than $R_\theta$ for a perfect crystal of the same thickness.

Case B: Primary Extinction, Small Secondary Extinction

For this case the domains are large enough to give complete extinction; yet in any slab of thickness dT of the crystal the total power reflected from the incident beam is small. This simply means that the whole depth of the crystal is bathed in the incident radiation. As is Case A

$$\mathcal{R}_\theta = \frac{R_\theta T_o}{t_o} e^{-\frac{\mu_o T_o}{\gamma_o}}$$

but now it is necessary to introduce the proper value of $R_\theta$. Since for large primary extinction $A >> 1$ where A is calculated for the individual crystallites of the mosaic,

$$\frac{R_\theta}{w'} = \frac{\pi}{2}$$

and

$$\mathcal{R}_\theta = \frac{\pi}{2} w' \frac{T_o}{t_o} e^{-\frac{\mu_o T_o}{\gamma_o}} \tag{2.53}$$

The total reflection by each crystallite or domain is independent of its size once it is large enough to make $A >> 1$. Hence, if the size of the crystallites increases, i. e. $t_o$ becomes larger, it follows that there can be fewer of them in the slab of thickness $T_o$, so the total power which is reflected must decrease. Thus $\mathcal{R}_\theta$ should vary inversely as $t_o$, and the width of the pattern is given by $W(\theta - \theta_B)$ and is independent of $\lambda$.

It will be helpful to compare the values of $R_\theta$ for a perfect

"thick" and "thin" crystal and the values of $R_\theta$ for Cases A and B of real crystals.

Table I

| Type | | Integrated Reflection Coefficient | Half-Width of Diffraction Pattern at Half-Maximum |
|---|---|---|---|
| Perfect | Thick | $\frac{r_o d_H K (\frac{F_H}{V}) \lambda}{2n \cos \theta_B}$ | $\frac{r_o d_H (\frac{F_H}{V}) K \lambda}{\pi n \cos \theta_B}$ |
| | Thin | $\frac{r_o^2 (\frac{F_H}{V})^2 K^2 \lambda^2 d_H t_o}{n (\cos \theta_B)^2}$ | $\sqrt{\frac{\ln 2}{\pi}} \frac{d_H}{t_o n}$ |
| Mosaic | Case A | $\frac{r_o^2 (\frac{F_H}{V})^2 K^2 \lambda^2 d_H T_o}{n (\cos \theta_B)^2}$ | $\eta \sqrt{\ln 4}$ |
| | Case B | $\frac{r_o (\frac{F_H}{V}) K \lambda T_o}{2n \cos \theta_B t_o}$ | $\eta \sqrt{\ln 4}$ |

$T_o$ is the plate thickness; $t_o$ is the thickness of the domain of coherence. Any other cases can be analyzed in terms of the two cases that have been given or by an extension of these. These results will be applied to the analysis of experimental results and design of a spectrometer in Part IV.

The Effect of Lattice Disorders and Thermal Motion

The effects of lattice disorders and thermal motion can be present even in the so-called perfect crystal lattice. These disorders are best described as small variations in the structure of the individual unit cells. The variations may or may not be periodic in the medium. In such a crystal the unit cells are assumed to be reproduced, on the average, throughout the whole crystal so that there is partial coherence between all parts of the lattice; in the mosaic there was assumed to

be complete incoherence between the domains. The scattering is expressed as the sum of two factors; the first is the ordinary Laue (Bragg) diffraction which is subject to the Bragg conditions. The intensity is described by the relations given previously. The structure factor F is replaced by the mean structure factor which is calculated on the assumption that all atoms are frozen in their mean positions. The second term is a diffuse scattering which is not subject to the Bragg conditions and is incoherent.

Since the absolute reflectivities for various crystal planes are known at x-ray wave-lengths, the wave-length dependence of the diffuse and coherent scattering is of interest for calculation of reflection coefficients at short wave-lengths. The effect of thermal motion on coherent scattering is expressed by the relation for the effective structure factor F' in terms of F, the factor for a perfect crystal.

$$F' = Fe^{-M}$$

$$M = \frac{6h^2 \sin^2 \theta}{mk \lambda^2 \Theta} f\left(\frac{T}{\Theta}\right) \qquad (2.54)$$

The quantity $\Theta$ is the characteristic temperature of the crystal, and T the Kelvin temperature. It is noticed that M is a function of $\frac{\sin \theta_B}{\lambda}$ for any characteristic reflection and thus independent of $\lambda$. This effect of temperature has been observed for x-rays and in quartz at room temperatures was found to be very low; hence it should also be low at all wave-lengths.

The effects of substitution disorders are not well known except in some few cases. However, the incoherent scattering will be a function of the mean square deviation of the structure factor and thus of

$\frac{\sin\theta}{\lambda}$. In quartz there should be little or no incoherent scattering due to lattice disorder.

## Part III

## Calculation of Luminosity of the Spectrometer

### Factors Influencing the Luminosity

The luminosity of the transmission type curved crystal spectrometer must be estimated for two cases of geometry, Case A: Real source and virtual image and Case B: Virtual source and real image. The factors entering in the calculation of the intensity of the diffracted radiation are four:

1. Source geometry
2. Spectral distribution of radiation
3. Focal aberration
4. Crystal diffraction pattern.

Each factor will be characterized by a distribution function measured along the focal circle or as is more convenient, in terms of the wave-length screw of the instrument. The first two profiles define the spectral character of the source under analysis, while the last two define the character of the analyzing apparatus. Fig. 21 shows the nature of the profiles.

The dispersion relation for the instrument together with the fact that the screw has a linear calibration in terms of wave-length makes it convenient to refer to all angular widths, wave-lengths, and linear distances at the focal position directly in terms of screw divisions. The conversion factor in each case will be obvious.

### Source Geometry

The source is assumed to be limited by a rectangular aperture which

may be defined by slits or may usually be just the physical dimension of the radioactive material placed at the focus of the apparatus. For the moment assume the geometric aperture of the system is identical for all points on the vertical axis of the source.* Assume, also, that the activity per unit width is constant over the width of the source. For the usual radioactive source in the form of a rectangular slab which is seen on edge this will be the case. It is also tacitly assumed that the intensity of radiation emitted by the source is independent of the angle of observation, at least within the geometric cone determined by the crystal aperture. Otherwise the analysis would become very difficult and impossible to check. If t is the total source width and $N_s$ is the activity in quanta per second per unit solid angle when the source is seen on edge, then the source distribution function becomes

$$N(x) = N_s f_s(x) \qquad (3.1)$$

$$= 0 \; ; \quad x < -\frac{t}{2}$$

$$\text{where } f_s(x) = \frac{1}{t} \; ; \quad -\frac{t}{2} \leq x \leq \frac{t}{2}$$

$$= 0 \; ; \quad x > \frac{t}{2}$$

if the activity is uniform over the width t. If $f_s(x)$ is not constant over the width, then the function is normalized so that

$$\int_{-\infty}^{\infty} f_s(x)\,dx = 1 \qquad (3.2)$$

The function $f_s(x)$ represents the fractional source strength per unit width at the setting x.

---

*The problem of vertical divergence will not be discussed here. For x-rays it is negligible. For gamma radiation the exact crystal diffraction pattern will determine whether it will affect the intensity.

Spectral Distribution of Radiation

The spectral distribution curve for the radiation in any given line may be approximated with sufficient accuracy by a "witch". We wish to normalize the distribution over any one line to unity so if $f_i(\lambda)$ is the distribution function, $\gamma_i f_i(\lambda)$ is the number of quanta per unit wave-length where $\gamma_i$ is the probability that any quantum emitted by the source corresponds to the line i and

$$\sum_i \gamma_i \int_{-\infty}^{\infty} f_i(\lambda)d\lambda = 1 \qquad (3.3)$$

Since $\sum \gamma_i = 1$, this implies $\gamma_i \int_{-\infty}^{\infty} f_i(\lambda)d\lambda = \gamma_i$. Rather than express the distribution in terms of $\lambda$, we use the dispersion relation and write

$$\int_{-\infty}^{\infty} f_i(x)dx = 1$$

where x is the screw setting measured from the center of the line.

$$f_i(x) = \frac{\Delta_i}{2\pi(x^2 + (\frac{\Delta_i}{2})^2)} \qquad (3.4)$$

Here $\Delta_i$ is the full width at half-maximum in the proper units.

Focal Aberration

The focal aberration is most conveniently expressed as a distribution function $f_g(x)$ such that in the region of the $\beta$ point, $f_g(x)dx$ represents the fraction of the crystal aperture from which the crystal planes intersect in the width dx at x. This expresses the fact that there exists aberration in the geometric optics of the system in a quantitative manner. The function $f_g(x)$ is normalized to unity, i. e.

$$\int_{-\infty}^{\infty} f_g(x)dx = 1 \qquad (3.5)$$

the function $f_g(x)$ can be determined from the focal picture (Fig. 10)

together with an areal sensitivity curve such as Fig. 14.* To simplify the analysis a square form is assumed such that

$$\begin{aligned} &= 0 \; ; \qquad x < -\frac{w}{2} \\ f_g(x) &= \frac{1}{w} \; ; \quad -\frac{w}{2} \leqslant x \leqslant \frac{w}{2} \\ &= 0 \; ; \qquad x > \frac{w}{2} \end{aligned} \tag{3.6}$$

where w is the width as given by the focal picture.

Crystal Diffraction Pattern

The crystal "window" or diffraction pattern is extremely difficult to predict for any given crystal. Since the crystals are used in the Laue arrangement and since the crystal is assumed to be nearly perfect, one may use the theoretical form for the window curve or at least one which is symmetrical. In general

$$T(x) = T_o f_X(x) \tag{3.7}$$

where T is the fraction of a plane parallel beam of radiation that would be reflected by the crystal when the angle of incidence is that corresponding to the setting x. Notice that

$$\int_{-\infty}^{\infty} T(x)dx = R_\theta$$

is the integrated reflection coefficient. For a "thick" crystal used in transmission

$$f_X(x) = \frac{1}{\left(\frac{2x}{\delta}\right)^2 + 1} \tag{3.8}$$

---

*Fig. 14 gives only the variation of counter sensitivity due to geometry. It may happen that all regions of the crystal are not equally effective for diffraction. A preliminary check of this fact made with x-rays showed considerable differences over the different regions of the crystal. A careful experimental determination of $f_g(x)$ would be difficult and would not yield any very valuable information.

where $\delta$ is the full width of the crystal diffraction pattern at half-maximum in the proper units. In the case of mosaic crystals this function might be replaced by a Gaussian distribution function where $T_o$ is no longer a constant but a function of $\lambda$ as is $f_X(x)$.

One may write the intensity for any setting of the spectrometer in terms of these four functions. Let S be the geometric solid angle and counter efficiency factor, i. e. the fraction of all quanta emitted by the source which produce counts when the source is lined up with the crystal and collimator in the zero position. The number of counts in the direct beam will be

$$R_D = N_S S \tag{3.9}$$

S may be a function of $\lambda$ due to the change in counter efficiency with wave-length or energy.

Case A: Real Source and Virtual Image

For the diffracted beam one must calculate the effective source. To each point of $f_s(x)$ in Fig. 21 there corresponds the spectral distribution $f_i(x - \xi)$. The resultant source is given by the fold of the source and spectral distribution functions.

$$P_i(x) = N_S S r_i \int_{-\infty}^{\infty} f_i(\xi) f_s(x - \xi) d\xi \tag{3.10}$$

To evaluate this integral one may make use of the properties of Fourier transforms. If $G_i(\xi)$ is the Fourier transform of $\frac{P_i(x)}{N_S r_i}$ and similarly, $g_i(\xi)$, $g_s(\xi)$ for $f_i(x)$ and $f_s(x)$ respectively, then a theorem on folds* states

$$G_i(\xi) = \sqrt{2\pi}\, g_i(\xi) g_s(\xi) \tag{3.11}$$

*This is easily verified by calculating the Fourier transform of both sides of (3.10) and comparing. Note that

$$g(\xi) = \frac{1}{\sqrt{2\pi}} \int_{-\infty}^{\infty} f(x) e^{-i\xi x} dx$$

Calculating $g_i(\xi)$ and $g_s(\xi)$ one finds

$$g_i(\xi) = \frac{1}{\sqrt{2\pi}} e^{-\left|\frac{\xi \Delta_i}{2}\right|} \tag{3.12}$$

$$g_s(\xi) = \frac{1}{\sqrt{2\pi}} \frac{\sin \frac{t\xi}{2}}{\frac{t\xi}{2}} \tag{3.13}$$

So

$$G_i(\xi) = \frac{1}{\sqrt{2\pi}} \frac{\sin \frac{t\xi}{2}}{\frac{t\xi}{2}} e^{-\left|\frac{\xi \Delta_i}{2}\right|} \tag{3.14}$$

Hence

$$P_i(x) = \frac{N_s r_i S}{2\pi} \int_{-\infty}^{\infty} \frac{\sin \frac{t\xi}{2}}{\frac{t\xi}{2}} e^{-\left|\frac{\xi \Delta_i}{2}\right|} e^{i\xi x} dx \tag{3.15}$$

Evaluating the integral one obtains*

$$P_i(x) = \frac{N_s r_i S}{\pi t} \left[ \tan^{-1} \frac{t + 2x}{\Delta_i} + \tan^{-1} \frac{t - 2x}{\Delta_i} \right] \tag{3.16}$$

This is the spectral distribution which the spectrometer "sees". x is measured from the center of the line i as it appears on the wave-length scale.

The window curve or analyzing function may be calculated in a similar manner by taking the fold of the functions T(x) and $f_g(x)$. To every part of the crystal there is associated its own diffraction function T(x). The fold of this function into the profile representing the geometrical aberration of focus then represents the summation of the diffraction patterns over all infinitesimal elements of the crystal. The window curve is given by

$$W(x) = T_o \int_{-\infty}^{\infty} f_X(x - \xi) f_g(\xi) dx \tag{3.17}$$

The Fourier transforms are:

---

*See Appendix A.

$$g_X(\xi) = \sqrt{\frac{\pi}{2}}\,\frac{\delta}{2}\,e^{-\left|\frac{\xi\delta}{2}\right|}$$

$$g_g(\xi) = \frac{1}{\sqrt{2\pi}}\,\frac{\sin\frac{w\xi}{2}}{\frac{w\xi}{2}}$$

Hence

$$H(\xi) = \sqrt{\frac{\pi}{2}}\,\frac{\delta}{2}\,\frac{\sin\frac{w\xi}{2}}{\frac{w\xi}{2}}\,e^{-\left|\frac{\xi\delta}{2}\right|} \tag{3.18}$$

and
$$W(x) = \frac{\delta T_o}{2w}\left[\tan^{-1}\frac{w+2x}{\delta} + \tan^{-1}\frac{w-2x}{\delta}\right] \tag{3.19}$$

The actual process of analysis of a spectral line consists of sliding the analyzing window W(x) over the spectral distribution $P_i(x)$ and plotting the resultant intensity as a function of position. The intensity in counts per second at any given setting is given by the expression

$$R_A(x) = \int_{-\infty}^{\infty} W(x-\xi)P_i(\xi)\,d\xi \tag{3.20}$$

If $\mathcal{G}(\xi)$ is the transform of $R_D(x)$

$$\mathcal{G}(\xi) = N_s S\, r_i T_o \sqrt{2\pi}\,\frac{\delta}{wt}\,\frac{\sin\frac{w\xi}{2}\sin\frac{t\xi}{2}}{\xi^2}\,e^{-|\xi|\left(\frac{\delta+\Delta_i}{2}\right)} \tag{3.21}$$

$$R_A(x) = N_s S\, r_i T_o\left(\frac{\delta}{wt}\right)\int_{-\infty}^{\infty}\frac{\sin\frac{w\xi}{2}\sin\frac{t\xi}{2}}{\xi^2}\,e^{ix\xi-|\xi|\left(\frac{\delta+\Delta_i}{2}\right)}\,d\xi \tag{3.22}$$

The integral* is given as two terms

$$\left\{\frac{\delta+\Delta_i}{4}\ln\frac{\left(\frac{w-t}{2}\pm x\right)^2+\left(\frac{\delta+\Delta_i}{2}\right)^2}{\left(\frac{w+t}{2}\pm x\right)^2+\left(\frac{\delta+\Delta_i}{2}\right)^2} + \left(\frac{w+t}{2}\pm x\right)\tan^{-1}\frac{w+t\pm 2x}{\delta+\Delta_i}\right.$$

$$\left. - \left(\frac{w-t}{2}\pm x\right)\tan^{-1}\frac{w-t\pm 2x}{\delta+\Delta_i}\right.$$

where the plus signs are one set of terms to be added to the set with

---

*See Appendix A for the evaluation of this integral.

the minus signs. Since it is the maximum of $R_A(x)$ that is desired, set $x = 0$. It is assumed now that x is measured from the position of the center of the diffracted line.

$$R_A(0) = N_s S \gamma_i T_o \left[\frac{\delta(\delta + \Delta_i)}{2wt}\right]\left\{\tfrac{1}{2} \ln \frac{(w-t)^2 + (\delta+\Delta_i)^2}{(w+t)^2 + (\delta+\Delta_i)^2} + \frac{w+t}{\delta+\Delta_i} \tan^{-1} \frac{w+t}{\delta+\Delta_i} - \frac{w-t}{\delta+\Delta_i} \tan^{-1} \frac{w-t}{\delta+\Delta_i}\right\} \quad (3.23)$$

Or setting

$$\frac{w-t}{\delta+\Delta_i} = \xi \quad \text{and} \quad \frac{w+t}{\delta+\Delta_i} = \eta$$

$$R_A(0) = N_s S \gamma_i T_o \left[\frac{\delta(\delta+\Delta_i)}{2wt}\right]\left\{\tfrac{1}{2} \ln \frac{\xi^2+1}{\eta^2+1} + \eta \tan^{-1}\eta - \xi \tan^{-1}\xi\right\} \quad (3.24)$$

Now for the x-ray regions the crystal diffraction width $\delta$ is such that $\Delta_i >> \delta$ for almost all lines. For example

$$\Delta_i \cong 0.1 \text{ div. for the WK } \alpha \text{ line}$$
$$\delta \cong 10^{-3} \text{ div. for a perfect crystal}$$
$$\delta \cong 10^{-2} \text{ div. for a mosaic crystal}$$

Also $w \cong t$ and in practice one might set $w = t$; hence

$$\frac{w+t}{\Delta_i} \cong \frac{2t}{\Delta_i}$$

$$\frac{w-t}{\Delta_i} \cong 0$$

Also $\delta$ may be given in terms of $R_\theta$, the integrated reflection coefficient. From equation (2.37) $R_\theta = T_o \frac{\pi\delta}{2}$. The $\delta$ which is used here is $2w_\theta$ of equation (2.37), but a factor of $\frac{1}{2}$ is replaced by $T_o$.

$$R_A(0) = \frac{N_s S \gamma_i}{\pi}\left[R_\theta \frac{\Delta_i}{wt}\right]\left\{-\tfrac{1}{2} \ln\left(\left(\frac{2t}{\Delta_i}\right)^2+1\right) + \frac{2t}{\Delta_i} \tan^{-1} \frac{2t}{\Delta_i}\right\} \quad (3.25)$$

If one calculates the ratio of peak line intensity to direct beam inten-

sity, $\Gamma_i$, for the line i, then in the general case

$$\Gamma_i = \left[\frac{R_\theta}{\pi}\frac{(\Delta_i + \delta)}{wt}\right]\left\{\tfrac{1}{2}\ln\frac{\xi^2+1}{\eta^2+1} + \eta\tan^{-1}\eta - \xi\tan^{-1}\xi\right\} \quad (3.26)$$

The factors which depend on energy are $R_\theta$, $\Delta_i$, $\delta$, $\xi$, and $\eta$.

If one considers the energy range 0.1 - 1.0 Mev., $\Delta_i$ will depend more on the nature of the radiation than on the energy. Since the crystals are certainly not perfect, $\delta$ may be of the order of $\Delta_i$ but probably much larger; hence assume $\delta >> \Delta_i$. Also since the width is probably due to mosaic structure or to the fact that only a constant limited number of crystal planes are effective, the width will remain constant. Hence set $\delta + \Delta_i \cong \delta$. Assume $w >> \delta$, $t >> \delta$, and $w - t \cong 0$ so that $\eta = \frac{2t}{\delta} >> 1$ and $\xi \cong 0$. Then

$$\Gamma_i = \frac{R_\theta}{\pi}\frac{\delta}{t^2}\left\{-\ln\left(\frac{2t}{\delta}\right) + \frac{2t}{\delta}\frac{\pi}{2}\right\} \simeq \frac{R_\theta}{t} \quad (3.27)$$

This expression is true for all lines for which the source has the width of the geometric source only. It expresses the fact that as the source width and crystal aberration approach the limit of the diffraction width, the maximum number of quanta will be diffracted by the crystal because all rays in the aperture cone will "see" a part of the crystal at the Bragg angle $\theta_B$.

Case B: Virtual Source and Real Image

The luminosity of the spectrometer for the case of a virtual source and real image depends on the same factors as for the case of a real source but in a slightly different manner. The relative luminosity for the two cases is of great interest.

Fig. 4 is a schematic drawing of the geometry for the case of a virtual source. One may assume that the same total activity is spread

over the area A such that the whole available aperture of the crystal is filled with radiation which may be diffracted to R. The solid angle available to an atom in A will be proportional to $R_\theta$, the integrated reflection coefficient. To make a true comparison of the two cases, it is necessary to express the intensity in the diffracted beam as a function of the same parameters as were used for Case A; namely $N_S$, the total activity of the source; S, the effective solid angle which the aperture system subtends at the focus taking the counter efficiency into account; $T_o$, the true reflection coefficient for plane parallel radiation; and $\gamma_i$, the fraction of the total number of photons in the line i. Again the aberration and crystal diffraction functions determine the analyzing tool or "window". Now

$$S = k \frac{hs}{r^2} \qquad (3.28)$$

where k is a factor which includes the counter sensitivity as well as blocking due to ribs and collimator partitions, h the horizontal aperture, s the vertical aperture, and r the equivalent distance. Assuming that the system is symmetric for sources at V or at A, the solid angle for the atom in A will depend on the resultant window curve and may be expressed in terms of S. The function $f_g(x)dx$ represents the fraction of the crystal area whose focal planes intersect in the range dx at the position x of the aberration distribution. The crystal window curve $T_o f_X(x)$ represents the fraction of a monochromatic plane parallel beam, passing through the crystal in such a direction as to intersect the focal circle at a point in the vicinity of V conjugate to the point x in the vicinity of R, which would be reflected when the crystal is set for reflection at some wave-length. Since radiation is falling at all angles

on the crystal, one takes the product integral of these two functions to obtain the fraction of all monochromatic quanta emitted by A which will pass through the slit dx at x. The aberration in this case limits the fraction of the total activity $N_s$ placed at A which can contribute at the setting. If there were no aberration, the whole source could contribute at a given setting just as in Case A any atom in the source could use the full aperture of the crystal. The vertical aperture h, the sensitivity and blocking factor k, and the distance r are the same as for Case A. In performing the product integral one is essentially integrating to get the horizontal aperture.

The remaining dependence of the "window" will be on the vertical aperture and counter sensitivity. These are given by the factor S/h. The window W(x) becomes

$$W(x) = \frac{ST_o}{h} \int_{-\infty}^{\infty} f_g(\xi) f_X(x - \xi)\, d\xi \qquad (3.29)$$

where h and $d\xi$ must be expressed in the same units. It is convenient to refer all measurements to screw divisions, so if $r_o$ is the factor converting millimeters at the focal circle to screw divisions, one must set $r_o h$ for h. The result is given by equation (3.19), Case A.

$$W(x) = \frac{S}{r_o h} \frac{\delta T_o}{2w} \left[ \tan^{-1} \frac{w + 2x}{\delta} + \tan^{-1} \frac{w - 2x}{\delta} \right] \qquad (3.30)$$

with a transform

$$H(\xi) = \frac{ST_o}{r_o h} \sqrt{\frac{\pi}{2}} \frac{\delta}{2} \frac{\sin \frac{w\xi}{2}}{\frac{w\xi}{2}} e^{-\left|\frac{\xi\delta}{2}\right|}$$

It is again convenient to take the slit at F and the distribution in $\lambda$ of the radiation as determining the unknown spectrum for analysis. In this case, however, the function $f_s(x)$ is defined so

$$= 0 \; ; \qquad x < -\frac{t}{2}$$

$$f_s(x) = 1 \; ; \quad -\frac{t}{2} \leq x \leq \frac{t}{2} \tag{3.31}$$

$$= 0 \; ; \qquad x > \frac{t}{2}$$

The reason that $f_s(x)$ is different from that for Case A is that one integrates over any radiation entering the slit.

$\gamma_i$ and $f_i(x)$ have the same meaning as before. Hence the spectral distribution function becomes

$$P_i(x) = N_s \gamma_i \int_{-\infty}^{\infty} f_i(\xi) f_s(x - \xi)\, d\xi \tag{3.32}$$

$$G_i(\xi) = \frac{t}{\sqrt{2\pi}} \frac{\sin \frac{t\xi}{2}}{\frac{t\xi}{2}} e^{-\left|\frac{\xi \Delta_i}{2}\right|}$$

and

$$P_i(x) = \frac{N_s \gamma_i}{\pi} \left[ \tan^{-1} \frac{t + 2x}{\Delta_i} + \tan^{-1} \frac{t - 2x}{\Delta_i} \right] \tag{3.33}$$

The function $P_i(x)$ represents the total number of quanta in the band of width t whose center is at the distance x from the center of the line. The final result in these calculations is independent of the order in which the folds are calculated. The choice made here seems to be the best for an understanding of the factors contributing to diffracted intensity. The window curve then analyzes the source curve $P_i(x)$ yielding the final intensity function.

$$R_B(x) = \int_{-\infty}^{\infty} W(x - \xi) P_i(\xi)\, d\xi \tag{3.34}$$

Solving as in Case A, the final result will be for a setting at the center of the line i

$$R_B(0) = \frac{N_s S T_o \gamma_i}{r_o h}\left[\frac{\delta(\delta+\Delta_i)}{2w}\right]\left\{\frac{1}{2}\ln\frac{(w-t)^2+(\delta+\Delta_i)^2}{(w+t)^2+(\delta+\Delta_i)^2}\right.$$

$$\left.\frac{w+t}{\delta+\Delta_i}\tan^{-1}\frac{w+t}{\delta+\Delta_i} - \frac{w-t}{\delta+\Delta_i}\tan^{-1}\frac{w-t}{\delta+\Delta_i}\right\} \qquad (3.35)$$

$R_B(x)$ then represents the total flux passing the analyzing slit as it is swept over the spectrum. Comparing equations (3.23) and (3.35) one sees immediately

$$\frac{R_A}{R_B} = \frac{r_o h}{t} \qquad (3.36)$$

if the same values of w and t are used. Since the screw has a pitch of approximately one mm. per revolution and in Fig. 7

$$C\beta = 76.25 \text{ in.}$$

$$CB = 90.5 \text{ in.}$$

and the linear aperture of the crystal is about 44 mm., the value of the ratio becomes

$$\frac{R_A}{R_B} = \frac{(44)(90.5)}{(0.1)(76.25)} = 520$$

In practice one could concentrate the same activity in a much smaller area and hence decrease w and t for Case B. The decrease in luminosity would probably be nearer a factor of 100, and the resolving power would be increased by a factor of possibly 3 or 4.

Dispersion and Resolving Power

The dispersion of a spectrometer for high energies must be large to obtain high resolving power. The dispersion is determined solely by the focal length and lattice spacing. Except in special cases the first order is best in order to obtain high atomic structure factors.

$$\frac{d\ell}{d\lambda} = \frac{Rn}{2d\cos\theta} = \frac{Rn}{2d} \qquad (1.2)$$

To get sufficient dispersion it is necessary to pick a crystal with a lattice spacing of the order of 1 to 2 Å. A dispersion of much less than one mm. per X. U. makes the resolving power diminish to the point where the advantage of the crystal method, i. e. high precision, is lost.

The resolving power decreases with wave-length since geometric factors as well as intensity prevent the source width and aberration width from decreasing beyond a certain limit. The crystal resolving power is always much smaller than any of the geometric factors. Since the luminosity varies inversely with w as long as $t \cong w$, an improvement in the focal aberration width would result in considerable increase in intensity. Hence t could be decreased proportionately. For a dispersion of one mm. per X. U. and if a resolution of $10^{-3}$ is required at one Mev., then $w \cong t = 0.01$ mm. Actually the experimental resolution is 1/3 to 1/5 the width of the line so $w \cong t = 0.05$ mm. is a good figure to attempt. In this spectrometer $w \cong t = 0.1$ mm., but w has been made as small as 0.05 mm. The radiation widths for energies above 0.1 Mev. are usually of the order of at most a few volts, i. e. the relative line width is about $10^{-5}$ and will not depend in a regular manner on the energy. This is almost an order of magnitude greater than the best resolution attainable. For comparison, the theoretical resolution of a perfect crystal is given by the relations (2.35) or (2.41). Compare $w_\theta$ for a "thick" crystal with the angle at which the diffraction occurs.

$$w_\theta = \frac{r_o d_H K(\frac{F_H}{V}) \lambda}{\pi n \cos \theta_B} \qquad (2.35)$$

If $\theta_B$ is small, $K \cong 1$, $\cos \theta_B \cong 1$ and $\sin 2\theta_B \cong 2\theta_B$; assume $n = 1$.

$$w_\theta = \frac{r_o d_H \left(\frac{F_H}{V}\right) \lambda}{\pi}$$

but $\lambda = 2d_H \sin \theta_B \cong 2d_H \theta_B$ so

$$\frac{w_\theta}{\theta_B} = \frac{2r_o (d_H)^2 \left(\frac{F_H}{V}\right)}{\pi}$$

For the quartz (310) planes

$$\frac{F_H}{V} = 0.12 \text{ Å}^{-3}$$

$$d = 1.178 \text{ Å}$$

$$\frac{e^2}{mc^2} = 2.82 \times 10^{-5} \text{ Å}$$

$$\frac{w_\theta}{\theta_B} = \frac{2(2.82 \times 10^{-5})(0.12)(1.178)^2}{\pi} = 3 \times 10^{-6}$$

This resolving power is much higher than necessary. It is just this fact that makes the luminosity very low. Only a mosaic crystal can have a low resolving power and yet have a reasonably large reflection coefficient.

## Part IV

### An Experimental Determination of Reflection Coefficients and the Energy of a Gamma Radiation of Radio-gold, $Au^{198}$

Experimental Arrangement for Measurement of Absolute Reflection Coefficients with X-Radiation

After a preliminary test with the gamma radiations of $Co^{60}$, having energies of 1.1 and 1.3 Mev. respectively, had failed to give a positive result, the measurement of the integrated reflection coefficient $R_\theta$ as a function of $\lambda$ was undertaken in an effort to establish by extrapolation the source strengths which might be needed. Actually, the quantity which was measured was $\Gamma_i$, the ratio of the peak intensity of the diffracted line corresponding to the wave-length $\lambda$ to the peak intensity in the direct beam if only the wave-length $\lambda$ were present.

$$\Gamma_i = \frac{R_A(0)}{{}_iR_D} \tag{4.1}$$

The reading in the direct beam was made by moving the source to the position which is the focus of the collimator. $\gamma_i$ is the fraction of all quanta emitted by the source which lie in the line of wave-length $\lambda$. From these data the value of $R_\theta$ was calculated by means of equations (3.26) and (3.27); the wave-length dependence of $R_\theta$ gives considerable information concerning the nature of the crystal structure.

To make a reliable determination of $\Gamma_i$, a source of known composition was needed. For practical reasons it is also desirable that the total source intensity be concentrated in a very few lines. In the x-ray region the fluorescent K radiation from an element of high atomic number is satisfactory since the continuous background from scattering can be kept small. Figure 22 shows a schematic drawing of the arrange-

ment. The x-ray tube excites in the scatterer its characteristic fluorescent radiation as well as the Compton scattered radiation, but very little of the Compton scattering is directed toward the crystal since the angle is about 110° and the atomic number is high. Nevertheless, to eliminate all question as to the effect of continuous scattered background a procedure utilizing the Ross method of balanced filters was employed. The true source for the spectrometer was the scattering foil mounted on the lucite support. The dimension 0.1 mm. for the thickness was chosen because it represents the width of the crystal aberration. The lucite mounting was milled away so that it touched the foil at ten points, thus presenting the least amount of matter for scattering into the spectrometer. The lead jaw was rotated about the focal axis so that the crystal aperture was just filled with radiation. Owing to the fact that the radiation emerges from the face of the wedge, those rays emerging at a more glancing angle will suffer greater self-absorption. This, however, did not invalidate the results.

The sources were prepared of pure metal foil 0.004 inches thick by grinding to shape in a special jig. Great care was taken to make the sources identical in geometrical width as seen by the spectrometer. This required mounting them so that their projected width was 0.004 inches (0.1 mm.) and no more. They were mounted on the lucite support by means of stopcock grease which was sufficiently tacky to hold them firmly in place, yet did not dry and distort the shape. As a matter of fact the reflection coefficient $\Gamma_i$ turned out to be rather insensitive to the exact geometry.

The x-ray tube had to be mounted so that its target remained at constant distance from the scatterer. Since the real source of the

spectrometer must move on a segment of a cardioid with respect to the room, it was necessary to fasten the tube rigidly to the source carriage N yet provide that it introduce no undue mechanical loading which might distort the structure of the instrument. This was done by providing a track on the side of the beam S along which the tube mounting rolled as the source carriage moved. In addition an overhead counterbalance system was provided to balance all gravitational loading.

A preliminary calculation had shown that an x-ray tube operating at 150 kvp. 10 ma. would generate sufficient fluorescent radiation for these measurements. Consequently the transformer, control panel, and tube were taken from a Philips "Searchray 150" outfit. The tube was a Eureka shockproof-mounted x-ray tube. All of the x-ray data were made running the tube at 155 kvp. 9 ma., and except in the case of thorium, there was adequate intensity. The tin K radiation was so soft that the counter sensitivity fell off rather seriously, but the increased production of characteristic K radiation made-up the difference.

The experimental method was to determine the counting rate at the zero setting of the spectrometer after first setting the $\beta$ point and the collimator center on zero. The counting rate in this position was due to all the radiation from the source, fluorescent as well as continuous. As mentioned above, the characteristic K radiation was the main component of this radiation. Then the reading at the peak of the $K\alpha_1$ line was taken. The ratios of intensities of the K lines of the elements as given by Compton and Allison[22b] were used in the formula (4.1). The data were corrected for the background counting rate in every case, and the root mean square deviations of $\Gamma_i$ were calculated from the actual data. In the case of tin the reflection coefficient

so measured had to be corrected for continuous scattered radiation by the use of Ross filters[27] whose K edges bracketed the K $\alpha_1$ and $\alpha_2$ lines. For higher atomic numbers the correction was shown by this method to be very small. A set constructed for gold permitted us to correct the results for tantalum and thorium by extrapolation. These results are presented in Table II. Two independent determinations at x-ray wave-lengths using different sources gave results which were in complete agreement. The determination of the reflection coefficients for the nuclear gamma-ray lines was made incidental to their energy determinations.

Table II

| Line | $\lambda$ X. U. | E Mev. | $\Gamma_i$ | $\Gamma_{i/R_\theta}$ From theory | $R_\theta$ X. U. | $R_\theta$ Radians |
|---|---|---|---|---|---|---|
| Sn $K\alpha_1$ | 489.57 | 0.0253 | $0.175 \pm .023$ | 2.27 | $7.70 \times 10^{-2}$ | $3.28 \pm 0.43 \times 10^{-5}$ |
| Ta $K\alpha_1$ | 214.88 | 0.0506 | $0.050 \pm .002$ | 3.20 | $1.56 \times 10^{-2}$ | $6.63 \pm 0.27 \times 10^{-6}$ |
| Au $K\alpha_1$ | 179.96 | 0.0688 | $0.044 \pm .004$ | 3.39 | $1.30 \times 10^{-2}$ | $5.52 \pm 0.50 \times 10^{-6}$ |
| Th $K\alpha_1$ | 132.3 | 0.0936 | $0.017 \pm .004$ | 3.62 | $4.69 \times 10^{-3}$ | $1.99 \pm 0.47 \times 10^{-6}$ |
| $Au^{198}$ | 30.09 | 0.411 | $0.0030 \pm .0001$ | 8.33 | $3.60 \times 10^{-4}$ | $1.53 \pm 0.05 \times 10^{-7}$ |
| $Co^{60}$ | 11.27 | 1.10 | $< 2.8 \times 10^{-4}$ | 8.33 | $3.4 \times 10^{-5}$ | $< 1.4 \times 10^{-8}$ |

Measurement of a Nuclear Gamma-Ray Wave-length and Energy

The experimental arrangement and method for the measurement of nuclear gamma ray energies has been completely described except for the source holder. The source holder for these investigations (see K of Fig. 8 or Fig. 22) consists of a set of lead jaws machined so that a thin foil sitting on edge at the focal position can irradiate only the crystal aperture. The aluminum inserts at the actual source position, being of low atomic number, will not scatter appreciably; hence the source will be truly defined by the foil. The source was set up and

checked beforehand to see if the axis of the foil was accurately parallel to the axis of focus. Any deviation would introduce an aberration proportional to the sine of the angle of deviation. The instrument was previously adjusted for optimum focus; the axis of the source bomb was centered on the source carriage and leveled with a precision level. Since the crystal holder blocks were ground with the generators of the cylinder accurately normal to the horizontal faces, the focal line was assumed to be accurately vertical when the crystal holder was leveled. The depth of focus for the instrument determines the depth of the source within the limits of self-absorption. Reference to Fig. 10 will show that the depth of focus of 5 mm. will result in a maximum source width of about 0.1 mm. However, the assumption that the focal aberration is a rectangular window will no longer hold. The presence of self-absorption in the source will decrease this aberration. It is evident that rather careful focusing is necessary if the optimum resolving power is to be attained.

The sources which were tried were in each case foils of pure metal 5 mm. wide by 30 mm. long by 0.1 mm. thick which had been activated by neutron bombardment in the pile at Oak Ridge. The disintegration schemes for gold and cobalt are given as follows:

Gold

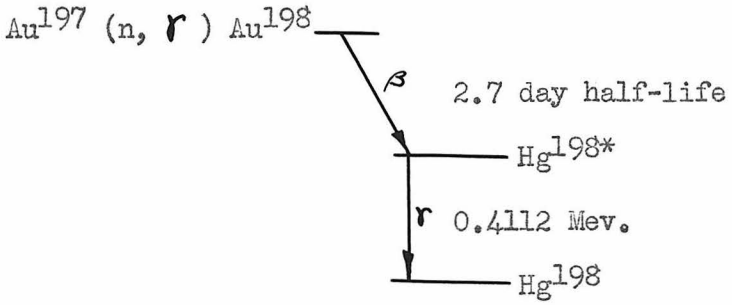

Cobalt

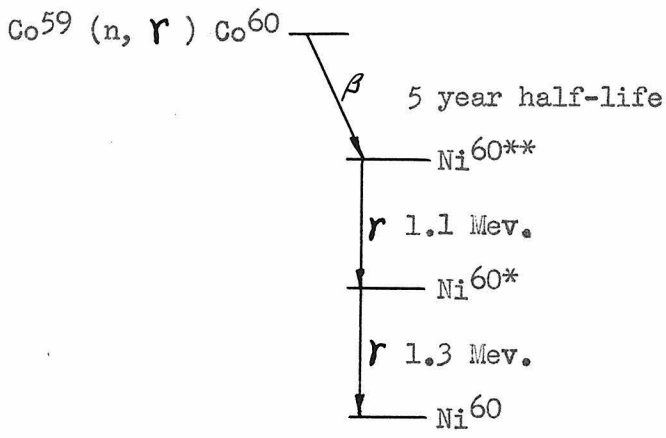


These schemes indicate only the lines which were of interest for this work. In each case the $\beta$ spectrum is believed to be simple. The gamma transitions occur on decay of excited states of the daughter elements to the ground state. There have been reported[28] two other lines in the case of gold at 0.157 Mev. and 0.207 Mev. corresponding to 15% of the intensity of the 0.41 Mev. line. These reactions were chosen because they had very good yields and the gamma radiations were fairly well known. The question of half-life is important when the material has to be shipped an appreciable distance.

The gold source had an activity of one curie when placed in the instrument, and it decayed through about three half-lives before all the data were accumulated. Owing to self-absorption the effective source was of the order of 1/5 of the total activity. The line profile for the 0.41 Mev. line was taken by turning the screw by hand from the left to the right side so that all backlash would be taken up. There was still a slight shifting of the lines (due to displacement of the point whose cause was later located), but this did not greatly affect the spacing between the lines which determines the wave-length and

energy. At the same time the readings at the central beam were taken with filters in place to reduce the counting rate sufficiently to permit its measurement. Fig. 23 shows some sample line profiles and Fig. 6 the profile of the central beam characteristic of our present lead collimator. The centers of the lines were located by extrapolation of the straight sides of the profile to an intersection and also by locating the center of the half-maximum point. These two methods gave consistent results. The symmetric shape of the profiles permits a more accurate location of the line position than would otherwise be possible. The half-width of 0.13 divisions and the shape are just that to be expected if the source and analyzer are approximately rectangular windows of width 0.13 divisions. The background was in part proportional to the source strength so that the ratio of peak height to background did not change with decay of the source until the background became constant. The data are given in Table III.

Table III

Preliminary Values of Wave-length and Energy

| Run No. | $\lambda_s$ X. U. | $\lambda_g$ cm. | $h\nu$ Mev. |
|---|---|---|---|
| 1 | 30.095 | $30.156 \times 10^{-11}$ | 0.41100 |
| 2 | 30.080 | 30.141 | 0.41121 |
| 3 | 30.065 | 30.126 | 0.41141 |
| 4 | 30.085 | 30.146 | 0.41114 |
| 5 | 30.083 | 30.144 | 0.41116 |
| | 30.082 ± 0.004 | 30.143 ± 0.004 | 0.41118 ± 0.00005 |

The errors given are the probable errors calculated from the statistical fluctuations of the experimental data only.

The calibration of the screw may be made by two methods. The one uses the quartz crystal spacing as measured by Cu K radiation and the measured values for the mean pitch P of the screw and the distance

$\overline{CV'}$ of Fig. 7.

$$P = 0.038440 \pm .000010 \text{ inches per turn} \quad \text{at } 25^\circ \text{ C}$$

$$\overline{CV'} = 90.522 \pm .010 \text{ inches}$$

$$d_{310}\ (18^\circ \text{ C}) = 1177.64 \text{ X. U.}^*$$

$$\frac{\lambda}{T} = \frac{2d_{310}\ P}{\overline{CV'}} \text{ X. U. per revolution}$$

From which one may obtain

$$\frac{\lambda}{T} = 1.0002 \pm 0.0003$$

The other method of calibration is to calibrate the instrument directly in terms of the $K\alpha$ lines of the heavy elements. These are known with an accuracy of about one part in 5,000. A somewhat rough calibration using tungsten $K\alpha_1$ $K\alpha_2$ lines and the lead $K\alpha_1$ line yields a mean value for $\lambda/T$ given by

$$\frac{\lambda}{T} = 0.9998 \pm 0.0002$$

The errors in the calibration arise from (a) differences in the coefficient of thermal expansion of quartz and steel, (b) errors in the standard micrometer used for the measurements, and (c) errors in the measured values of x-ray wave-lengths. However, the precision given and the agreement between the two essentially independent methods leads to the belief that the calibration is sufficiently accurate for the present measurements. For further work it appears desirable to obtain a more precise determination of tungsten K radiation for calibration.

---

*The value of $d_{310}$ was calculated from $d_{100}$ by the relation $d_{310} = \frac{d_{100}}{(13)^{\frac{1}{2}}}$. The value of $d_{100}$ is given in terms of the Cu $K\alpha$ lines by Berquist.(29) The temperature coefficient of expansion normal to the axis is $1.45 \times 10^{-5}$/X. U./deg. from 18° C.(30) The value parallel to the axis is $0.90 \times 10^{-5}$/X. U./deg. These coefficients were used to correct the crystal spacing to 23° C, the ambient temperature.

There may be some very small random errors as well as systematic errors inherent in the instrument due to misalignment or frictional loading on the spindle M (Fig. 8). These introduce errors of the order of one part in 5,000 which should be corrected to take full advantage of the precision possible. Finally, the periodic correction to the screw of the order of 0.005 X. U. is indicated by a preliminary calibration using a standard decimeter. This correction is neglected in the present work.

The reduction of the data given in Table III was accomplished as follows: The nominal instrument readings were converted to Siegbahn X. U. by the factor 1.0000 ± 0.0003. The conversion factor from the Siegbahn to the absolute centimeter scale is 1.00203 and from centimeters to energy units in Mev. is 12394.2 ± 0.9 x $10^{-8}$ (the wave-length associated with an energy of 1 ev.).[31] With these data the final precision determination of the energy of this gamma-ray of gold $Au^{198}$ is reported as

$$0.4112 \pm 0.0002 \text{ Mev.}$$

The probable deviation for the final result is caused by the lack of a precision calibration of the instrument and to the small random motion of the $\beta$ point. If the determination of line position from the experimental data were the limiting factor, a precision of one part in 5,000 could be quoted.

At this time absorption curves were taken with tin and lead since these data were necessary to reduce the observed data to a reflection

coefficient determination.* The values of the linear absorption coefficients for 0.4112 Mev. radiation are measured to be

$$\mu_{Sn} = 0.777 \text{ cm.}^{-1}$$

$$\mu_{Pb} = 2.28 \text{ cm.}^{-1}$$

By comparing the peak of the line with the peak of the central beam, extrapolated to zero absorber, the value of $\Gamma_i$ was calculated to be $0.0030 \pm 0.0001$.

The cobalt sample had an activity of about 50 mc. Since the half-life is very long, a very careful exploration of the lines at 1.10 and 1.30 Mev. was made. No line could be detected, the reflected intensity being equal to or less than the statistical fluctuations of the background counting rate. However, a maximum possible value for the reflection coefficient could be assigned assuming that one could have observed a line if its height had been three times the statistical fluctuation. This led to a value for $\Gamma_i \leq 2.8 \times 10^{-4}$. These data are presented in Table II with the x-ray reflection coefficients.

Interpretation of the Experimental Reflection Coefficient Data

The experimental determinations of $\Gamma_i$ were reduced to $R_\theta$ by the use of the expressions calculated in Part III, Case A. The expression for $\Gamma_i$ has a different form in the x-ray and the gamma-ray regions, equation (3.26) being correct for x-rays and equation (3.27) for gamma-rays. With the appropriate approximations equation (3.26) becomes

*The absorption curves were taken with the source turned so that the effects of self-absorption would not be so large. An attempt had been made to observe the lower energy radiation with the spectrometer, but its very high self-absorption made this observation impossible. The curve for tin showed a slight upward curvature at zero absorber thickness; this indicates the presence of a soft component, the energy or intensity of which was difficult to determine from the absorption curve alone.

$$\Gamma_i = \left[\frac{R_\theta}{\pi}\frac{\Delta_i}{wt}\right]\left\{-\tfrac{1}{2}\ln\left(\left(\frac{2t}{\Delta_i}\right)^2+1\right) + \frac{2t}{\Delta_i}\tan^{-1}\frac{2t}{\Delta_i}\right\} \qquad (3.26)$$

and $$\Gamma_i = \frac{R_\theta}{t} \qquad (3.27)$$

It is assumed that at all times the source width equals the aberration width. The value of w is taken from the appropriate focal picture made just before the determination of $\Gamma_i$; from it $w \cong 0.12$ div. The assumption of a square window for the aberration profile is justified only by lack of a better assumption and the difficulties in making a calculation of $\Gamma_i$ for other windows. The linear width of the sources used is 0.10 mm. or, when converted to screw divisions, 0.12 divisions. The values of $\Delta_i$ were taken from Compton and Allison[22c] for tungsten and silver, and by linear interpolation the values for the other scatterers were calculated. Physically, the difference between equations (3.26) and (3.27) corresponds to the fact that for x-rays the "window" of the spectrometer is greater than the line width while for gamma radiation it is not. The values of $R_\theta$ calculated by the expression above are given in units of screw revolutions. To convert to radians these values must be divided by (90.5)(26); the screw has 26 threads per inch, and the distance from the crystal to the screw is 90.5 inches. The values of $R_\theta$ in the last column are given in radians and may be compared with theory. These data are plotted in Fig. 24.

The slope of the curve of $R_\theta$ versus $\lambda$ on a log log plot is slightly greater than two. However, the discrepancy, when compared with a curve of slope two, is not outside the deviations which might be accounted for by the assumptions made on the reduction of $\Gamma_i$ to $R_\theta$. A comparison with the theoretical values for $R_\theta$ calculated from equation (2.52) for the case of a mosaic crystal with small primary and secondary extinction

indicates very good agreement.

$$R_\theta = \frac{QT_o}{\gamma_o} \tag{2.52}$$

$$Q = r_o^2 \left(\frac{F_H}{V}\right)^2 \frac{\lambda^2 d_H \,(1 + \cos^2 2\theta_B)}{2n \cos \theta_B} \tag{2.44}$$

$$r_o = 2.82 \times 10^{-5} \text{ Å}$$

$$\left.\begin{aligned} F_{310} &= 13.8 \\ V &= 112.0 \text{ Å}^3 \end{aligned}\right\} \text{ from Appendix B}$$

$$n = 1$$

$$d_H = 1.1776 \text{ Å}$$

$$T_o = 1 \text{ mm.}$$

The assumption of $\cos \theta_B \cong 1$ and $\frac{1 + \cos^2 2\theta_B}{2} \cong 1$ will be valid for all Bragg angles of interest. Hence

$$\frac{Q}{\lambda^2} = (2.82 \times 10^{-5})^2 \left(\frac{13.8}{112.0}\right)^2 (1.1776)$$

$$= 1.42 \times 10^{-11}$$

$$R_\theta = 1.42 \times 10^{-4} \lambda^2$$

if $\lambda$ is in Å units. The value of $R_\theta/\lambda^2$ calculated from the experimental data is

$$\frac{R_\theta}{\lambda^2} = 1.5 \times 10^{-4}$$

This agreement is much better than should be expected from either experiment or theory. It is of interest to compare the value of $R_\theta/\lambda$ which would obtain had the crystal behaved as a perfect lattice. For the corresponding range of $\lambda$ the crystal would be "thick". Hence

$$\frac{R_\theta}{\lambda} = \frac{r_o d_H \left(\frac{F_H}{V}\right) K}{2n \cos \theta_B} \tag{2.37}$$

$$\cong \frac{r_o d_H \left(\frac{F_H}{V}\right)}{2}$$

$$\frac{R_\theta}{\lambda} \cong \frac{(2.82 \times 10^{-5})(1.178)(\frac{13.8}{112.0})}{2}$$

$$= 2.1 \times 10^{-6}$$

Hence, at a wave-length of 0.1 Å the mosaic crystal will give about five times the intensity of the perfect crystal. This curve is plotted in Fig. 24 also. It cannot be extrapolated below about 50 X. U. because at short wave-lengths the quartz crystal of one mm. thickness no longer behaves as a "thick" crystal, so the curve must change to the corresponding curve for a "thin" crystal, i. e. the slope must change from one to two. By equation (2.29) the extinction distance for the (310) planes of quartz is 0.3 mm. at 100 X. U. and 1 mm. at 30 X. U. Hence, beyond the point of intersection the two curves must be identical. These curves bring out the interesting fact that for every thickness of crystal, with the assumption of very small extinction, the mosaic crystal will have the higher reflection coefficient until the curves intersect. For shorter wave-lengths the reflection coefficient is identical for either perfect or mosaic crystals.

The quartz slabs are probably very nearly perfect before bending. There may be some rupture of the lattice near the surface during the polishing of the plates, but it is doubtful whether this affects the diffraction pattern.* However, the reflection curve definitely indicates that the curved plate is a mosaic crystal or at least that the domains over which coherent diffraction takes place are small. This same effect has been observed by others[32] for a quartz plate subjected to inhomo-

*Mr. W. West in this laboratory has taken two-crystal antiparallel rocking curves with plates cut from the same piece of quartz and polished in the same manner. At 707 X. U. the rocking curve width was four sec. of arc which is strong evidence that there is little or no surface effect.

geneous stresses. This is not true for homogeneous stresses however. No attempt will be made to explain this phenomenon since it is the subject of further research. These experimental results can be used to indicate the range of usefulness of the focusing curved crystal spectrometer and the design requirements.

Design Requirements and Range of the Curved Crystal Method for Gamma Radiation Spectroscopy

It is possible to state the conditions which must hold if direct spectroscopy of gamma radiation is to be a successful tool. All the factors - dispersion, precision, resolving power, and luminosity - are related, but it may be well to discuss them as separate factors.

Dispersion

The dispersion equation

$$\frac{\Delta\lambda}{\Delta\ell} = \frac{2d}{Rn} \qquad (1.2)$$

shows that a large focal distance and small planar spacing is necessary. However, a large atomic structure factor requires a small value for n/d. The atomic structure factors do not decrease as rapidly for high atomic number as for low with increasing n/d, so it is of considerable advantage to use an element of rather high Z for the scatterer. The choice of crystal is rather seriously limited, because it must have planes of rather small spacing yet have a reasonable structure factor. If the dispersion is to be one X. U./mm., which is a minimum value for operation to one Mev. and above, $\frac{2d}{R}$ becomes $10^{-3}$ if d is in Ångstrom units and R in millimeters. The limitations of physical size force one to use lattice spacings of one Å or smaller.

Precision

The precision of the spectrometer is controlled by the precision in the mechanical construction, wave-length screw, front pivot, and various adjustments. If the dispersion is large, the problems of precision are not as great. In an instrument with a dispersion of one X. U./mm. it is not difficult to make settings precise to 0.005 mm. provided care is taken to observe the principles of kinematic design and the parts are carefully made and assembled. Systematic errors can be detected by careful calibration; one of these, however, can never be evaluated. If any one of the four window curves is asymmetrical and at the same time reflected about the $\beta$ point, it will be impossible to make a precise determination of an energy save by increasing the resolution, since the line will have an asymmetric profile which is reflected in the $\beta$ point. The effect of the non-uniform background can be corrected because in most cases it is small. Assuming the window curves are symmetric, a precision of one part in 2,000 is possible at one Mev. with this instrument. The precision is inversely proportional to the wave-length because the dispersion is constant. It should be noted that the precision is not entirely limited by the resolution, but by the mechanism itself.

Resolving Power

A discussion of resolving power has already been made. The resolving power is limited at present by the geometrical aberration of focus of the crystal. This may be due to non-uniform curvature of the plate or to the inherent mosaic structure of the crystal. The crystal one uses must have a very small angular distribution of the mosaic domains

and at the same time be very uniform over rather large areas. Few such crystals, except quartz, exist in large enough pieces. Artificially grown crystals are large enough, but their mosaic structure makes the resolving power too low. However, careful testing of crystals with a two-crystal spectrometer may reveal a suitable one. The problem of bending a slab is very serious. The stresses set up in a thick quartz slab bent to a cylinder force the ratio t/R to be less than $10^{-3}$ where t is the plate thickness. The only method for increasing t is to permit plastic deformation or to use a multiplicity of superposed plates. It may be possible to bend crystals, similar to sodium chloride, by re-crystalization[33] in a saturated solution. However, this may destroy the focusing properties. A geometric focal width of 0.05 mm. is the minimum width which has been obtained with this instrument. The resolution at present is of the order of 0.05 X. U. which is adequate.

Luminosity

The effective luminosity of the instrument as it stands is about $10^{-8}$, i. e. this represents the fraction of all quanta in a source which will be registered. This will vary from $10^{-7}$ to $10^{-9}$ depending on the energy. The luminosity is closely related to the resolution, and in general if the resolution is increased, the luminosity must decrease. This is true only as long as the source which is under investigation is wide compared with the analyzer. Nuclear line widths are so narrow that only the physical width of the source contributes to the composite width. At present the source volume, i. e. the volume in which the active material may be placed, is fixed by the resolution of the crystal (geometrical aberration). To increase the volume would decrease the

resolution and not increase the diffracted intensity. Hence, sources of high specific activity (one curie per gram) are required. This is a serious limitation to the application of the instrument especially for high energy radiation.

The choice of a crystal is the most serious problem. It should be rather thick (5 mm.) and have the property that when it is bent, the mosaic structure is not disturbed too much. The relative angular disorientation of the planes in all parts of the crystal should be less than 10 sec. of arc with respect to the initially flat face which is pressed against the defining clamp. At the same time the domains of the mosaic structure should be large enough to insure primary extinction. Such a crystal would have a large reflection coefficient which varies as $\lambda$ rather than $\lambda^2$. The luminosity of the present instrument can be increased by at most a factor of about two with certainty; to do better than this requires considerable investigation of crystals. It should be pointed out that only by increasing the reflectivity of the crystal and by redesigning the collimator to decrease scattering will the line contrast be increased.

The counter sensitivity for Geiger counters may be increased by a factor of three or four; if higher sensitivity is needed, development of the scintillation counters must be undertaken. In this case an increase of sensitivity of five to ten may be possible. Hence, the over-all effective luminosity may be made $10^{-7}$, but until the crystal can be improved, an increase in the solid angle factor or counter sensitivity will not appreciably affect the luminosity.

Range of Application

The present luminosity, $10^{-8}$, and small focal volume together with the present design of the collimator limit the instrument to the determination of a few gamma energies below one Mev. to be used as standards for the field of nuclear physics. The sources at present must be 50 mc. or greater in strength with a specific activity of 1000 mc. per gram. With the improvements suggested it is possible that sources as low as five mc. would be satisfactory. The energy range of the instrument is from 0.025 to 1.7 Mev., but above one Mev. the low contrast due to large background will make measurements very difficult.

Appendix A

Evaluation of the Integrals of the Luminosity Function

$$I = \int_{-\infty}^{\infty} \frac{\sin \frac{t\xi}{2}}{\frac{t\xi}{2}} e^{ix\xi - \left|\frac{\xi\Delta_i}{2}\right|} d\xi \qquad (3.15)$$

The real part of the integrand is even while the imaginary part is odd; hence

$$I = 2 \int_{0}^{\infty} \frac{\sin \frac{t\xi}{2}}{\frac{t\xi}{2}} \cos x\xi \; e^{-\frac{\xi\Delta_i}{2}} d\xi$$

By the addition formula

$$2 \sin \frac{t\xi}{2} \cos x\xi = \sin \left(\frac{t}{2} + x\right)\xi + \sin \left(\frac{t}{2} - x\right)\xi$$

$$I = \int_{0}^{\infty} \left\{ \frac{\sin \left(\frac{t}{2} + x\right)\xi}{\frac{t\xi}{2}} + \frac{\sin \left(\frac{t}{2} - x\right)\xi}{\frac{t\xi}{2}} \right. e^{-\frac{\xi\Delta_i}{2}} d\xi$$

Since

$$\int_{0}^{\infty} \frac{\sin a\eta}{\eta} e^{-b\eta} d\eta = \tan^{-1} \frac{a}{b} \qquad (34)$$

the integral becomes

$$I = \frac{2}{t} \left[ \tan^{-1} \frac{(t + 2x)}{\Delta_i} + \tan^{-1} \frac{(t - 2x)}{\Delta_i} \right]$$

The integral arising in the evaluation of $R_A(x)$ is of the form:

$$I = \int_{-\infty}^{\infty} \frac{\sin \frac{w\xi}{2} \sin \frac{t\xi}{2}}{\xi^2} e^{ix\xi - |\xi|\left(\frac{\delta + \Delta_i}{2}\right)} d\xi$$

The real part of the integrand is even while the imaginary part is odd; hence

$$I = 2 \int_{0}^{\infty} \frac{\sin \frac{w\xi}{2} \sin \frac{t\xi}{2}}{\xi^2} \cos x\xi \; e^{-\xi\left(\frac{\delta + \Delta_i}{2}\right)} d\xi$$

Applying the addition formulae twice

$$2 \sin \frac{w\xi}{2} \cos x\xi = \sin \left(\frac{w}{2} + x\right)\xi + \sin \left(\frac{w}{2} - x\right)\xi$$

and

$$\sin \left(\frac{w}{2} \pm x\right)\xi \quad \sin \frac{t\xi}{2} = \tfrac{1}{2} \cos \left(\frac{w - t}{2} \pm x\right)\xi \; - \tfrac{1}{2} \cos \left(\frac{w + t}{2} \pm x\right)\xi$$

$$I = \tfrac{1}{2} \int_0^\infty \left[ \frac{\cos \left(\frac{w - t}{2} + x\right)\xi \; - \cos \left(\frac{w + t}{2} + x\right)\xi}{2} \right] e^{-\xi\left(\frac{\delta + \Delta_i}{2}\right)} \, d\xi$$

$$+ \tfrac{1}{2} \int_0^\infty \left[ \frac{\cos \left(\frac{w - t}{2} - x\right)\xi \; - \cos \left(\frac{w \; t}{2} - x\right)\xi}{2} \right] e^{-\xi\left(\frac{\delta + \Delta_i}{2}\right)} \, d\xi$$

The two integrals are identical except for parameter.

Consider the integral

$$I = \int_0^\infty \frac{\cos \alpha x - \cos \beta x}{x^2} \, e^{-rx} dx$$

Integrate by parts replacing limits by $\varepsilon$, R and taking the limit as $\varepsilon \to 0$ and $R \to \infty$.

$$I = - \frac{\cos \alpha x - \cos \beta x}{x} \, e^{-rx} \Big|_\varepsilon^R - r \int_\varepsilon^R \frac{\cos \alpha x - \cos \beta x}{x} \, e^{-rx} dx$$

$$- \int_\varepsilon^R \frac{\alpha \sin \alpha x - \beta \sin \beta x}{x} \, e^{-rx} dx$$

$$\lim_{\varepsilon \to 0} \quad \frac{\cos \alpha x - \cos \beta x}{x} \longrightarrow 0$$

At upper limits the exponential insures convergence since $r > 0$.

Hence

$$I = r \int_0^\infty \frac{\cos \beta x - \cos \alpha x}{x} \, e^{-rx} dx + \int_0^\infty \frac{\beta \sin \beta x - \alpha \sin \alpha x}{x} \, e^{-rx} dx$$

$$I(\nu) = \int_0^\infty e^{-rx} \sin \nu x \, dx = \frac{\nu}{r^2 + \nu^2}$$

The integral is uniformly convergent for real $\nu$; hence, if one integrates over $\nu$

$$\int_\alpha^\beta \int_0^\infty e^{-rx} \sin \nu x \, dx \, d\nu = \int_\alpha^\beta \frac{\nu \, d\nu}{r^2 + \nu^2}$$

$$\int_0^\infty e^{-\gamma x} \frac{\cos \alpha x - \cos \beta x}{x} dx = \tfrac{1}{2} \ln \frac{\gamma^2 + \beta^2}{\gamma^2 + \alpha^2}$$

Also

$$\int_0^\infty e^{-\gamma x} \frac{\alpha \sin \alpha x - \beta \sin \beta x}{x} dx = \alpha \tan^{-1} \frac{\alpha}{\gamma} - \beta \tan^{-1} \frac{\beta}{\gamma}$$

Hence

$$I = \frac{\gamma}{2} \ln \frac{\gamma^2 + \alpha^2}{\gamma^2 + \beta^2} + \beta \tan^{-1} \frac{\beta}{\gamma} - \alpha \tan^{-1} \frac{\alpha}{\gamma}$$

where

$$\alpha = \left(\frac{w - t}{2} \pm x\right)$$

$$\beta = \left(\frac{w + t}{2} \pm x\right)$$

$$\gamma = \frac{\delta + \Delta_i}{2}$$

## Appendix B

### Calculation of Structure Factor for Quartz (310) Planes

$\alpha$ quartz has the space group $D_3^4$ or $D_3^6$, and the atom centers are at the following positions in the unit cell:

Si (u,0,0; $\bar{u}$,$\bar{u}$,1/3; 0,u,2/3)

O (x,y,z; y - x,$\bar{x}$,z + 1/3
$\bar{y}$,x - y,z + 2/3; x - y,$\bar{y}$,$\bar{z}$
y,x,$\bar{z}$ + 2/3; $\bar{x}$,y - x,$\bar{z}$ + 1/3)

where the parameters as given by Brill et al.[35] are:

$u = 0.465 \pm .003$

$x = 0.415 \pm .003$

$y = 0.272 \pm .003$

$z = 0.120 \pm .002$

The coordinates of the atoms in the unit cell are tabulated in the table. The atomic structure factors are taken from Compton and Allison.[22a] The factors for Si and O are used because the exact nature of the binding will not affect the structure factor for the values of $\frac{\sin \theta_B}{\lambda}$ of interest.

$$\frac{\sin \theta_B}{\lambda} = \frac{1}{2d} = 0.425$$

$f_O = 2.72$

$f_{Si} = 6.89$

The unit cell for the hexagonal crystal has the constants

$a = 4.903$
$c = 5.393$ at 18° C

and contains three $SiO_2$ molecules. The crystal structure factor is given by

$$F_H = \sum_i f_i e^{i\vec{s}\cdot\vec{r}}$$

$$\sum_i f_i e^{i2\pi(h_1x_{i1} + h_2x_{i2} + h_3x_{i3})}$$

for $H = (310)$

$$|F_H| = \sqrt{A^2 + B^2}$$

where

$$A = \sum_i f_i \cos 2\pi(h_1x_{i1} \quad h_2x_{i2})$$

$$B = \sum_i f_i \sin 2\pi(h_1x_{i1} \quad h_2x_{i2})$$

The calculated value for $|F_{310}|$ becomes 13.8. The volume of the unit cell is given by

$$V = ca^2 \sin\frac{\pi}{3} = \frac{\sqrt{3}}{2} ca^2$$

$$V = 1.12 \times 10^2 \text{ Å}^3$$

Structure Factor Calculation for $\alpha$ Quartz

| Atom | f | $x_1$ | $x_2$ | $x_3$ | $\phi$ | cos $2\pi\phi$ | sin $2\pi\phi$ | f cos $2\pi\phi$ | f sin $2\pi\phi$ |
|---|---|---|---|---|---|---|---|---|---|
| Si | 6.89 | 0.465 | 0 | 0 | 1.395 | 0.1750 | 0.9846 | | |
| | | -0.465 | -0.465 | 0.333 | -1.860 | -0.2850 | -0.9585 | | |
| | | 0 | 0.465 | 0.667 | 0.465 | 0.8938 | 0.4486 | | |
| | | | | | | 0.7838 | 0.4747 | 5.400 | 3.271 |
| O | 2.72 | 0.415 | 0.272 | 0.120 | 1.517 | 0.0537 | 0.9985 | | |
| | | -0.143 | -0.415 | 0.453 | -0.844 | 0.6645 | -0.7473 | | |
| | | -0.272 | 0.143 | 0.787 | -0.673 | 0.7820 | -0.6233 | | |
| | | 0.143 | -0.272 | -0.120 | 0.157 | 0.9877 | 0.1564 | | |
| | | 0.272 | 0.415 | 0.547 | 1.231 | 0.3330 | 0.9430 | | |
| | | -0.415 | -0.143 | 0.213 | -1.388 | 0.1816 | -0.9834 | | |
| | | | | | | 3.0025 | -0.2561 | 8.167 | -0.697 |
| | | | | | | | | 13.567 | 2.574 |

$F_{310}$ 13.8

References

(1) E. Rutherford and E. Andrade, Phil. Mag. 27, 854 (1914); 28, 262 (1914).

(2) J. Thibaud, Thesis (Paris, 1925), Ann. de Physique 5, 75-152 (1926).

(3) M. Frilley, Thesis (Paris, 1928), Ann. de Physique 11, 483 (1929).

(4) M. Gouy, Ann. de Physique 5, 241 (1916).

(5) J. W. M. DuMond and H. A. Kirkpatrick, Rev. Sci. Inst. 1, 88 (1930).

(6) Y. Cauchois, J. de Phys. et Rad. 3, 320 (1932).

(7) Y. Cauchois, J. de Phys. et Rad. 4, 61 (1933).

(8) Y. Cauchois, Ann. de Physique 1, 215 (1934).

(9) H. H. Johann, Zeits. f. Physik 69, 185 (1931).

(10) J. W. M. DuMond, Rev. Sci. Inst. 18, 626 (1947).

(11) J. W. M. DuMond, D. A. Lind and E. R. Cohen, Rev. Sci. Inst. 18, 617 (1947).

(12) F. Norling, Arkiv for Math. och Fysik 27A, No. 27 (1941).

(13) H. Bradt, P. C. Gugelot, O. Huber, M. Medicus, P. Preiswerk and P. Scherrer, Helv. Phys. Acta 19, 77 (1946).

(14) E. Bleuler and W. Zunti, Helv. Phys. Acta 19, 376 (1946).

(15) S. J. DuToit, Rev. Sci. Inst. 18, 31 (1947).

(16) G. Wentzel, Zeits. f. Physik 43, 1 (1927).

(17) A. Sommerfeld, Wave-Mechanics, translated by H. L. Brose (Dutton, 1930), pp. 164-177 and 212-225.

(18) W. H. Zachariasen, Theory of X-Ray Diffraction in Crystals (Wiley, 1945).

(19) W. Franz, Zeits. f. Physik 90, 623 (1934).

(20) W. Franz, Zeits. f. Physik 95, 652 (1935).

(21) W. Franz, Zeits. f. Physik 98, 314 (1935).

(22a) A. H. Compton and S. K. Allison, X-Rays in Theory and Experiment (D. Van Nostrand, 1935), p. 781.

(22b) Ibid., pp. 638-641.

(22c) Ibid., pp. 745-746.

(23) C. G. Darwin, Phil. Mag. 27, 325 (1914); 27, 675 (1914).

(24) P. P. Ewald, Ann. der Physik 54, 519 (1917); 54, 577 (1917); Zeits. f. Physik 2, 232 (1920); Physik. Zeitschr. 26, 29 (1925).

(25) J. A. Prins, Zeits. f. Physik 63, 477 (1930).

(26) M. Kohler, Ann. der Physik 18, 265 (1933).

(27) P. Kirkpatrick, Rev. Sci. Inst. 10, 186 (1939).

(28) P. W. Levy and E. Grueling, Phys. Rev. 73, 83 (1948).

(29) O. Berquist, Zeits. f. Physik 66, 496 (1930).

(30) A. H. Jay, Proc. Roy. Soc. 142, 237 (1933).

(31) J. W. M. DuMond and E. R. Cohen, Rev. Mod. Phys. 20, 82 (1948).

(32) C. S. Barrett and C. E. Howe, Phys. Rev. 39, 889 (1932).

(33) R. M. Bozorth and F. E. Haworth, Phys. Rev. 53, 538 (1938).

(34) E. B. Wilson, Advanced Calculus (Ginn and Co., 1912).

(35) R. Brill, C. Hermann and C. Peters, Ann. der Physik 41, 233 (1942).

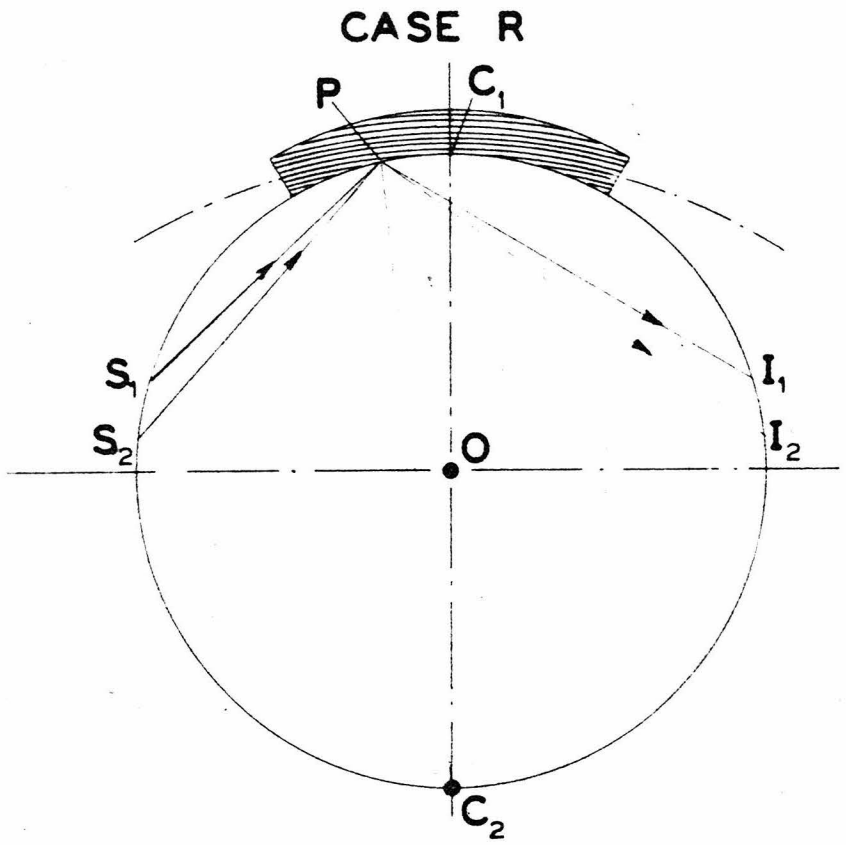


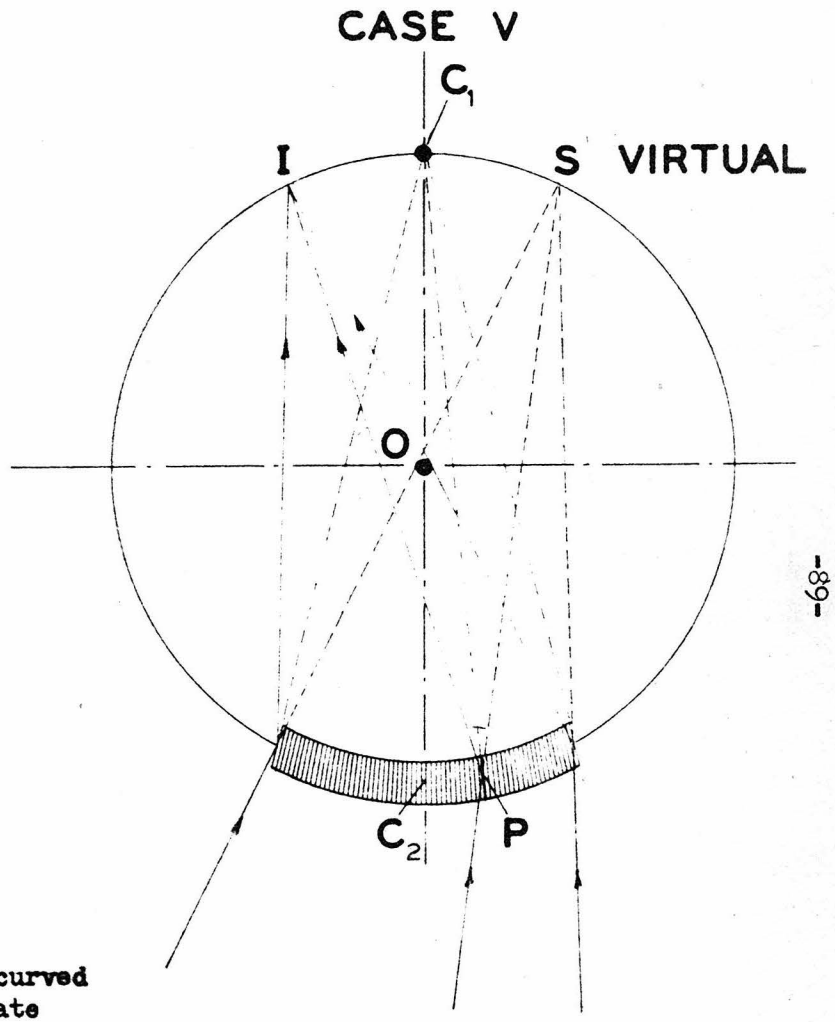


Fig. 1. Case R shows the exact solution for the reflection type curved crystal focussing spectrometer in which there are two real conjugate foci S and I. The reflecting boundary surface of the crystal coincides with the focal circle (center at O) while the atomic reflecting planes are curved so as to be concentric about the center $C_2$ on the circumference of the focal circle.

Case V shows the exact solution for the transmission type curved crystal focussing spectrometer. In this type there is one real focus I and one virtual focus S. The atomic reflecting planes converge to a point $C_1$ on the focal circle (center at O) while the neutral axis of the bent lamina coincides with the focal circle.

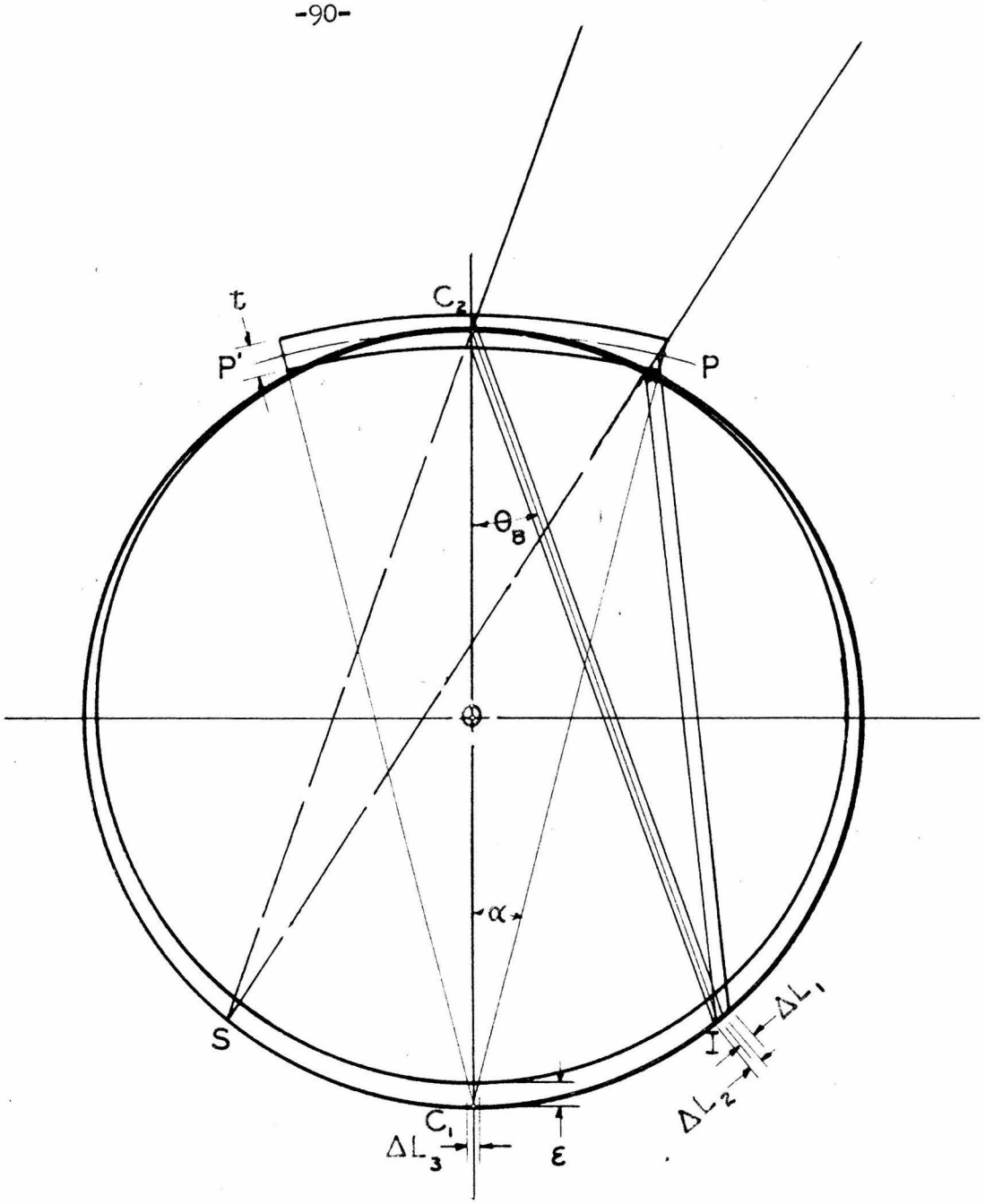


Fig.2 Geometry of aberrations which may occur in a focusing crystal spectrometer.

$L_1$ - aberration caused by failure of crystal to lie on focal circle.
$L_2$ - aberration caused by finite crystal thickness.
$L_3$ - aberration caused by improper focusing.

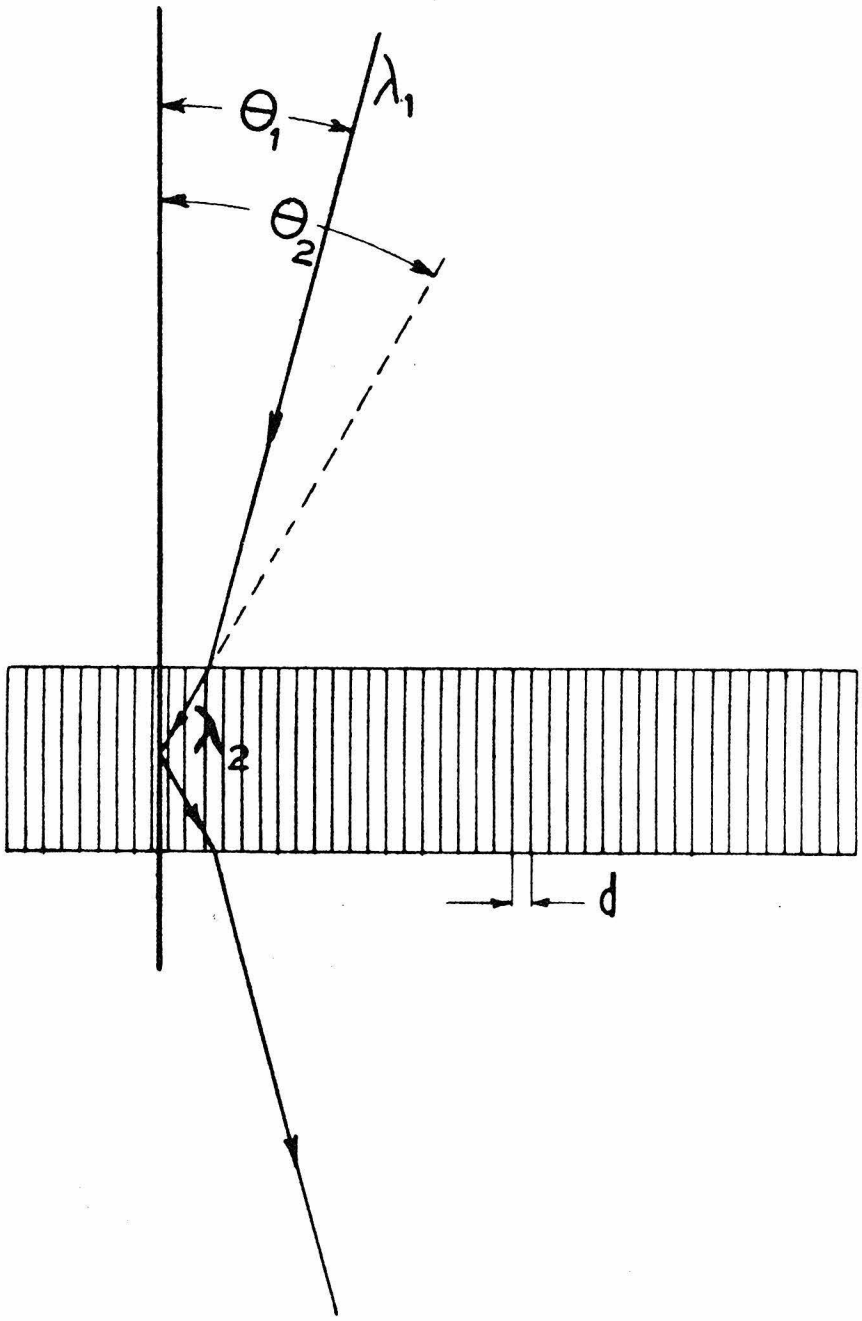


Fig. 3. Geometry demonstrating the absence of correction for refractive index when the atomic reflecting planes are normal to the exit and entry faces of the lamina in the transmission type spectrograph.

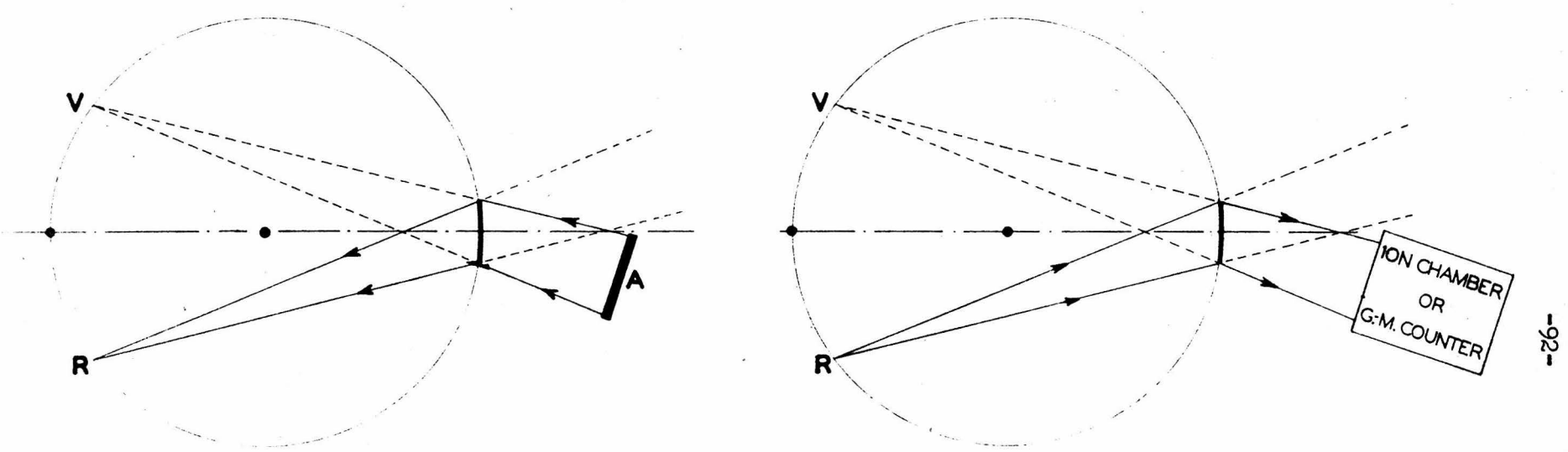


Fig. 4. Two ways of using the transmission type curved crystal spectrometer. An extended source may be placed at A in which case spectral lines will be focussed as at R. This case is appropriate for the study of fluorescence excited in a screen placed at A but is uneconomical if the total intensity from the source is a limiting factor. For gamma ray spectra the source may be placed at R, and the intensity, measured in an ion chamber or counter, is thus plotted as a function of the position of the source R on the focal circle.

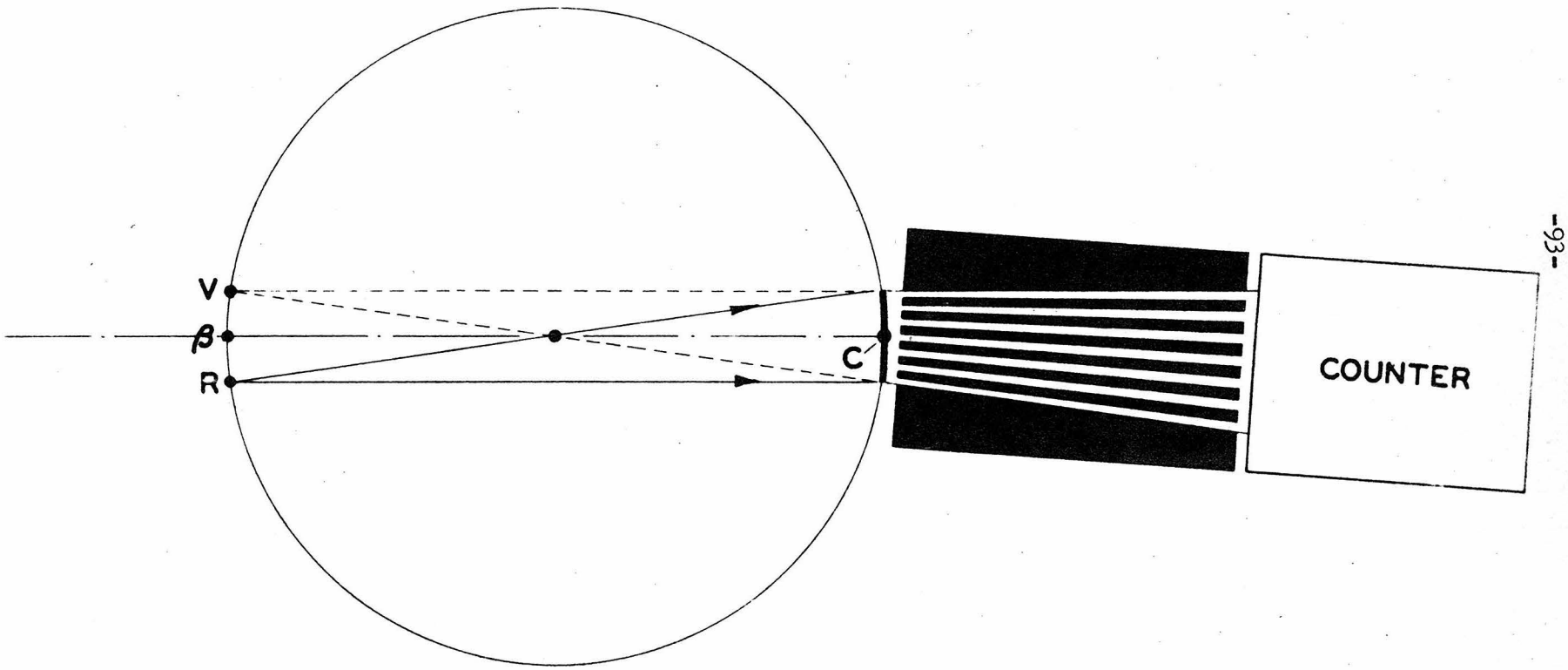


Fig. 5. To illustrate how the tapering lead collimator is used to suppress the beam directly transmitted through the crystal from R and to permit free passage of the monochromatic diffracted beam whose virtual source is V. The drawing is not to scale. Dimensions transverse to the beams are greatly exaggerated.

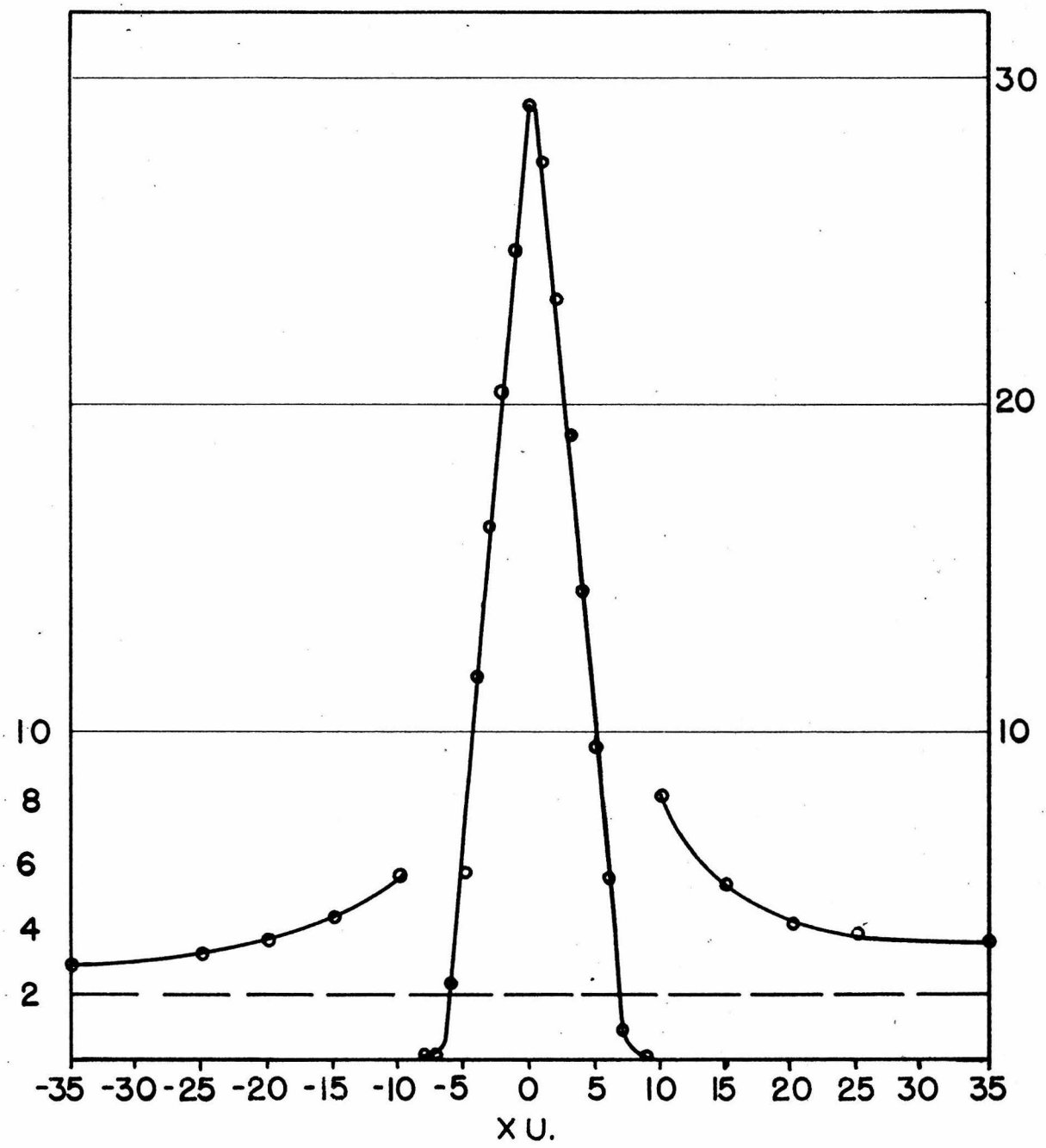


Fig.6 Transmission profile of collimator for a narrow source placed on the focal circle. The left scale of ordinates applies to the regions outside ±10 X.U., while the right scale multiplied by the factor $10^3$ applies within ±10 X.U. The dashed line represents the irreducible background on the left ordinate scale.

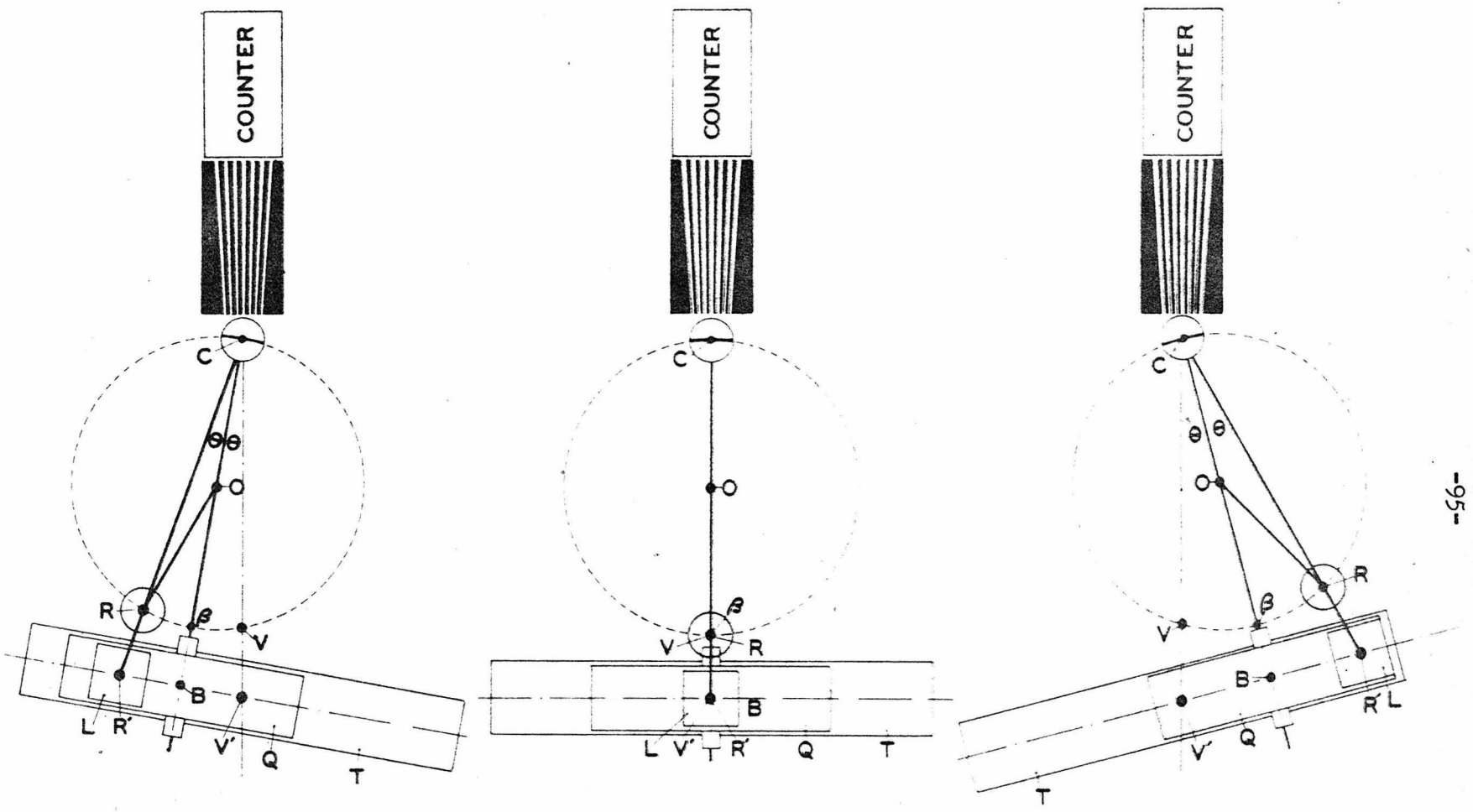


Fig. 7. To illustrate schematically the geometry of the gamma ray spectrometer. The view at center shows the instrument at the zero wave-length position while the views to left and right show different wave-length settings for reflections to left and to right of the atomic reflecting planes. The constant distances CR' and CV' are made rigorously equal. Displacements of the carriages L and Q effected by means of precision screws are proportional to the sine of the Bragg angle θ and hence proportional to wave-lengths. The drawing is not to scale. The aperture of the crystal at C and the width of the collimator are exaggerated.

Fig.8 Isometric Drawing of Complete Spectrometer.

Legend

| | |
|---|---|
| A | Front pivot pad |
| B, C | Pads at the rear corners |
| D | Protection counters |
| E | Lead collimator |
| F | Focal circle beam |
| G | Main counter |
| H | Lead shielding for counters |
| J | $\beta$ point adjustment lever |
| K | Source holder for radio-isotope |
| L | Small carriage |
| M | Front pivot axel |
| N | Source carriage |
| O | Center pivot of the focal circle |
| P | Crystal holder table |
| Q | Screw carriage |
| S | Source beam |
| T | Swinging track |
| U | Photographic spectrum cassette |
| V | Track pivot |
| W | Wave-length drum |
| Y | Wave-length vernier |
| Z | Wave-length revolution counter |

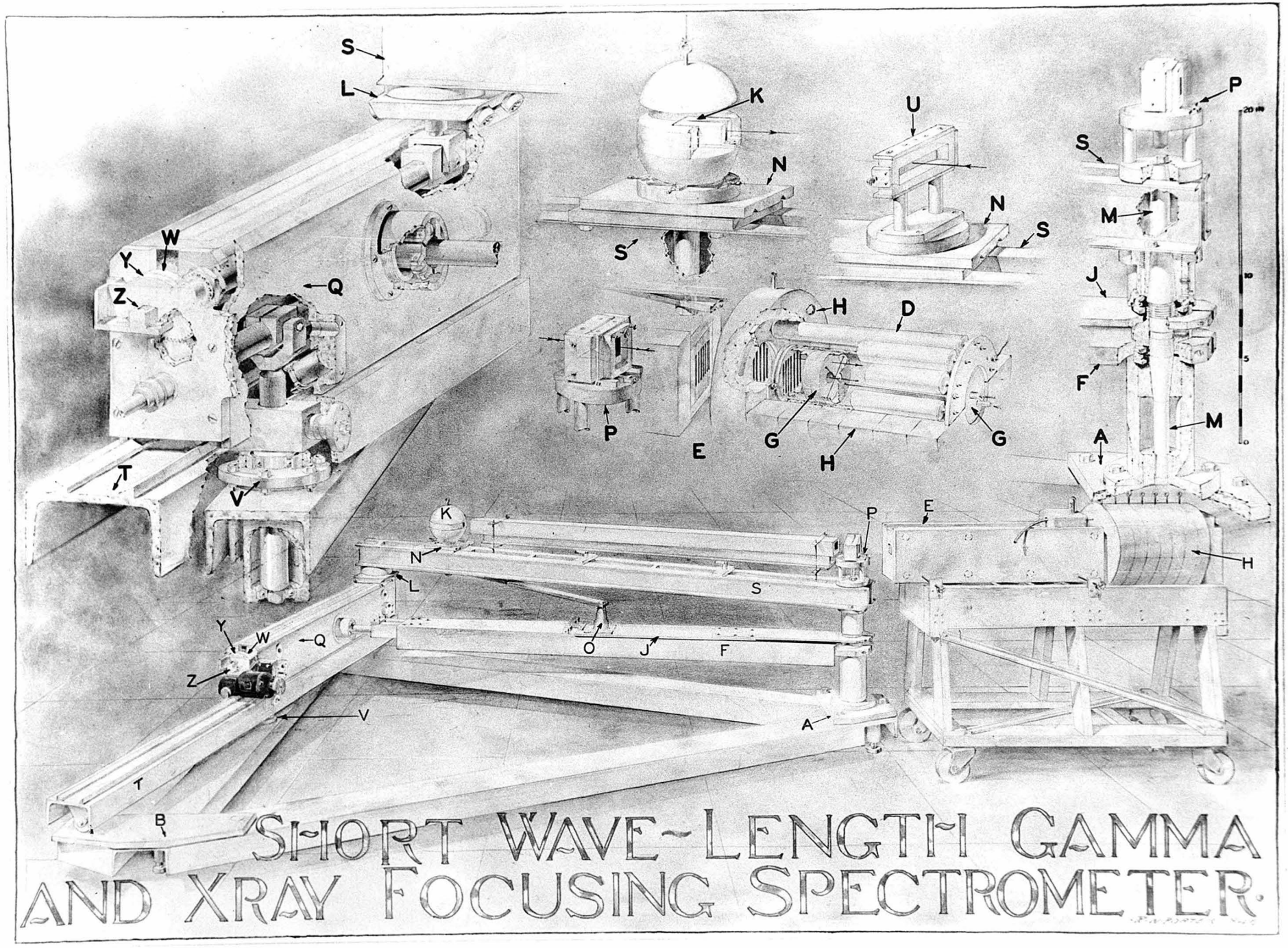


# SHORT WAVE-LENGTH GAMMA AND XRAY FOCUSING SPECTROMETER.

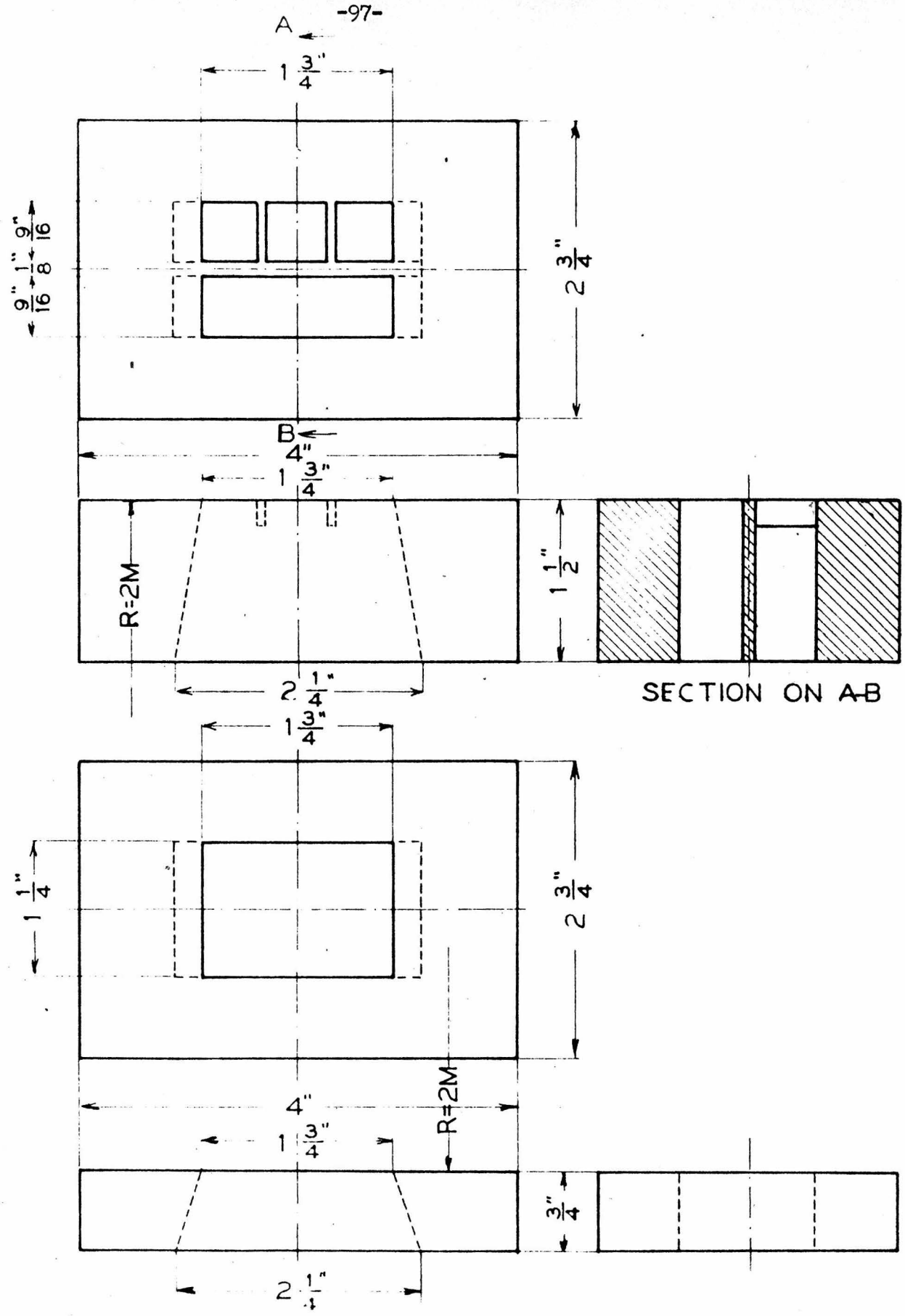


Fig. 9. Working drawing of the convex and concave stainless steel clamping blocks showing the windows for the radiation. The upper drawing is the convex block.

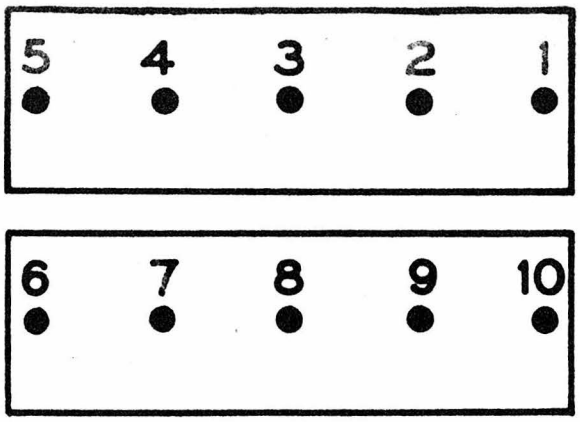


NUMBERING SCHEME GIVING
POSITIONS STUDIED IN CRYSTAL APERTURE

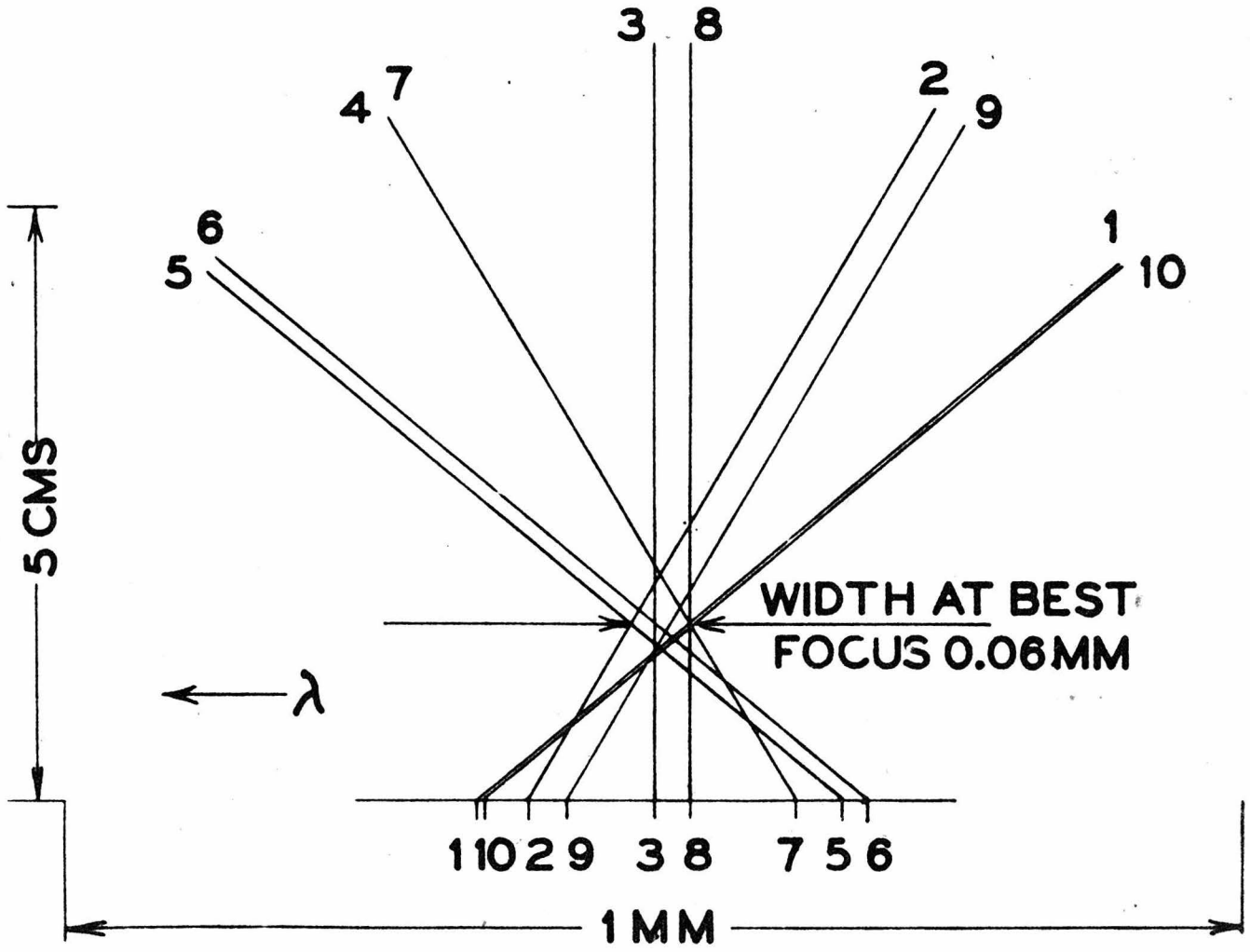


Fig. 10. Ray diagram used for determining by successive x-ray exposures the quality of focussing in the curved crystal transmission spectrometer. The transverse or horizontal scale of this diagram in 100 times the vertical scale. The ten positions in the crystal aperture are shown above.

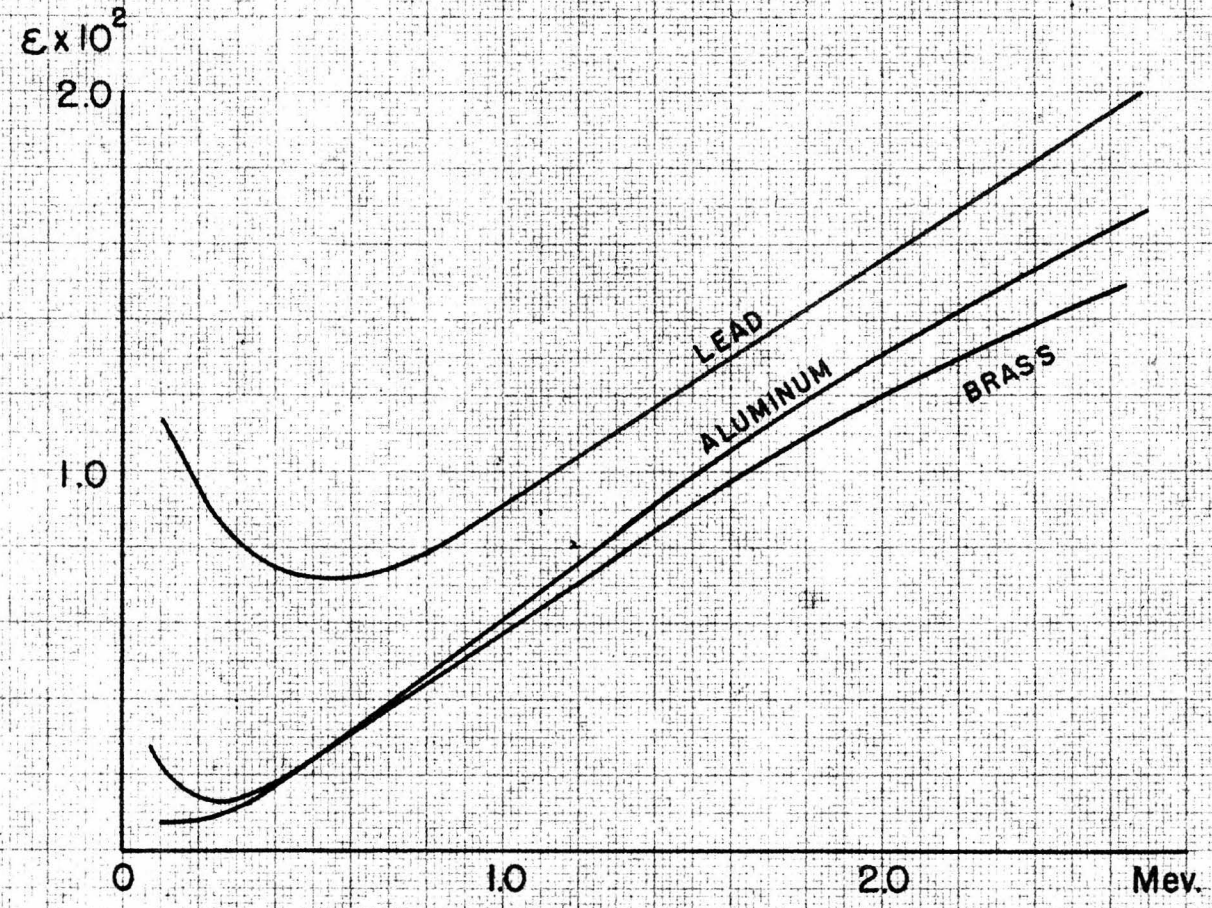


Fig.11 Absolute sensitivity of a cylindrical counter as a function of quantum energy. The cathode wall thickness is adjusted in each case to give the maximum sensitivity. From Bradt et.al. Helv. Phys. Acta 19 77 (1946).

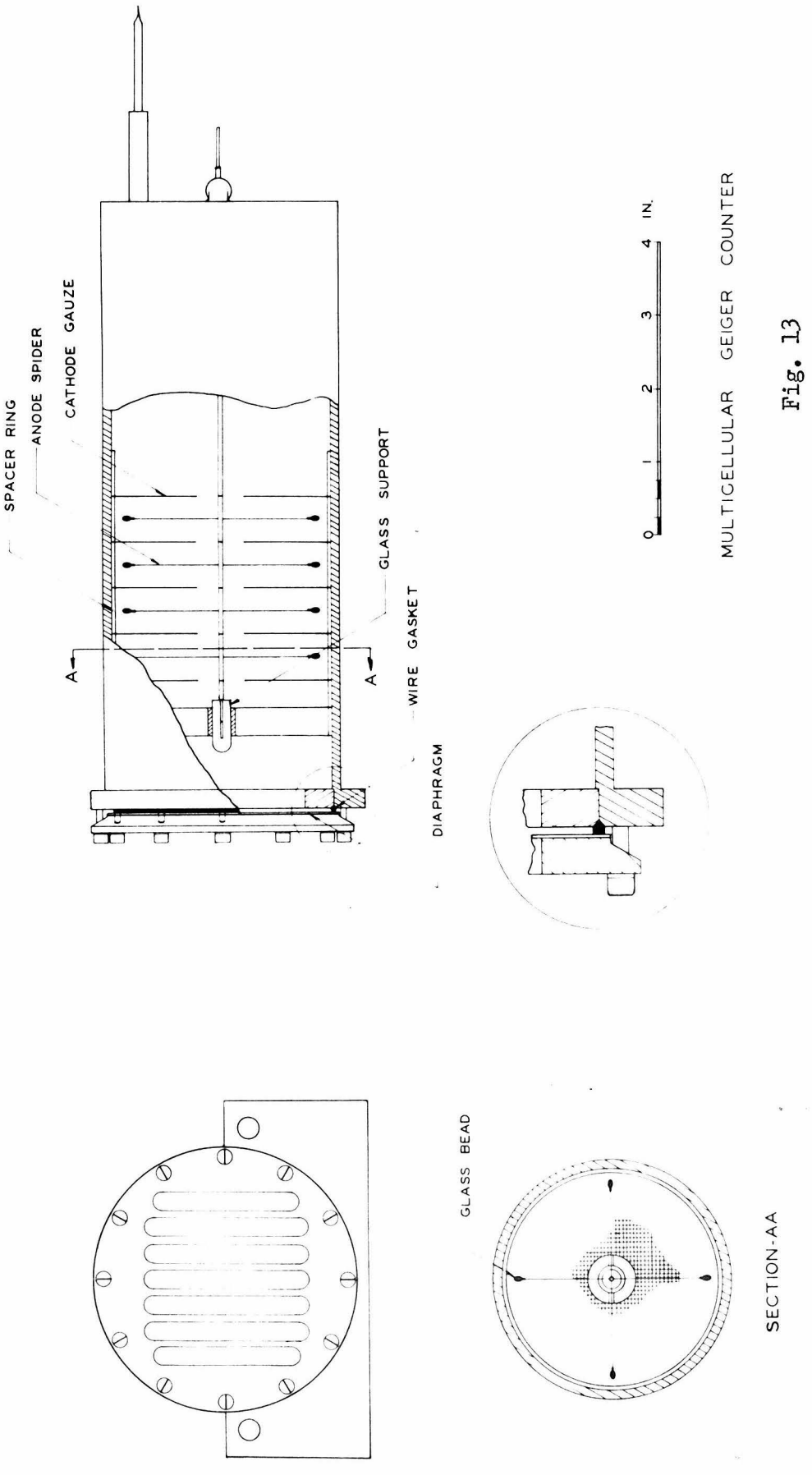


MULTICELLULAR GEIGER COUNTER

Fig. 13

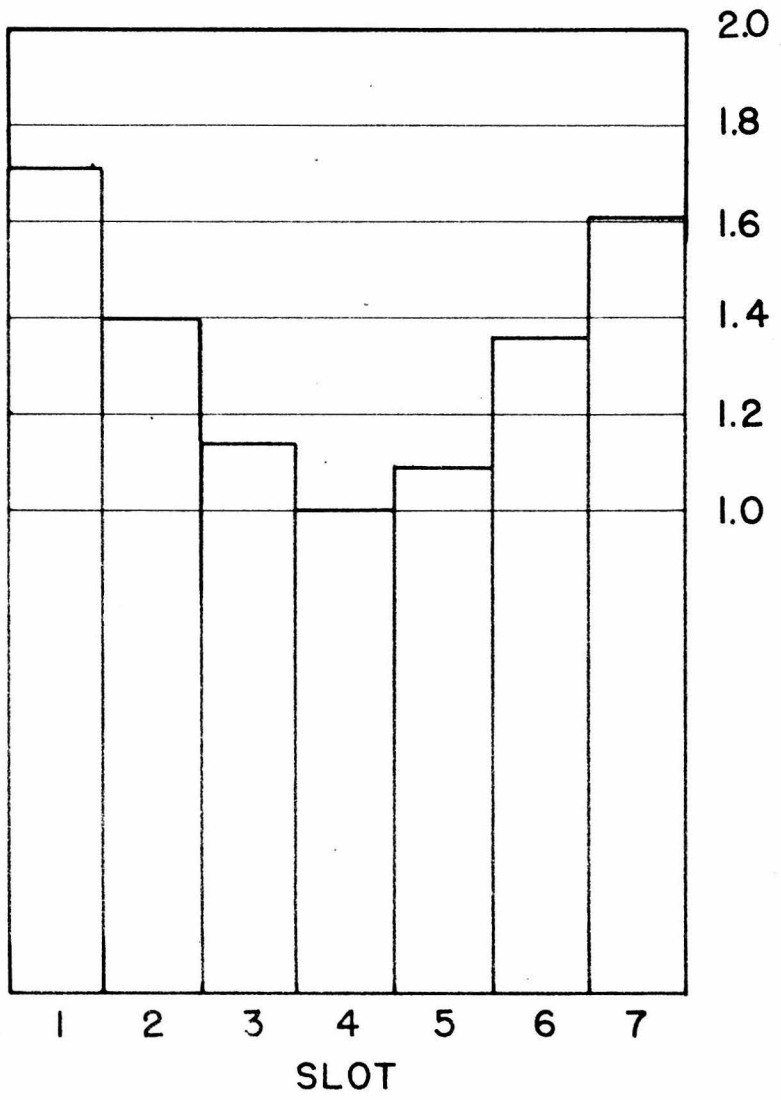


Fig.14 Counter sensitivity over the window slots relative to the central slot (4).

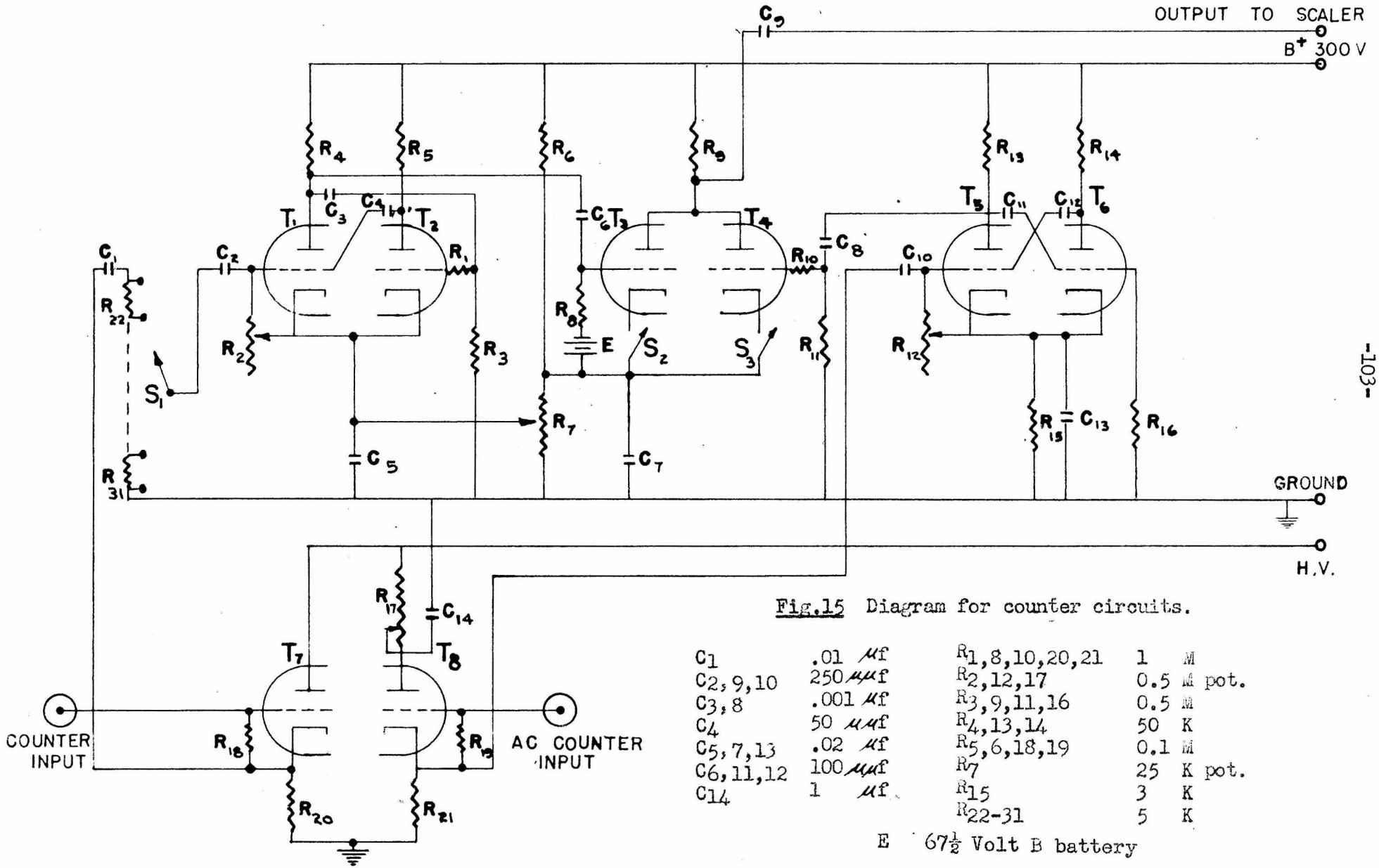


Fig.15 Diagram for counter circuits.

| | | | | |
|---|---|---|---|---|
| $C_1$ | .01 μf | $R_{1,8,10,20,21}$ | 1 | M |
| $C_{2,9,10}$ | 250 μμf | $R_{2,12,17}$ | 0.5 | M pot. |
| $C_{3,8}$ | .001 μf | $R_{3,9,11,16}$ | 0.5 | M |
| $C_4$ | 50 μμf | $R_{4,13,14}$ | 50 | K |
| $C_{5,7,13}$ | .02 μf | $R_{5,6,18,19}$ | 0.1 | M |
| $C_{6,11,12}$ | 100 μμf | $R_7$ | 25 | K pot. |
| $C_{14}$ | 1 μf | $R_{15}$ | 3 | K |
| | | $R_{22-31}$ | 5 | K |

E $67\frac{1}{2}$ Volt B battery

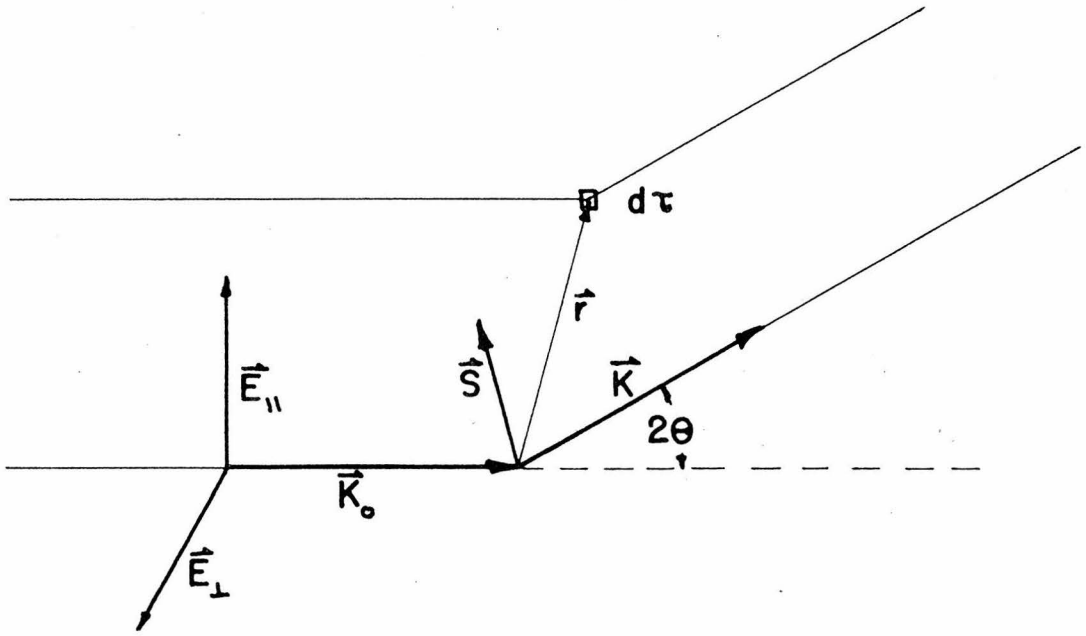


Fig. 16

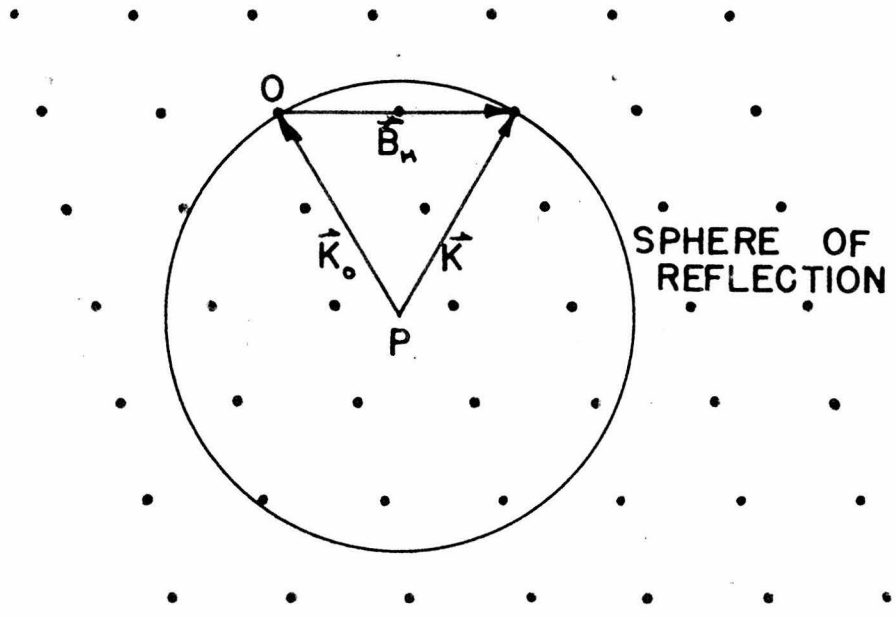


Fig.17 The Bragg Law expressed as a vector relation in the reciprocal lattice. Note that $|k| = |k_0| = \frac{1}{\lambda}$.

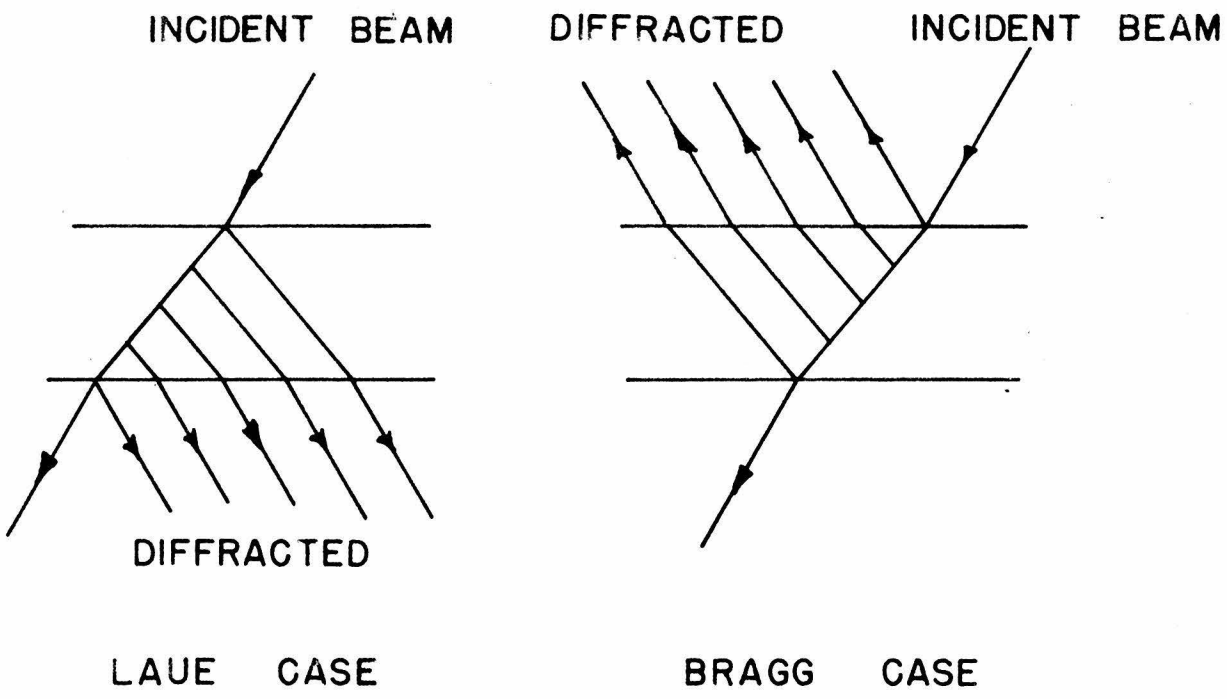


Fig.18 Shows the differences between Laue reflection (atomic planes normal to plate) and Bragg reflection (atomic planes parallel to plate). Actually the cases represent a very narrow beam incident on a "thin" crystal.

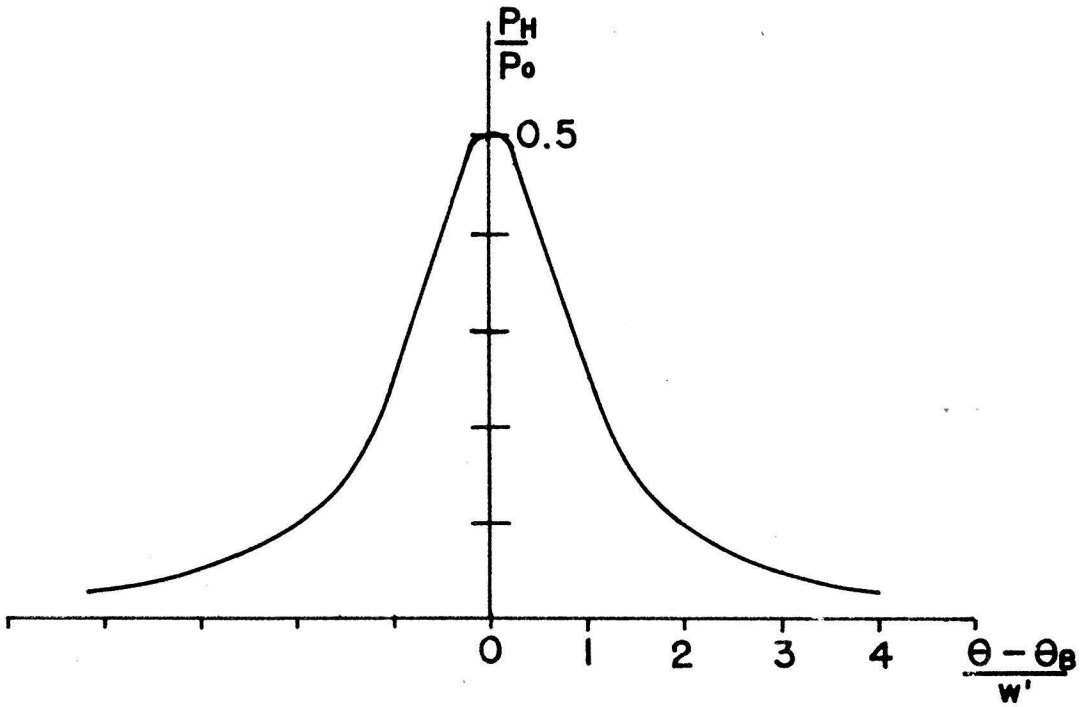


Fig.19 Diffraction pattern for the Laue case of a thick perfect crystal.

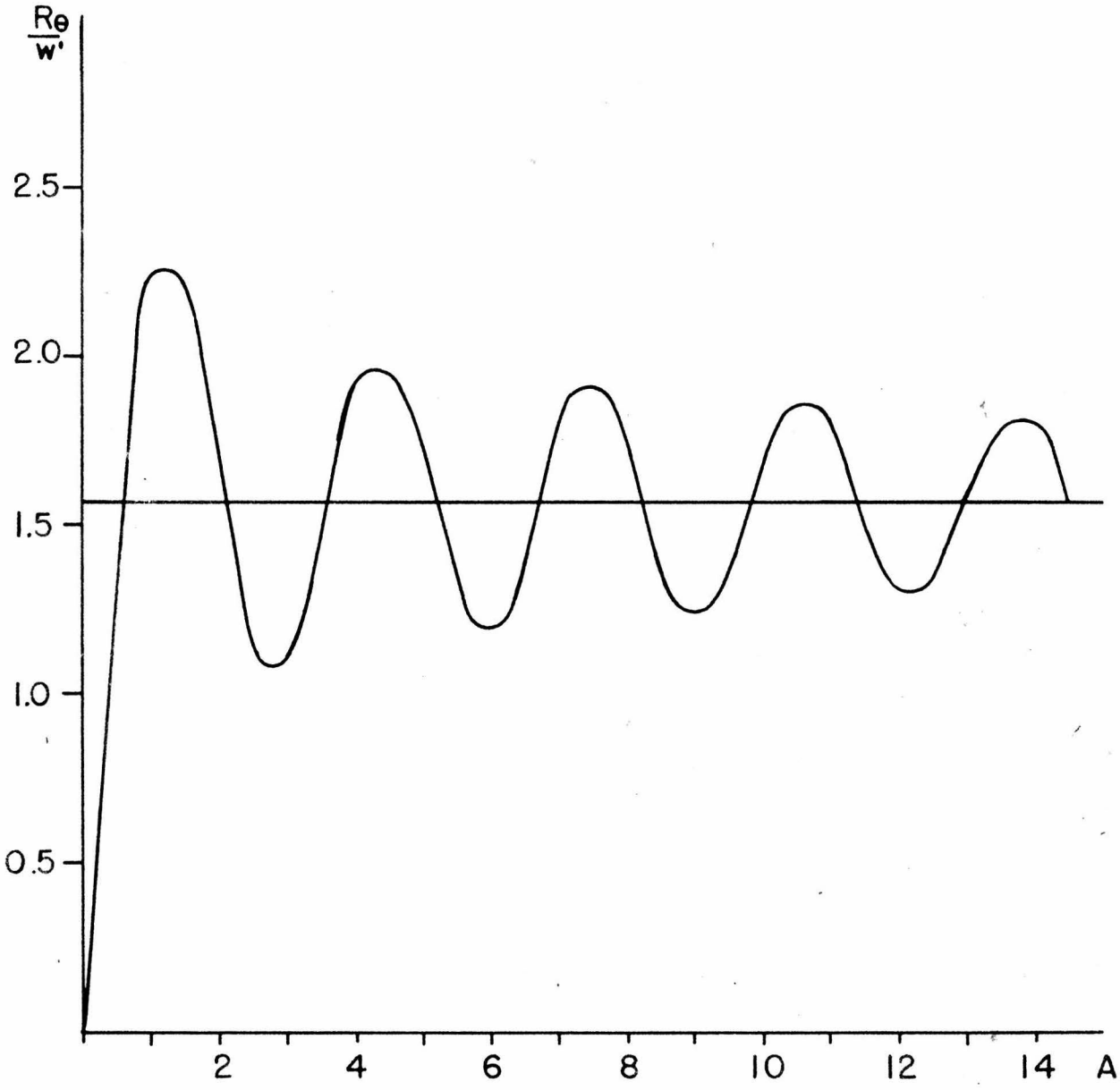


Fig.20 Plot $\frac{R_\theta}{w'}$ as a function of A. For large A the value of $\frac{R_\theta}{w'} = \frac{\pi}{2}$ is shown by the full line.

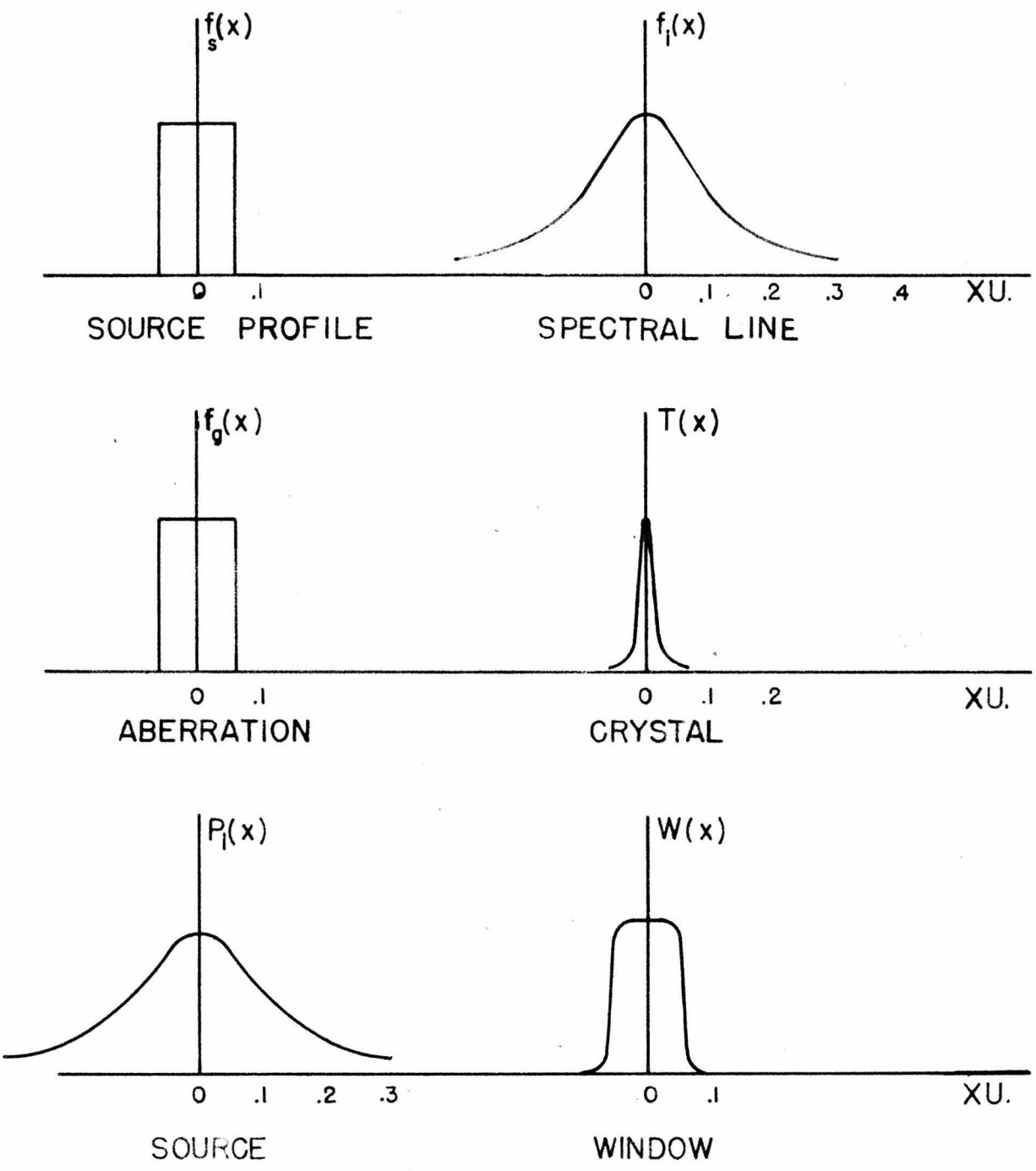


Fig.21 Plot of the four profiles contributing to the spectrometer response. $P_i(x)$ is the fold of the source functions $f_s(x)$ and $f_i(x)$ and constitutes the true source under analysis. $W(x)$ is the fold of $f_g(x)$ and $T(x)$ and constitutes the analysing window of the spectrometer. The fold of $P_i$ with W yields the actual line profile. The widths are plotted to true scale for the case of Sn K$\alpha$ radiation but the heights are adjusted arbitrarily.

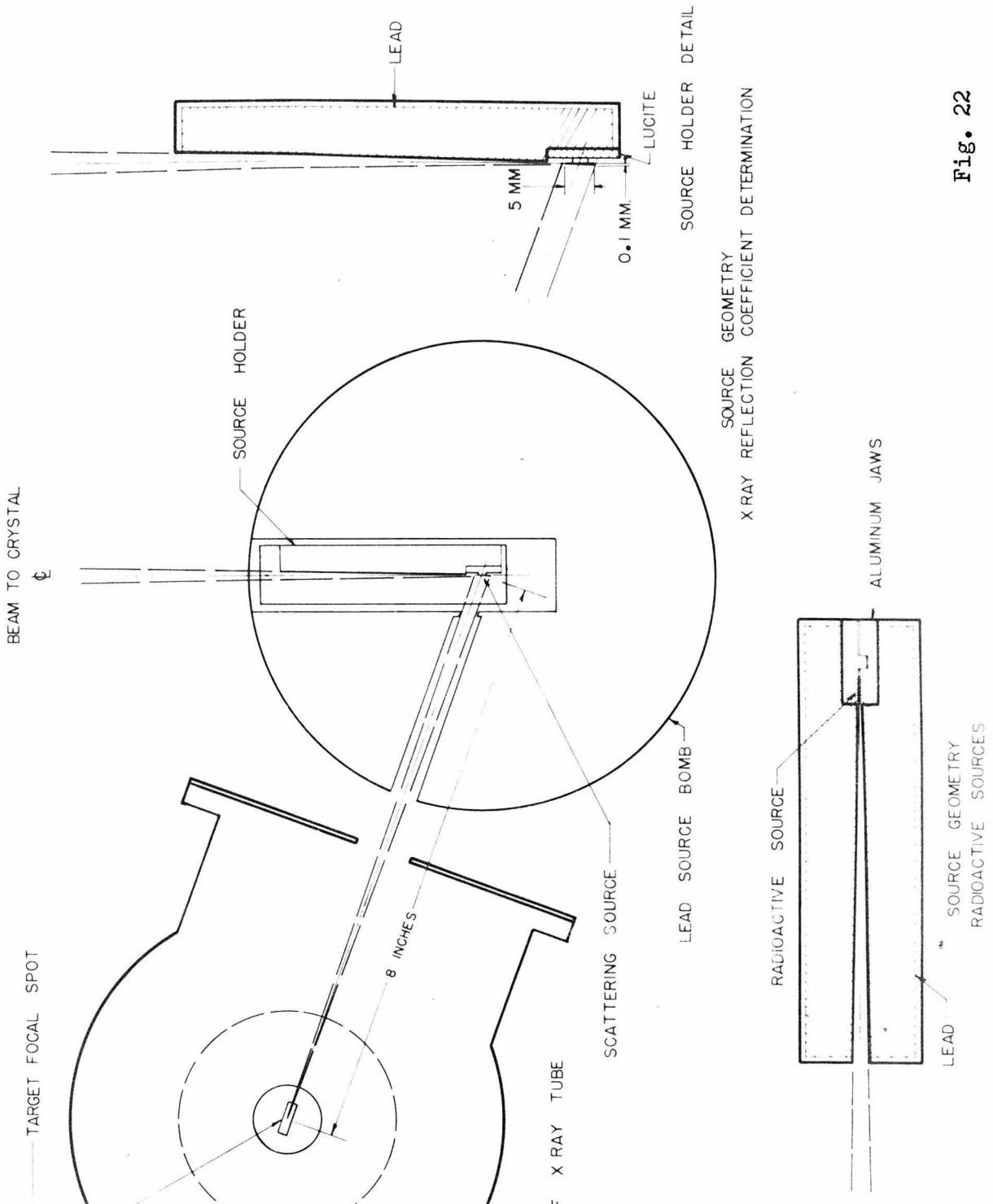
LEAD
LUCITE
5 MM
0.1 MM
SOURCE HOLDER DETAIL
SOURCE GEOMETRY
X RAY REFLECTION COEFFICIENT DETERMINATION
BEAM TO CRYSTAL
SOURCE HOLDER
TARGET FOCAL SPOT
8 INCHES
SCATTERING SOURCE
LEAD SOURCE BOMB
SHOCKPROOF X RAY TUBE
ALUMINUM JAWS
RADIOACTIVE SOURCE
LEAD
SOURCE GEOMETRY
RADIOACTIVE SOURCES

Fig. 22

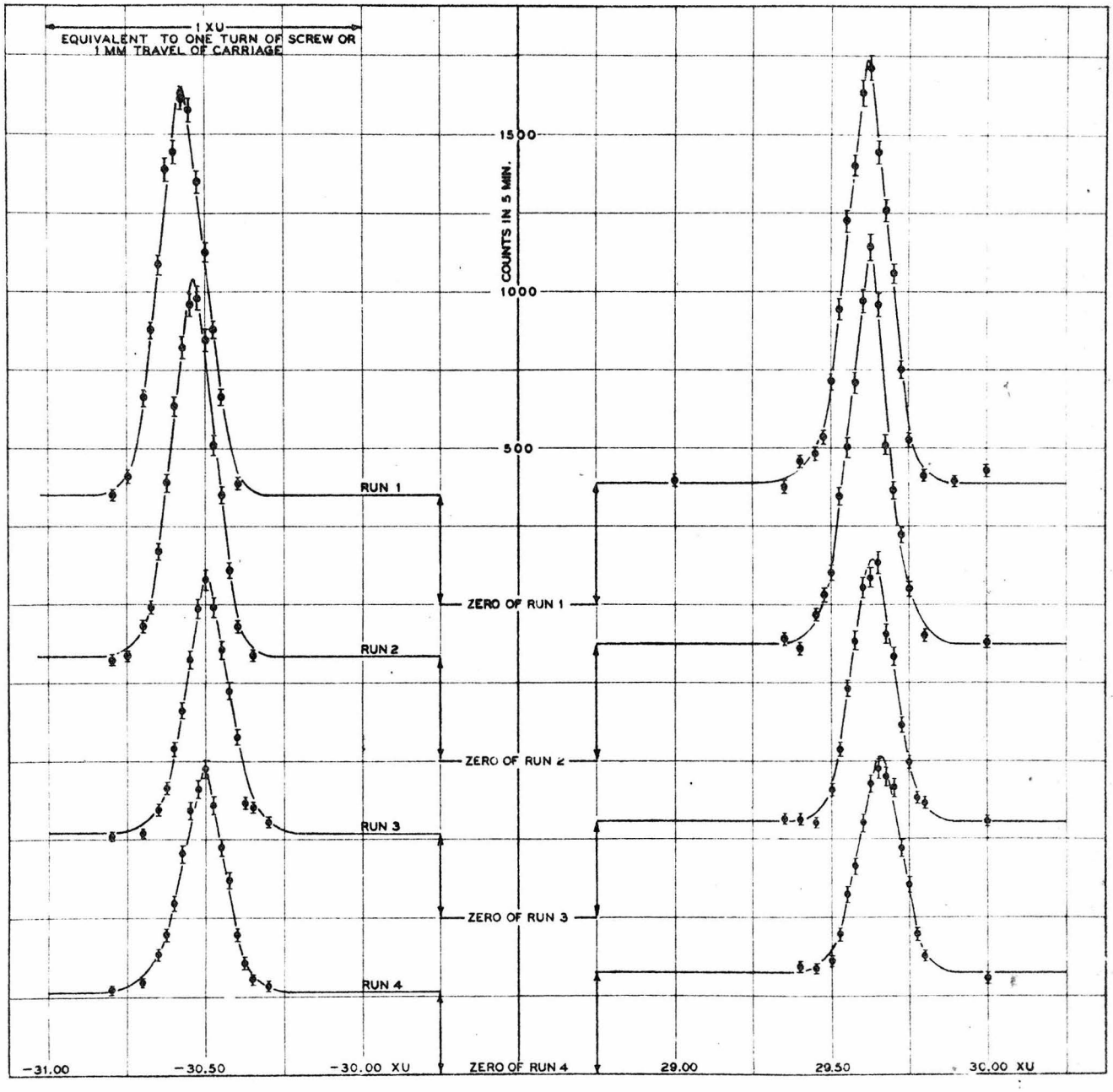


Fig.23 Actual line profiles of the $Au^{198}$ 0.4112 Mev line as obtained with the spectrometer.

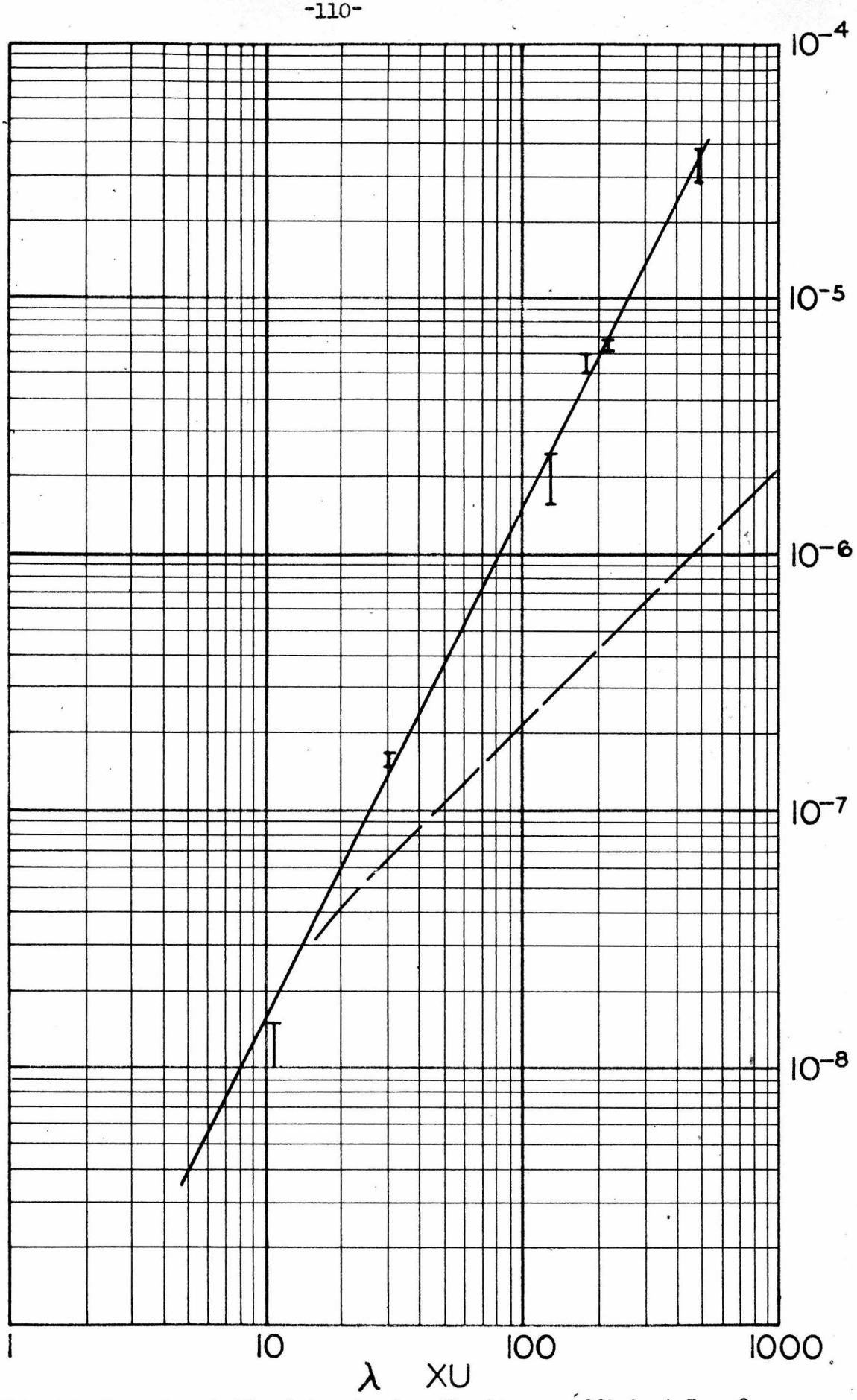


Fig.24 Experimentally determined reflection coefficient $R_\theta$ for quartz (310) planes as used in the spectrometer. The ordinate scale is in radians. The dashed curve shows the theoretical values for $R_\theta$ if the crystal were assumed to be perfect.